Spectral Analysis of Phonocardiographic Signals Using Advanced Parametric Methods

Herkole P. Sava

A thesis submitted for the degree of Doctor of Philosophy.

The University of Edinburgh.

- July 1995 -

Abstract

The use of spectral analysis of heart sounds has been found to be an effective method for detecting different valvular diseases, monitoring the condition of prosthetic heart valves and studying the mechanism of heart action. In this context, the method of analysis is of crucial importance because diagnostic criteria depend on the accuracy of estimating the spectrum of heart sounds. The research detailed in this thesis investigates the performance of several advanced signal processing techniques when analysing heart sounds, and investigates the feasibility of such a method for monitoring the condition of bioprosthetic heart valves.

A data-acquisition system was designed and developed which records and digitises heart sounds in a wide variety of cases ranging from sounds produced by native heart valves to mechanical prosthetic heart valves. Heart sounds were recorded from more than 150 patients including subjects with normal and abnormal native, bioprosthetic, and mechanical prosthetic heart valves. The acquired sounds were pre-processed in order to extract the signal of interest. Various spectral estimation techniques were investigated with a view to assessing the performance and suitability of these methods when analysing the first and second heart sounds. The performance of the following methods is analysed: the classical Fourier transform, autoregressive modelling based on two different approaches, autoregressive-moving average modelling, and Prony's spectral method.

In general, it was found that all parametric methods based on the singular value decomposition technique produce a more accurate spectral representation than conventional methods (i.e. the Fourier transform and autoregressive modelling) in terms of spectral resolution. Among these, Prony's method is the best. In addition a modified forward-backward overdetermined Prony's algorithm is proposed for analysing heart sounds which produces an improvement of more than 10% over previous methods in terms of normalised mean-square error. Furthermore, a new method for estimating the model order is proposed for the case of heart sounds based on the distribution of the eigenvalues of the data matrix. Five parameters are used to describe the spectral composition of heart sounds: the distribution of the number of frequency components, the distribution of the amplitudes of frequency components, the distribution of the energy of frequency components, the frequency of the largest amplitude component, and the frequency of the largest energy component. Results show that the relative distribution of the amplitudes of spectral components is strongly related to the functioning of the heart valves, whereas the number of frequency components and their relative energy are more dependent on the characteristics of lung-thorax system. Clear differences have been found with respect to the distribution of amplitude of the frequency components for different kinds of heart valves and amongst the normal and malfunctioning cases of the same valve. The diagnostic potential of spectral analysis combined with pattern classification methods is investigated for the case of Carpentier-Edwards bioprosthetic valves implanted in the aortic position. The structure presented in this thesis is based on the combination of a modified overdetermined forward-backward Prony's method combined with an adaptive single layer perceptron classifier. Results show 100% correct classification of the normal and malfunctioning cases of Carpentier-Edwards bioprosthesis for the investigated patient population. It is believed that this high accuracy in correct classification can mostly be attributed to the accurate representation of the information contained in heart sounds by the modified forward-backward overdetermined Prony's method. Thus, the proposition of this thesis is that when the appropriate signal processing and classification methods are used to analyse heart sounds, the diagnostic potential of spectral phonocardiography can be exploited with a high degree of success. In the long term a larger population of patients with implanted Carpentier-Edwards bioprosthesis is needed in order to validate the clinical use of the method.

Declaration of originality

I hereby declare that this thesis and the work reported herein were composed and originated entirely by myself, in the Department of Electrical Engineering at the University of Edinburgh.

Acknowledgements

Contents

prosthetic heart valve.

Figure 2.2:   Star-Edward prosthetic heart valve.

The main advantages of the tilting disc prosthesis over the caged ball valve are the ease of insertion in the aortic position, the narrow sewing ring, and the absence of a protruding cage which is particularly helpful to the surgeon when working in a small aortic root or small-volume left ventricle. Nevertheless, the reported incidence of mechanical malfunction of implants in the mitral position has been higher with disc valves than with ball valves [48].

Although a standardised procedure has not yet been developed for the determination of the functional characteristics of valves, some general characteristics for mechanical prostheses can be derived:

- The number of MPHV implants is much higher nowadays compared with bioprosthetic implants.

- The main advantage of all MPHV is that they have an excellent record of durability: more than 20 years in the case of caged–ball valves. However, patients with any mechanical prostheses, regardless of design or site of placement, require long-term anticoagulation because of the incidence of thromboembolism [49–51]. The incidence of thromboembolism tends to be slightly higher for prostheses in the mitral position; the reported incidence of mechanical malfunction of mitral valves has been higher with disc valves [48], thrombosis in the tricuspid position is quite high, and for this reason a bioprosthesis is preferred in this position.

- Mechanical failure is another well-known complication of these valves. Whether it is a change in ball characteristics leading to ball escape in ball valves, leaflet es-

cape in bileaflet valves or strut fracture in tilting disc valves, these complications may causes acute severe heart failure associated with instantaneous death especially in the aortic position. However, in the mitral position mechanical failure is compatible with life for several hours [51–54].

- Ischemic stroke in patients with MPHV is often considered to result in a high rate of mortality and morbidity. For this reason these types of valves are not recommended for elderly patients, since this group of patients is known to experience more difficulties with anticoagulation therapy.

2.4.2   Bioprosthetic heart valves

In a search for a solution to the thromboembolic complications of MPHV, prosthetic heart valves constructed from biological tissue were developed. Carpentier-Edwards porcine xenograft is most commonly used among the bioprosthetic heart valves. The valve is specially treated so that they not only become tougher and more resistant to wear, but are also rendered incapable of causing rejection by the human body.

However, despite recent improvements in tissue fixation and preservation techniques, tissue deterioration ultimately leading to valve failure is a major problem associated with the operation of the Carpentier-Edwards biprosthesis. Bioprosthetic valves are less durable than mechanical valves because the valve leaflets begin to degenerate after being implanted for 5 years or more. Therefore a further follow-up operation is needed which carries an operative mortality of more than 10% in many centres [53,55].

Regarding these problems, attention is being focussed on techniques for early detection of valvular malfunction. However, detecting abnormal function of a valve can be difficult because even a properly functioning prosthetic valve may cause turbulent flow and have some degree of stenosis and regurgitation. Moreover, significant valve problems may not cause noticeable haemodynamic changes until later, or in the worst case, until sudden catastrophic failure occurs.

2.5   Spectral analysis of heart valve sounds

Work using SPCG began in the early 1970s. An early example of SPCG was published by Kingsley [56] followed by Yoganathan *et al* [30,31], Iwata *et al* [27], and Hearn *et*

al [26]. In the early 1980s Stein *et al* [32,42] and Durand *et al* [20,57] analysed the closing sounds produced by prosthetic heart valves.

These early studies showed the improvement that digital signal processing methods could provide over analogue-based techniques [56,58–60] in the investigation of the origin of heart sounds and the diagnostic potential of phonocardiography.

With respect to native heart valves, several studies have been conducted in order to investigate the relationship between heart valve motion and the spectral composition of the respective heart sound [24–31,61,62]. These studies have shown that the spectral signature of S1 is composed of peaks in the low frequency range (10 to 50 Hz), medium frequency range (50 to 140 Hz), and sometimes even in frequencies greater than 300 Hz. In an attempt to relate spectral components to heart valve motion it was suggested that the frequency components up to 50 Hz are caused by the ventricular vibrations [26], whereas the peaks in the medium frequency range are related to the closure of the mitral heart valves. In the case of S2, it was found that S2 has more high-frequency components than S1 [31]. The spectrum of S2 was observed to contain spectral peaks in the low (10-80 Hz), medium (80-220 Hz), and high-frequency ranges (220-400 Hz). From the power spectrum produced by the Fast Fourier transform (FFT), it was shown that S2 contains two to three peaks and the dominant peak was located somewhere between 30-70 Hz. It has also been shown that the aortic valve size parameters correlate best with the spectral energy in the range 120-140 Hz [62]. This suggested that frequencies ranging between 120-140 Hz should be related to the condition of the aortic heart valve.

Computer programs have also been developed for automated classification of cardiac diseases based on frequency domain features of PCG signals along with time domain information [29,61,63]. These techniques make use of one of the linear classification techniques such as discriminant methods or other linear classifiers using parameters of linear prediction method.

Regarding MPHV, two categories of studies can be distinguished: *in vitro* [17,64–66] and *in vivo* [48,56,58,67–72]. Studies *in vitro* have allowed the study of fluid flow through prosthetic valves, measurements of pressure drop, reflux volume, velocity profiles and turbulence. They also give information about the design, size, and orientation of implantation on the sound made by a valve in a closely controlled dynamic state. From the findings of frequency characterisation these studies have shown that the frequency spectra of sounds produced by MPHV reach more than 15 kHz [65] and with the

simulation of thrombosis not only does the intensity of higher frequency components drop, but, even more, a shift of energy from the higher frequency components to the lower frequencies becomes evident [64]. Information provided by these studies improves the understanding of results obtained from the *in vivo* studies, which are of crucial importance because they are directly related to the actual function of the prosthetic heart valve, thus they give a good understanding of the condition of the patient.

In vivo closing sounds of MPHV in the mitral and aortic position have been analysed by several investigators [48, 56, 58, 67–72]. The conclusion of these studies is that: due to the fact that the strut and ring are composed of hard materials which produce higher-frequency components than the valvular sound of the natural heart, MPHV contain higher frequencies than those of the natural heart valves, and in the case of ball variance or thrombosis, the high frequency components decrease in the very early stages after implantation. The adhesion of thrombosis onto the prosthetic valves may interfere with high-frequency components because of their buffering effect or may decrease the natural frequency of the material of the prosthetic valve. Kagawa *et al* [67] have reported that the normalised maximum frequency (NMF) of the power spectrum, which is defined as the frequency component occurring at the -30 dB level relative to the strongest frequency component, decreases during the post-operative course with thrombosis.

Koymen *et al.* used another approach to detect malfunction of MPHV [68–71]. They suggested that the anatomy of the thorax plays the most important factor in the power distribution of the spectral components associated with S1 and S2. This was based on the fact that the frequencies of the two major resonance modes, between 200-600 Hz, are not different in patient groups implanted for up to 32 months in the post-operative period. However, the energy ratio of the higher resonance mode to that of the lower resonance mode decreases during the postoperative course with the accumulation of thrombus.

In 1987, Stein *et al* [54] evaluated *in vitro* the potential of using spectral analysis of the opening sound produced by Bjork-Shiley convexo-concave valve as a non-invasive indicator of strut fracture. They found a clear difference of the dominant frequency between the normal and the malfunctioning case. This work was extended for the *in vivo* case by Durand *et al* [79] and clear differences were also observed between spectral composition of normally and malfunctioning cases.

Several studies were also conducted by different authors to investigate the spectral signature of the bioprosthetic heart valves either in the mitral or aortic position [10,32,37, 42,57,73–77]. Degenerated calcified mitral and aortic bioprosthetic heart valves were characterised either by mean dominant frequencies [32,77] or feature vectors comprising the two most dominant frequencies [10]. The presence of high frequency components, i.e. greater than 400 Hz, were observed in the case of stiffening Ionescu-Shiley bioprosthetic heart valves. Bayesian classifiers were extensively used to evaluate the diagnostic potential of spectral features derived from sounds produced by fifty-seven normally functioning and forty-nine degenerated Hancock porcine bioprostheses [78]. Results show that the best performance was above 94% [78].

Although a lot of work has been done regarding the SPCG, it must be emphasised that most of these studies make use of the FFT [48,56,58,67,72,79] or autoregressive modelling [62,80], which, as will be shown later in this thesis, are not appropriate techniques to represent accurately the spectral composition of S1 and S2. In this context, the availability of the spectral investigations presented in the above-mentioned works requires further investigations especially with regard to the accuracy of the method used to represent S1 and S2. This accurate representation of S1 and S2 is of paramount importance when one bears in mind the controversies still present about the origin of heart sounds and the fact that the diagnostic potential of the SPCG method is, almost, entirely dependent on the spectral characteristics presented by the power spectrum.

In an attempt to overcome the inherent limitation of the FFT, several autoregressive moving average modelling algorithms [10,37,57,76] and Prony's method [68–71] were used by other investigatiors. With regard to the accuracy of representation of S1 and S2, it was found that no single spectral estimation technique can estimate accurately the two most dominant peaks of the spectrum produced by bioprosthesis [57,74].

From a signal processing point of view, there are two main drawbacks with the studies based on parametric methods: (a) the criteria used to select the model order, and (b) a neglect of certain specific characteristics of S1 and S2 such as their transient nature. It must be said that not only does the model order vary widely from one study to another, but the same model order has always been used to analyse data from different patients. The discrepancy in the latter case consists in the fact that while some of these studies [68–71] are assuming that the anatomy of thorax is the most important factor in the distribution of the power spectrum, the same model order has always been used to analyse data from subjects with totally different thorax sizes. As a result of individual

characteristics of the thorax in different subjects, one would expect that the model order should be varied from one subject to another. One possible way to investigate the impact of the thorax system on the distribution of the power spectrum would have been to compare the power spectrum in the case of patients who underwent heart valve surgery *before* and *after* the operation, especially when a MPHV was implanted. In this method, the heart valve is the only factor that has changed after surgery and the lung-thorax system remains more or less the same in both cases. Thus the differences in the spectrum *before* and *after* surgery can give useful information regarding the impact of the lung-thorax system on the number, location, and the relative energy of spectral components in heart sounds.

The use of non-reliable estimators for classifying the condition of prosthetic heart valves is another drawback of some of these studies. For instance in the studies using the NMF as a criterion for detecting the malfunctioning of MPHV, it is not clear whether the NMF has decreased because the discrete frequency values have decreased, or whether the resonant frequencies have remained constant but the energies of higher frequency modes have declined due to the smearing of the initially impulsive excitation of the valve, as the thrombosis develops [69]. An even more serious problem is that NMF does not seem to be a stable estimator, because different values for this parameter have been reported in different studies [24, 26, 56, 58–60, 67], even for the same kind of valve. This is related to the fact that NMF is very dependent on analogue preprocessing and the monitoring technique used.

In the overall context, further investigations are required to understand better the impact of the lung-thorax system and heart valves on the spectral composition of the externally recorded PCG and the reliability of spectral parameters used in diagnostic methods of monitoring the condition of cardiac system.

2.6   Summary and conclusion

This chapter described the area of SPCG by first introducing the relationship between heart valve motion and PCG signals. A brief review of prosthetic heart valves, their advantages and disadvantages was also given. The chapter concluded by presenting a review of the most important investigations regarding the spectral composition of S1 and S2 for the cases of native and prosthetic heart valves.

Chapter 3

Data Acquisition and Conditioning of the Phonocardiographic Signal

This chapter discusses the design and development of a data-acquisition system for digitising and recording PCG signals. A description will be given of the factors taken into consideration in the design in particular the frequency bandwidth of the recording system, cardiac transducers, and PCG preamplifier and anti-aliasing filters. A description of the procedure for recording PCG signals from patients is also given. This chapter also provides a breakdown of the population of subjects investigated in this research and the pre-processing analysis of the data.

3.1 Design and development of the data acquisition system

The procedure for recording, processing and analysing the PCG used in this thesis is illustrated in Figure 3.1. This procedure can be divided into two main parts; data collection and data analysis. Data collection is primarily concerned with the design of a hardware systems for PCG capture and the recording procedure. Whereas data analysis includes all the stages of numerical analysis. This procedure can further be divided into two main steps; (a) the investigation of the performance of digital signal processing methods when applied to the analysis of the PCG signal and justifying results obtained, and (b) investigating the potential of classification techniques for automatic detection of different classes of heart valve malfunctions.
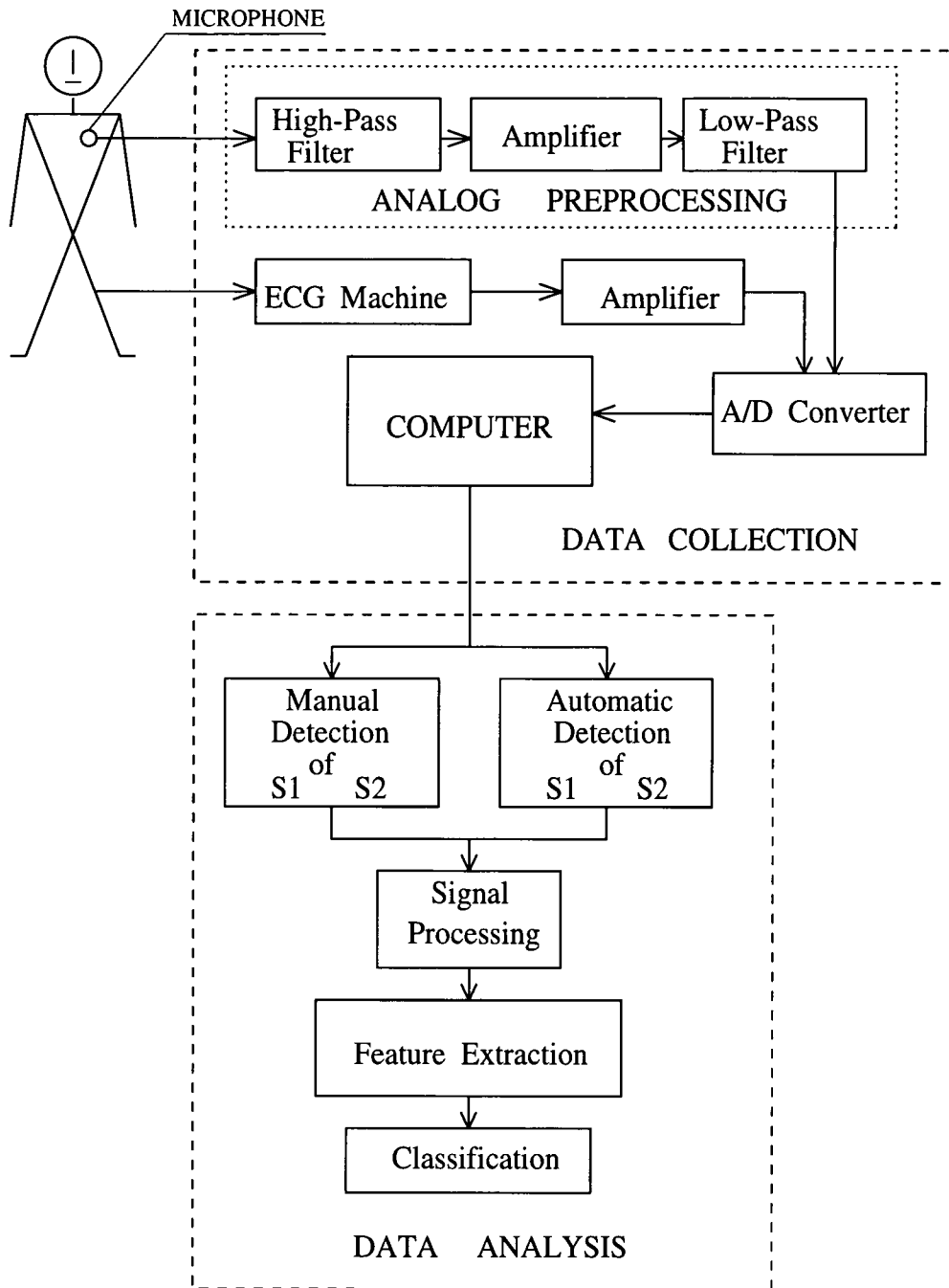
Figure 3.1: Block diagram of the data recording and processing system used to analyse S1 and S2.

During the design of the recording system a number of significant hardware and software design considerations were taken into account:

(i) The need for the complete system to be portable to facilitate the transportation

of equipment between recording venues.

(ii) The need for operation from both a standard mains electricity supply as well as a battery.

(iii) The need for the system to provide a full graphical display of the signals being acquired before and during the recording of sounds.

(iv) The need for interactive recording software in order to locate the optimum position in which to place the transducer during the recording procedure.

(v) The need for a fully flexible recording system in order to record the PCG signal in a very wide variety of cases ranging from sounds produced by native heart valves to MPHV.

To fulfil these design criteria an Elonex LT-320X laptop personal computer and a twelve-bit ADC 42 input/output expansion card marketed by Blue Chip Technology were selected. In total, the data acquisition system comprises three items of hardware: a portable computer fitted with an analogue-to-digital converter, the phonocardiographic transducer, and a small box containing some conditioning circuitry, i.e. analogue preprocessing.

3.1.1 Analogue preprocessing

The aim of this stage is to emphasise those frequencies which are associated with opening and closure of the heart valves under consideration, and to de-emphasise those frequencies which do not arise from heart valve motion.

As was described in the previous chapter, the frequency composition of the closing sounds produced by native and bioprosthetic heart valves is quite different from sounds produced by MPHV in terms of frequency component distribution and respective intensity levels. The majority of studies have shown that for the case of native heart valves the frequency components of S1 and S2 lie below 1 kHz [24, 25, 28, 30, 31]. However, there are indications that in some cardiac diseases the spectral composition can extend up to 1.5 kHz [23, 81]. The same can also be said for the case of bioprosthetic heart valves [20, 37]. Whereas in the case of MPHV higher frequency components are to be expected. In some cases [65] frequencies more than 10 kHz have been reported to be present in the spectral composition of S1 and S2 produced by the closure of MPHV

in vivo. As the sensitivity of the available kinds of phonocardiographic transducers, which remains the most limiting component of the recording system, in these bands is different, it was decided to design a system with two separate recording channels. The first channel is to record heart sounds produced by the closure of native heart valves and bioprosthesis, and the second channel records MPHV. This allows a high-quality recording of these signals with the proper sensitivity for all the subject cases.

The cut-off frequency of the first channel was selected to be 2 kHz. It must be said that the data from bioprosthetic heart valve cases investigated in this thesis were recorded with a system described by Bedi [82] because they were collected prior to use of the recording system presented here. The only difference between the system proposed here with that used in Bedi's system [82] is the cut-off frequency of the channel, i.e. in Bedi's system [82] the cut-off frequency of the anti-aliasing filter is 1 kHz instead of 2 kHz. The reason for the choice of a higher cut-off frequency was to obtain the full benefit of the transducer characteristics and to investigate if there are frequency components between 1 kHz and 2 kHz for the cases of bioprosthetic heart valves and native heart valves.

The second channel in the recording system is used to record PCG signals from MPHV. In this case two factors decide the bandwidth of these recordings: (a) the spectrum of the sounds produced by mechanical prostheses, and (b) the low–pass filter characteristic of the lung-thorax system [30,38]. According to studies *in vitro*, the spectrum of sounds produced by MPHV exists up to and above 10 kHz [65] with sound intensity much higher than that of natural valves. However, it was decided that the cut-off frequency of the second channel should be 10 kHz. This decision was made because the frequency components above 10 kHz are relatively weak in intensity and the lung-thorax system further attenuates these frequencies. Furthermore the frequencies above 10 kHz do not yield information about valve malfunctioning [64,67].

With respect to the low frequency components of the PCG signals, it has been shown that the peak frequencies in the lower part of the spectrum (10-50 Hz) are related to ventricular vibrations [26]. Therefore, a high pass filter with cut-off frequency of 50 Hz was used in order to ensure that the low-frequency signals would not dominate the high-frequency signals. As a result of the above mentioned considerations, the analogue preprocessing block consists of a third-order high-pass Butterworth filter with a cutoff frequency of 50 Hz, two alternative sixth-order low-pass filters with respective cutoff

frequencies of 2 kHz and 10 kHz, and a variable PCG pre-amplifier. The PCG pre-amplifier is used to amplify the output of the phonocardiographic transducer to occupy the input voltage range of the ADC converter, which is ±5V.

The layout of the recording system is shown in Figure 3.2. Lead II of ECG signal was also recorded to provide a time-reference for the automated detection of the beginning of each cardiac cycle. A pre-amplifier is also provided for the lead II of the ECG signal.
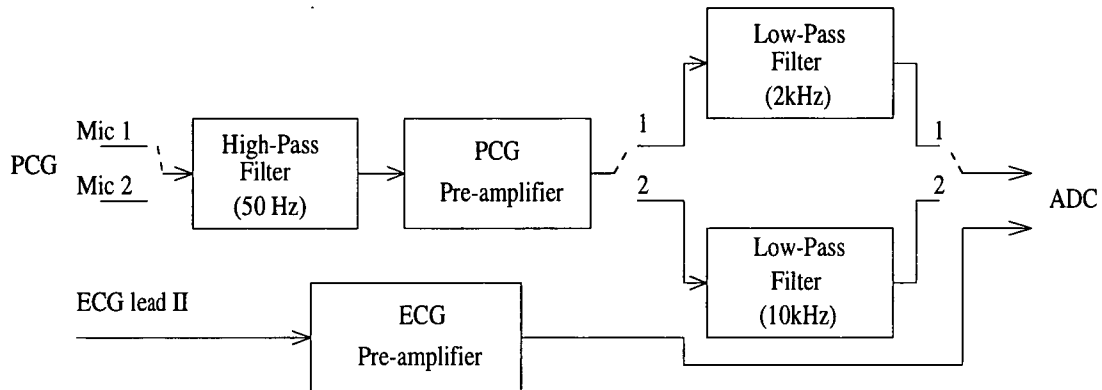
Figure 3.2:   The layout of the PCG analogue preprocessing used in this thesis.

The design of analogue filters was based on a high-performance, low-noise, low-power operational amplifier, the TL074 manufactured by Texas Instruments. An instrumentation amplifier, Burr-Brown (OPA 2111KP), was used for the pre-amplifiers. Figure 3.3 and Figure 3.4 gives the measured amplitude and phase response of both channels.
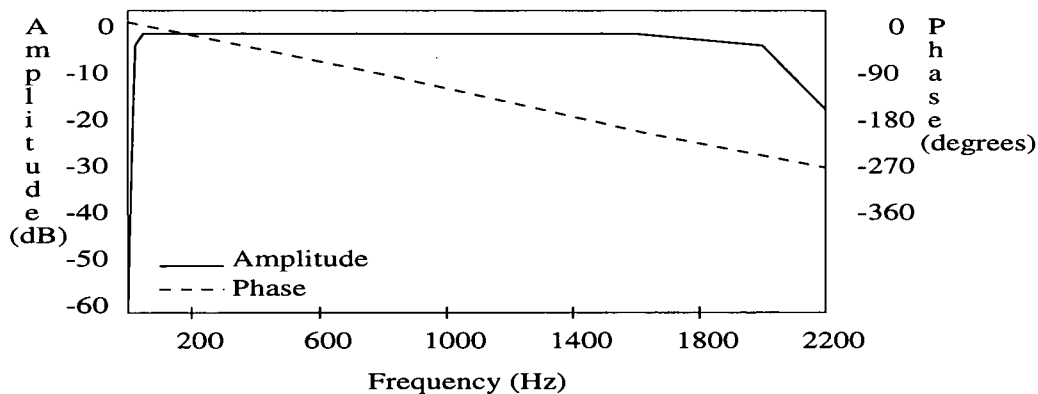
Figure 3.3:   The measured amplitude-phase response of the first channel.

From these two figures, it can be seen that both channels have a flat amplitude response and a linear phase characteristic inside the frequency bands of interest, which

are respectively 50-2000 Hz and 50-10000 Hz. The ECG and PCG signals were then digitised to 12-bits at a sampling rate of 5 kHz for the first channel and 20 kHz for the second one.
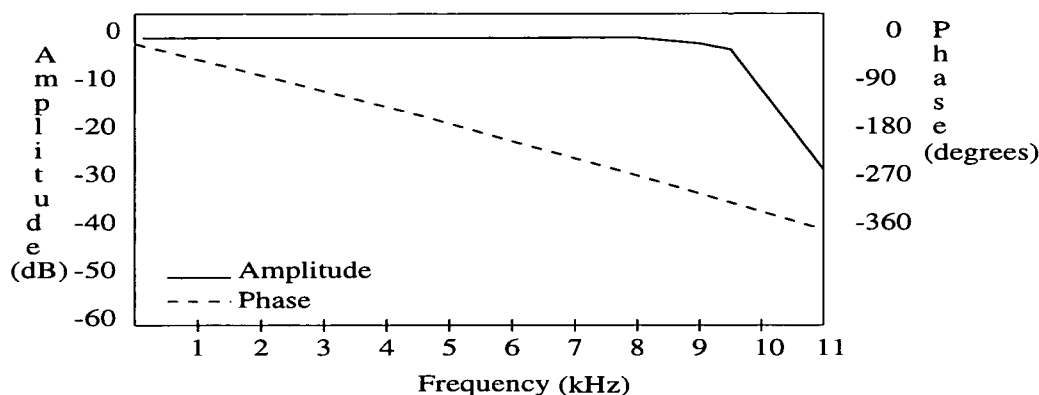
Figure 3.4:   The measured amplitude-phase response of the second channel .

3.1.2   Phonocardiographic transducer

In PCG-y a conversion of mechanical vibration into an electrical signal is required. This is accomplished by a vibration pick-up, the so-called microphone. A variety of microphones are now available for recording heart sounds in either a clinical or experimental context. Two major types of phonocardiographic transducers are commercially available: air-coupled and direct coupled devices [83]. Air-coupled microphones are characterised by a cavity which is placed at the appropriate heart sound recording site on the chest surface. The air in the closed cavity acts as a transmission medium between the chest surface and a membrane coupled to a mechanical-electrical transducing device. Direct-coupled transducers, on the other hand, such as contact microphones, have an area which is directly applied to the chest surface making contact with a transducing element [21,85,86]. Both types of cardiac microphone use one of several transducing elements, e.g. piezoelectric, moving-coil, capacitor.

The principal advantages of the air-coupled microphones are the ease with which they can be calibrated, and a flat frequency characteristic over a very wide band, i.e. more than 100 kHz. However, they suffer from the effect of ambient noise on the recorded signal. In contrast to air-coupled microphones, contact microphones have a considerably lower sensitivity to ambient noise and better low frequency (i.e. up to 2-3 kHz) response. Moreover, contact microphones eliminate the existence of a mismatch impedance between the lung-thorax system which is present in the case of an air-coupled

microphone. Schwartz [87] has shown that only 1% of the total energy of the PCG signal is picked up by air-coupled microphones. But unfortunately, contact microphones are difficult to calibrate and as a results of the static force required to achieve a good coupling they do not faithfully record frequencies over 2-3 kHz. From the above mentioned consideration, it can be seen that contact microphones outperform air-coupled microphones below 2 kHz. Above 2 kHz, due to limitations in response of contact microphones, air-coupled microphones are necessary for accurate PCG signal capture. In order to overcome this problem, two different microphones were chosen to be used in this thesis.

A Hewlett-Packard (21050A) contact microphone, which has a very flat frequency response for frequencies up to 2 kHz [83, 85], was used to obtain the PCG recording in channel one, which is mainly used for recording of PCG signals in the case of native and bioprosthetic valves.

As the second channel is designed for recording of sounds produced by MPHV which contains frequency components up to 10 kHz, an air-coupled microphone is needed to perform the recording in this case. The techniques used for recording heart sounds using air microphones can be divided into two categories: either recording the sounds at a distance from the chest [72], or using some mechanical construction to ensure better transmission of heart sounds thereby reducing the ambient noise [88]. Since the latter case provides a more robust technique for reducing the effect of the ambient noise on the PCG signal, it was decided to implement that one. In this case, the performance of the recording system is not only determined by the electrical properties of the transducing element incorporated into the microphone but also by the mechanical construction which houses the transducing element as well as the manner in which microphone is applied to the chest. These factors will influence the frequency response of the total system. Suzumura and Ikegawa [88] have analysed the characteristics of several types of air cavities for a phonocardiographic microphone and the sensitivity of the microphone to room noise. They found that the vibrations of the chest wall as a result of room noise were the dominant factor in conducting the room noise to the microphone. The mechanical impedance of the microphone and cavity depth determine the dip frequency, which decreases as the cavity depth increases. Verburgh and Van Vollenhoven [21] summarised important characteristics for air microphones in cylindrical cavities. A description of these microphones is made by introducing the concepts of mechanical or acoustical impedance. The acoustical impedance of the thorax surface is defined as

the mechanical impedance which can be measured at a certain site with an external unidirectional vibration source, perpendicular to the surface with a defined contact area [89]. The acoustic impedance (Z) of a material is equal to the product of its density (ρ) and the velocity of sound within it (c). The impedance seen by the skin of the cavity is given by [21]:

$$Z_s = \frac{\rho}{S} \frac{S Z_l \cos(kl) + i\rho c \, \sin(kl)}{\rho c \, \cos(kl) + i S Z_l \sin(kl)}$$

where:

Z_s =acoustic impedance at the skin side Z_l =acoustic impedance of the transducer

S =area of cavity perpendicular to axis $\rho =$ air density

c =velocity of sound in air k =wave number= $\frac{2\pi}{\lambda} = \frac{\omega}{c}$

l =length of the cavity λ =wavelength

ω =angular frequency

In a cylindrical cavity, resonance may occur for plane waves in the axial direction of the cavity and for cylindrical waves perpendicular to the axis. It has been found that for a cavity with length 1 cm and a diameter 3 cm the resonance mode occurs at 10 kHz which is at the upper frequency extreme of our second recording channel. Thus, a Knowles BL 1994 air-coupled microphone is used to record the PCG signal with channel two. This microphone has a flat frequency response from 20 Hz to 10 kHz [84]. Direct contact between the microphone and the chest of the patient is avoided by using a cylindrical plastic 'housing' device with diameter 3 cm and height 1 cm. The overall mass of the microphone and 'housing' is 32 grams. The mass of the phonocardiographic transducer is an important parameter regarding the loading effect which is particularly severe for high frequencies [85,89]. However, it has been shown that for a total mass of air-coupled microphone less than 50 grams the loading effect has little impact on the recording sensitivity of high frequencies [83].

Taking into account the better sensitivity characteristics of the contact microphone in the lower part of the spectrum than the air-microphones, the recordings were also carried out with the Hewlett-Packard transducer even for MPHV. This results in a better recording of the PCG signal in the case of MPHV for frequencies up to 2 kHz. Furthermore, it has been demonstrated that in the case of the opening sounds produced by the Bjork-Shiley convexo-concave valve, the frequency analysis of the lower region of the spectrum (i.e. up to 1 kHz) is a promising region in which to detect leg separation of the valve [79]. In this context, it would be of interest to investigate more fully the

lower region of the spectrum (i.e. up to 2 kHz) of the closing sounds produced by the MPHV.

3.2   Recording protocol

Recordings were performed with the subjects supine and with the patient's head elevated. In addition to greatly facilitating the recording of sounds, a greater appreciation of heart sounds is obtained with the subject in this position [49]. The microphones were placed on the patient's chest using a retaining rubber belt to ensure that the transducer remained in the ideal position during the recording.

As it was described earlier heart sounds S1 and S2 are caused by vibration of the whole cardiovascular system triggered by pressure gradients. However, there are some locations on the chest where the contribution of valve movements is the 'primary source' of acoustic energy and these locations are called the auscultatory areas, namely: the second right interspace, often called the **'aortic'** area; the second left interspace or**'pulmonary'** area; the lower left sternal edge or **'tricuspid'** area; and the cardioapex or the **'mitral'** area. As the interest in this research is concentrated on S1 and S2, the recordings were carried out with the microphone placed in the **mitral** and the **aortic** positions. Figure 3.5 illustrates the locations of these recording sites.
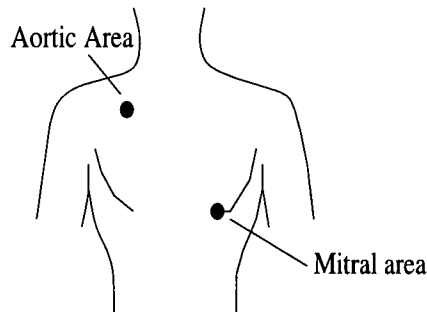
Figure 3.5:   Recording area of PCG signals.

The recording software package was written in the 'Turbo C' language for DOS systems. It allows the timebase and amplitude variables of both channels to be preset prior to recording. At the start of the recording, a tone is emitted by the computer. This is followed by a second tone later to indicate the end of sampling. A final-third tone is emitted after the acquired samples have been stored on disc. Figure 3.6 illustrates a typical example of the graphical display provided by the acquisition software during the recording stage using channel one with a sampling rate of 5 kHz. The top trace (channel 1) shows an ECG signal, while the bottom trace (channel 2) shows a PCG signal.

PCG ACQUISITION SOFTWARE

CH1

CH2

F1	F2	F3	F4	F5	F6	F7	F8	F9	F10	F11	F12
+	–	+	–	+	–	+	–		o		

CH1 Amp/Div   CH1 Tme/Div   CH2 Amp/Div   CH2 Tme/Div   PD   REC   D/L   SAVE

Control Panel

CH1 Amplitude = 0.188 V/div
CH1 Timebase = 0.48 s/div 9.6 s

CH2 Amplitude = 2.06 V/div
CH2 Timebase = 0.48 s/div 9.6 s

DEMO Mode

press Q to quit program

Patient Details

Patient No. – C12
Name –   Diane Patience
Age/DOB – 54
Sex –   F
Weight – 9 stone
Height – 5.4
Obesity Measure – 2
Time – Mon Oct 31 12:03:05 1994
DOI –   Feb. 94
Valve type – Carbomedics
Condition –   Normal
Murmurs –   none
Other Info. – After Surgery

Figure 3.6: Typical example of the graphical display provided by the acquisition software during the recording of sounds using the air-coupled microphone.

29

A modified recording procedure was used in the case when channel two was used. As the sampling rate was 20 kHz, a real-time display of the PCG signal on the computer screen was not possible. The procedure adopted in this case was to find the best position for the phonocardiographic transducer by running the graphic display program with a sampling rate of 5 kHz. Then a fifteen-second recording at 20 kHz was stored on disc. In addition, an interactive manual program to aid the detection of S1 and S2 was also written. The desired portion of the signal is selectable by the operator either by the mouse or the keyboard. The chosen portion is expanded automatically to full scale (the duration is also displayed), and is stored on the hard disk.

The duration of the PCG recordings is another parameter which needs to be decided. It have been suggested [27] that a time of 5 seconds is sufficient to diagnose heart diseases from the PCG. However, based on the fact that spectral components of mechanical prostheses are much higher in frequency than those from normal native valves, and the SNR is low in the higher frequency part of the spectrum [90], the length of the recording time was increased to 15-20 cardiac cycles, which is approximately 12-16 seconds, in order to reduce further the random effect of the ambient noise. Therefore all the recordings were carried out for this length of time.

3.3 Patient population

The population of subjects investigated for this thesis were chosen over a very wide range of subjects. These included subjects with normal and malfunctioning native heart valves as well as both types of prosthetic heart valves, i.e. bioprostheses and MPHV.

All subjects with MPHV or bioprostheses were contacted who had undergone artificial heart valve implantation at The Royal Infirmary of Edinburgh between 1990 and 1992 and these subjects were asked to attend a recording session at the Astley Ainslie Hospital in Edinburgh. This involved first writing to the patients' physicians to confirm the subject's present state of health, and then directly to the subject. In total, more than 200 recordings were obtained from more than 150 different subjects. The condition of each prosthesis was diagnosed by a cardiologist with all patients undergoing a physical examination which included: assessing the symptomatic state of the subject at

the time of recording, auscultation, electrocardiography, chest X-rays and ultrasound echocardiography.

The information regarding all the patients investigated in this thesis is given in appendix A.

3.4 Phonocardiogram preprocessing

Arising from the mechanical activity of the heart, the PCG signal can be seen as a composition of deterministic and non-deterministic components. As S1 and S2 are assumed to be generated under an identical set of hemodynamic conditions [25], they can be seen as a summation of deterministic transient signals with the random background noise such as thoracic muscular activity, respiratory sounds, ambient noise, and instrumentation noise. Therefore, to minimise the background noise interference on the acoustic signature of S1 and S2, a time-averaging of multiple occurrences of the respective sounds is needed. As a result of this time–averaging the signal-to-noise ratio (SNR) is improved by $\sqrt{N}$ (*N*-number of averages) [25, 38, 91] and the beginning point of each sound can be better determined [4]. Signal averaging may also be helpful in circumventing the difficulties caused by the beat-to-beat variation of heart sounds [20, 25].

To extract an ensemble average of S1 and S2 from the PCG, a technique based on coherent averaging was implemented.This technique is initiated by selecting a reference template of S1 and S2 from each PCG record under investigation, locating the beginning of each cardiac cycle, and matching the reference template with similar successive occurrences, i.e. the other S1 and S2 components within each of the remaining cardiac cycles.

This process firstly requires the detection of the beginning of each cardiac cycle. There are several algorithms to accomplish this using either the spectral tracking of the PCG [27, 29] or the time relationship between the ECG events (i.e. QRS complex) and the PCG [37, 57]. The QRS complex is defined as three nodes of the ECG concurrent with ventricular depolarisation. As only one QRS complex occurs within each cardiac cycle, the starting point of this event can be used to locate the beginning of each cardiac

cycle.

In this research detection of the QRS complex is achieved using an algorithm based on the amplitude and the first derivative of the ECG signal [93]. The threshold values are selected based on the morphological characteristics of ECG signals and the practical experience of several investigators [93–95].

Firstly, a threshold, MAX, is calculated as a function of the peak value of the ECG

$$\text{MAX} = 0.4\max\left(x[n]\right) \tag{3.1}$$

where $x[n]$ represents the ECG signal. The data is then rectified

$$x_r[n] = \begin{cases} x[n] & \text{if} & x[n] \geq 0, & 1 \leq n \leq N \\ -x[n] & \text{if} & x[n] < 0 & 1 \leq n \leq N \end{cases} \tag{3.2}$$

The rectified ECG is passed through a low-level clipper:

$$x_{rc}[n] = \begin{cases} x_r[n] & \text{if} & x[n] \geq \text{MAX} & 1 \leq n \leq N \\ \text{MAX} & \text{if} & x_r[n] < \text{MAX} & 1 \leq n \leq N \end{cases} \tag{3.3}$$

Then, the first derivative is calculated at each point of the clipped, rectified signal:

$$x_d[n] = x_{rc}[n+1] - x_{rc}[n-1] \quad 2 \leq n \leq N-1 \tag{3.4}$$

A QRS candidate occurs when $x_d[n] \geq 0.2$.

The second step in the computation of S1 and S2 ensemble average consists in detecting every S1 and S2 contained in the PCG signal. This process was achieved automatically using cross-correlation between the reference template of S1 and S2 with the PCG signal.

The cross-correlation function is a signal processing operation that provides a valuable tool for the comparison of two signals. As the template will always be of a shorter duration than the PCG, the cross-correlation of the PCG with S1 or S2 for positive lag is defined to be [96]:

$$\hat{r}_{xy} = \begin{cases} \sum_{n=l}^{M+l-1} x[n]y[n-l] & \text{for} \quad 0 \le l \le N - M \\ \sum_{n=l}^{N-1} x[n]y[n-l] & \text{for} \quad N - M \le l \le N - 1 \end{cases} \tag{3.5}$$

where $x[n]$ and $y[n]$ represent the PCG and the template sound respectively. N and M represent the length of the PCG and the sound template respectively.

As the amplitude of the PCG and the template do not affect the shape of the cross-correlation estimate, the cross-correlation function is normalised to the range -1 to +1. This normalised cross-correlation estimate can be expressed as a percentage termed the **Correlation Coefficient**, where a normalised cross-correlation coefficient of +1 equals a perfect temporal match between two signal events. The normalised cross-correlation estimate of the PCG with the template $\hat{\rho}_{xy}[l]$ is defined to be:

$$\hat{\rho}_{xy}[l] = \frac{\hat{r}_{xy}[l]}{\sqrt{\hat{r}_{xx}[0]\hat{r}_{yy}[0]}}; \tag{3.6}$$

where $\hat{r}_{xx}[0]$ and $\hat{r}_{yy}[0]$, are the autocorrelation estimates at zero lag of the PCG and the closing template sound respectively.

S1 or S2 contained in each cardiac cycle are selected from the greatest value of 'Correlation Coefficient' between the reference template with each cardiac cycle.

Following on from the detection of S1 and S2 sounds, time-averaging is then performed on the collected S1 and S2 sounds to produce respectively an ensemble average of first and an ensemble average of second heart sounds. Only sounds achieving a cross-correlation coefficient of 80% or more were admitted into the ensemble average. The 80% threshold value of cross-correlation coefficient was fixed in order to reject automatically any artefact or large variations in sound morphology.

Figure 3.7 and Figure 3.8 show the procedure of extracting an ensemble average S1 and S2 respectively from a healthy subject. From Figure 3.7(d) and Figure 3.8(d) it can be shown that the cross-correlation coefficient between the reference template of S1 and S2 with their successive occurrences is greater than 90% throughout the whole PCG recordings. This finding shows that S1 and S2 have a very consistent temporal signature throughout the PCG and also suggests that S1 and S2 represent a deterministic signal to a great extent.
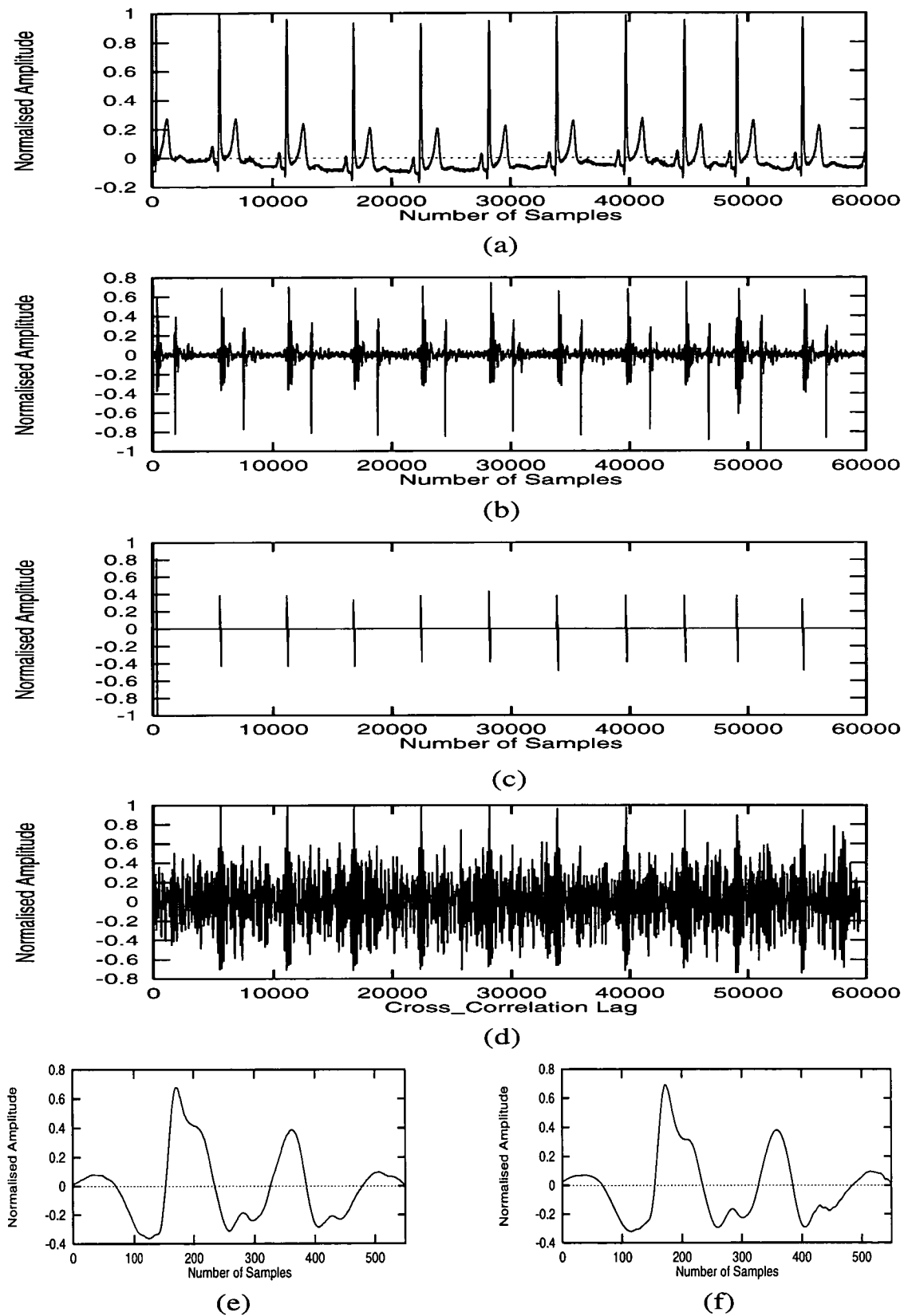
Figure 3.7: Procedure for extracting the S1 ensemble average for the case of a healthy subject: (a) the ECG signal, (b) PCG signal, (c) QRS complex detection, (d) cross-correlation coefficient between an S1 template and the PCG signal, (e) the template signal , (f) the ensemble average of S1.

34

(a)

(b)

(c)

(d)

(e)

(f)
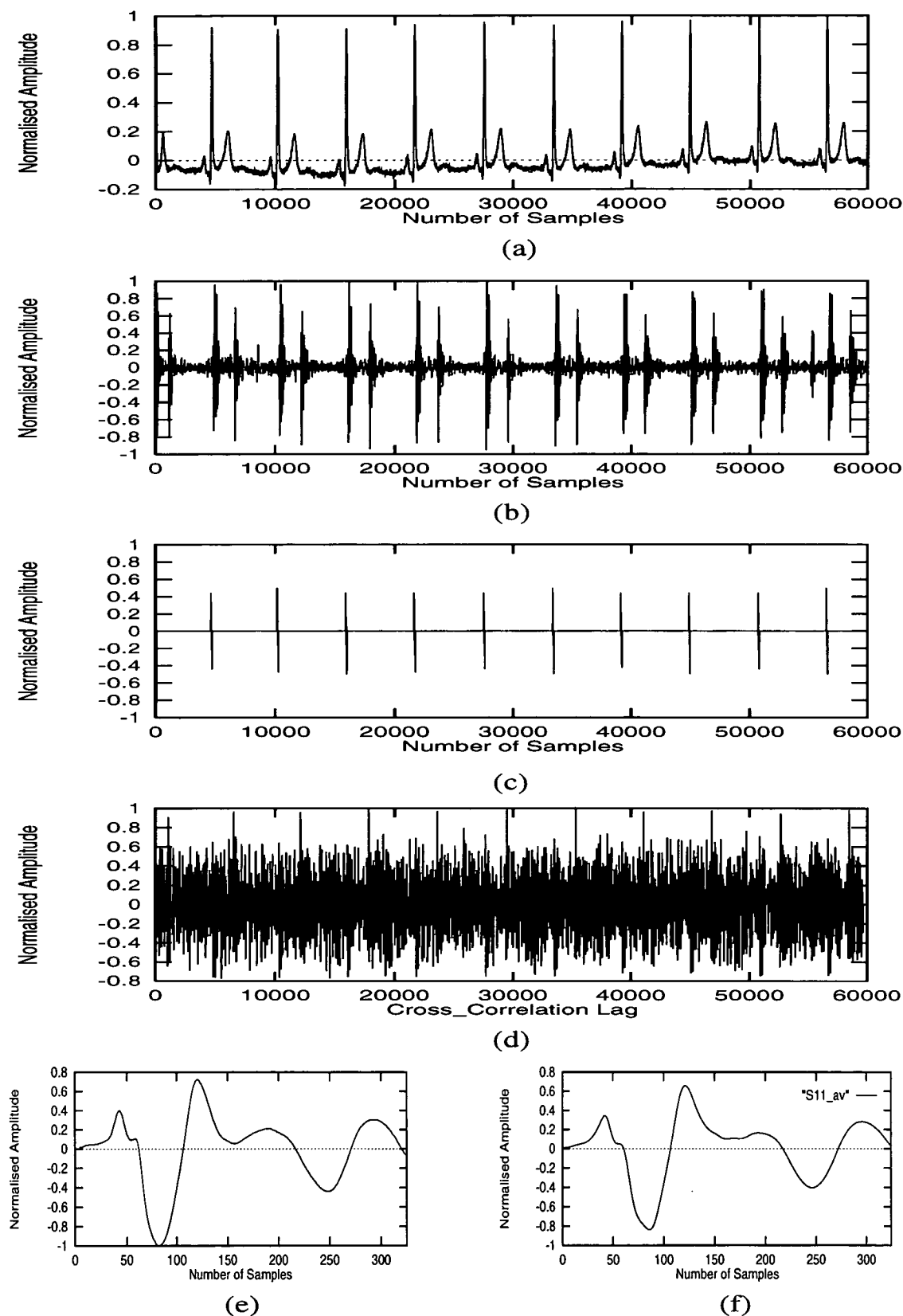
Figure 3.8: Procedure for extracting the S2 ensemble average for the case of a healthy subject: (a) the ECG signal, (b) PCG signal, (c) QRS complex detection, (d) cross-correlation coefficient between an S2 template and the PCG signal, (e) the template signal, (f) the ensemble average of S2.

35

3.5 Conclusion

This chapter has investigated the design and development of a data-acquisition system to digitise and record the PCG signals in a wide variety of cases.

After an investigation of the spectral characteristics of S1 and S2 for the cases of native heart valves, MPHV, bioprosthetic heart valves, and the characteristics of phonocardiographic transducers, it was decided to design a two-channel system. One of the channels of the system is used to record native heart valve sounds and the second channel is used to record higher frequencies generated by the operation of MPHV. This design results in a more sensitive data-recording system with the ability to cover a relatively extensive band of the PCG signal. Moreover, it allows a more accurate investigation of the low-part of the spectrum for the case of MPHV, where the main part of the signal energy is believed to be found. Channel one has a frequency response from 50 Hz to 2 kHz and the second channel extends this upper frequency limit to 10 kHz. The data acquisition system is based on a laptop computer and a small hardware box and provides a portable, high-quality, and easy-to-use system for the recording procedure.

A semi-automatic technique is described for time-averaging S1 and S2 sounds throughout the length of the recorded PCG signal. This procedure detects the beginning of each cardiac cycle based on a QRS detection algorithm and time alignment of sounds included in the ensemble average is obtained using the cross-correlation method. This procedure provides a less noisy and better estimate of the temporal sound signature of S1 and S2.

Chapter 4

Spectral Analysis Techniques

4.1   Introduction

There are many mathematical transformations in common use in engineering and the physical sciences. The concept behind a transformation is that a function of one or more independent variables may be represented as a different but nevertheless equivalent function of a new set of variables. The main reason for performing a transformation is to improve the detectability of some aspects of the signal which are not easily detected in its original domain.

In this context, the transformation of a signal from the temporal domain to its frequency-domain representation is one of the most common examples of signal processing in applied science. The advent of fast, cheap computing power together with fast algorithms has made spectral analysis very popular. In biomedical engineering the use of spectral analysis often gives information about an underlying causal process from a knowledge of the frequency components contained in a particular signal. The spectrum may therefore give information which can be used for diagnostic purposes or for elucidation of physiological dynamics [97, 98].

This chapter describes the spectral methods investigated in this research. The performance of the following methods is analysed: the FFT, autoregressive modelling (AR) based on two different approaches: Burg algorithm (ARB) with four different types of weighting function and sinusoidal signal identification (SSI), several algorithms for autoregressive moving average modelling (ARMA), and Prony's spectral method. In addition a modified forward-backward overdetermined Prony's method is proposed

that, as it will be seen in the next chapter, is more precise in terms of the mean-least-square-error than other versions of Prony's method for representing heart sounds. In this chapter the accuracy of the above mentioned methods is examined by applying them to simulated signals similar in nature to S1 and S2.

4.2   Power spectrum estimation

The spectrum analysis of a random process is, in concept, not obtained directly from the process $x(t)$ itself, but is based on knowledge of the autocorrelation function. The Wiener-Khintchin theorem [96] states that for a wide sense stationary random process, $x(t)$, the power spectrum density (PSD), $P_{xx}(f)$, is defined as the Fourier transform of the autocorrelation sequence, $r_{xx}[m]$

$$P_{xx}(f) = \sum_{m=-\infty}^{\infty} r_{xx}[m] exp(-j2\pi fm) \tag{4.1}$$

where

$$r_{xx}(\tau) = \mathrm{E}\left[x(t+\tau)x^*(t)\right] \tag{4.2}$$

and E[.] is the statistical expectation operator. The PSD function has a Fourier series interpretation in which the autocorrelation lags plays the role of the Fourier coefficients. It therefore follows that these coefficients may be determined from the PSD function through the Fourier series coefficient integral expression.

Two philosophically different families of PSD estimation methods may be identified in the literature namely: nonparametric and parametric methods [100]. Both these approaches are discussed below.

4.3   Nonparametric methods of PSD estimation

Nonparametric techniques, often called classical techniques, of spectral analysis utilise various combinations of the Fourier transform, windowing, and autocorrelation function

and make no assumption (other than stationarity) about the observed data sequence, hence the name nonparametric [99]. Classical spectral estimators fall into two categories: direct and indirect [104]. The PSD estimate based on the direct approach operates via a fast Fourier Transform (FFT) on the raw data to transform it to the frequency domain and produce the estimate. The direct approach is often known as the periodogram. Indirect methods first estimate the autocorrelation sequence and then transform it to the frequency domain-an application of the Wiener-Khintchin theorem. The indirect approach is often referred to as the correlogram.

The periodogram is an estimate of a PSD made on the basis of the modulus squared of the Fourier transform and the simplest form is given by

$$\hat{P}_{xx}[k] = \frac{1}{N} |X[k]|^2 \tag{4.3}$$

where $X[k]$ is the discrete Fourier transform (DFT) of the finite data sequence. The DFT is the name often given to the calculation of the Fourier series coefficients for a discrete signal which is either periodic or assumed to be periodic with a period equal to the length of the recording. Algebraically the forward and reverse DFT transformation for finite set of N signal samples, $x[0], x[1], \cdots, x[N-1]$ are respectively expressed by:

$$X[k] = \sum_{n=0}^{N-1} x[n] exp(-jkn\frac{2\pi}{N}) \tag{4.4}$$

$$x[n] = \frac{1}{N} \sum_{k=0}^{N-1} X[k] exp(jkn\frac{2\pi}{N}) \tag{4.5}$$

The development of the FFT algorithms in 1960 by Cooley and Tukey [101], amongst others, gave a fast and efficient means by which the DFT could be evaluated.

The correlogram estimates the PSD based on the estimated autocorrelatin coefficients of the signal which is assumed stationary, or more strictly ergodic. In this case the estimated PSD is given by

$$\hat{P}_{xx}[k] = \frac{1}{N} \left| \sum_{n=0}^{N-1} \hat{r}_{xx}[n] exp(-jkn\frac{2\pi}{N}) \right|^2 \tag{4.6}$$

where $\hat{r}_{xx}[n]$ is an estimated sequence of the autocorrelation lags.

These two approaches to spectral analysis are made computationally efficient by using the FFT, and both produces acceptable results for a large class of signals. In spite of these advantages, there are several performance limitations which are associated with the FFT approach [97–99]. The most significant limitation is that of frequency resolution, i.e., the ability to distinguish the spectral response of two or more closely-spaced frequency components. The frequency resolution in Hertz is proportional to the reciprocal of the time duration in seconds of the signal event under analysis. A second limitation arises because of the implicit windowing of the data that occurs when processing with the FFT. Windowing manifests itself as 'leakage' in the spectral domain, i.e., energy in the main lobe of a spectral response 'leaks' into the sidelobes, obscuring and distorting other spectral responses that are present. Skilful selection of tapered data windows can reduce sidelobe leakage, but always at the expense of reduced resolution.

These two performance limitations of the FFT approach are particularly troublesome when analysing short data records, as is often the case for heart sounds. It has been shown that S1 and S2 are transient signals with sinusoidal components contaminated by noise and length 10-60 ms [20,68].Therefore the resolution of a FFT is of the order of 30-100 Hz. This poor resolution combined with the effect of noise often means that different peaks of S1 and S2 cannot be correctly estimated. These drawbacks of the classical spectral analysis method has lead to the need for employing more accurate methods in the analysis of heart sounds.

4.4 Parametric spectral estimation techniques

In an attempt to alleviate the inherent limitations of the FFT approach to spectral analysis, many alternative spectral estimation procedures have been proposed. These alternatives, called **parametric**, model-based, data adaptive, modern, or high resolution methods, assume a generating model for the process, from which the spectrum is calculated [100]. The most recent methods are based on the linear algebraic concepts of sub-spaces associated with a data matrix or correlation matrix and have as a result been called 'sub-space' methods. All of these methods are fundamentally different from the classical methods in that they are not based on the Fourier transformation of the data sequence or its estimated correlation function.

The parametric methods considered in this thesis are based on modelling the data sequence (i.e. heart sounds) $x(n)$ as the output of a linear system characterised by a rational system function of the form

$$H(z) = \frac{B(z)}{A(z)} = \frac{\sum_{k=0}^{q} b[k] z^{-k}}{1 + \sum_{k=0}^{p} a[k] z^{-k}} \qquad (4.7)$$

where $a[k]$ and $b[k]$ are parameters describing the system and p and q are respectively the number of poles and zeros of the model. In (4.7) the $A(z)$ and $B(z)$ represent the z-transform of the AR branch and moving-average (MA) branch of an ARMA model. In PSD estimation, the input sequence is not observable. However, if the observed data are characterised as a stationary random process, then the input sequence is also assumed to be stationary random process. In such a case the PSD of the data is

$$P_{xx}(f) = |H(f)|^2 \, P_{ww}(f) \qquad (4.8)$$

where $P_{ww}(f)$ is the PSD of the input sequence and $H(f)$ is the frequency response of the model. If the input signal is white, i.e. $P_{ww}(f)$ has a constant variance, independent of frequency, which is equal to σ_{ww}^2, then the output PSD further simplifies to [99]

$$P_{xx}(f) = |H(f)|^2 \, \sigma_{ww}^2 \qquad (4.9)$$

in which case the PSD is completely characterised by the amplitude response of the filter and the variance of the white noise.

The parametric approach to spectral estimation can be divided into three steps. In step one, an appropriate parametric time-series model is selected to represent the measured data record. In step two, an estimate of the parameters of the model is made. In the final step, the estimated parameters are inserted into the theoretical power spectral density expression appropriate for that model. Figure 4.1 represents graphically the parametric spectral analysis [102]. The parametric methods are capable of obtaining stable spectra with very good resolution from a relatively small data length. The degree of improvement in resolution and spectral fidelity is determined by the appropriateness of the model selected and its ability to fit the measured data or auto-correlation sequence (either known or estimated from the data).
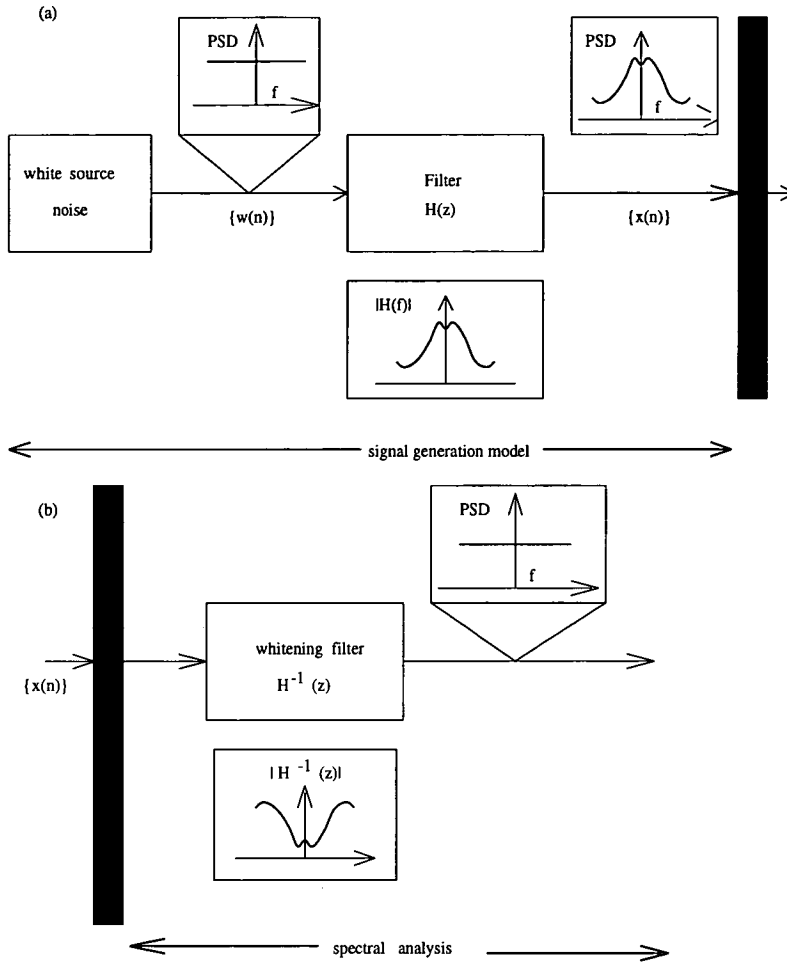
Figure 4.1:   Parametric spectral analysis; (a) signal generation model, (b) analysis filter.

4.5   Autoregressive spectral analysis

The most straightforward approach to parametric spectral estimation is to assume that the signal generating filter, $H(z)$, is autoregressive in nature. This is the case when all the $b[k]$ parameters in (4.7), except $b[0] = 1$, are zero. In this case the output signal is given by

$$x[n] = w[n] + \sum_{i=1}^{p} a[i]x[n-i] \qquad (4.10)$$

and the transfer function

$$H(z) = \frac{1}{1 + \sum_{k=0}^{p} a[k] z^{-k}} \qquad (4.11)$$

where $w[n]$ represents the white noise process and the summation is performed over the p previous outputs. Although other approximations are also possible, the AR model assumes that the signal comprises a set of resonances or sinusoids which is an appropriate model for the most practical signals [99,102]. Amongst different algorithms for estimating the PSD of an AR model, Burg algorithm (ARB) is one of the most popular ones [103].

4.5.1   The Burg algorithm

This algorithm is the most popular approach for an AR model and utilises a constrained least squares estimation procedure to obtain p estimated autoregressive parameters from N data samples, with the constraint that the AR parameters satisfy the Levinson–Durbin recursion. The ARB algorithm computes the reflection coefficients in the equivalent lattice structure specified by [104]

$$\hat{k}_p = \frac{-2 \sum_{n=p+1}^{N} w_{p-1}[n] e_{p-1}^{f}[n] e_{p-1}^{b*}[n-1]}{\sum_{n=p+1}^{N} w_{p-1}[n] \left[\left| e_{p-1}^{f}[n] \right|^2 + \left| e_{p-1}^{b}[n-1] \right|^2 \right]} \qquad (4.12)$$

where $w_{p-1}[n]$ is an arbitrary weighting function, $e_p^{f}[n]$ and $e_p^{b}[n]$ are the forward and backward prediction errors respectively and '$*$' denotes the complex conjugate operator.

The AR coefficients, $a_p[n]$, which are subject to the Levinson recursion are estimated from:

$$a_p[n] = a_{p-1}[n] + k_p a_{p-1}^{*}[p-n] \qquad (4.13)$$

where it is understood that the pth order reflection coefficient in the lattice realisation is $k_p = a_p[p]$.

The PSD may be obtained from the estimated AR parameters:

$$P[f] = \frac{\hat{\sigma}_{wp}^2}{\left| 1 + \sum_{k=1}^{p} \hat{a}[k] exp(-j2\pi f k) \right|^2} \qquad (4.14)$$

43

where $\hat{\sigma}_{wp} = r_{xx}[0] \prod_{k=1}^{p} \left[1 - |\hat{a}[k]|^2 \right]$ is the estimated minimum mean–square value for the p–th order predictor.

In this study four different $w_p[n]$ functions are used:

- The original uniform Burg function (ARB-B)

$$w_{p-1}[n] = \frac{1}{(N - p)} \tag{4.15}$$

- A Hamming taper function(ARB-H)

$$w_{p-1}[n] = 0.54 + 0.46 \left[\cos \left(\frac{2n - (N + p - 1)}{(N - p)} \right) \pi \right] \tag{4.16}$$

- An "optimum" parabolic weighting function (ARB-O)

$$w_{p-1}[n] = \left[\frac{6(n - p)(N - n + 1)}{(N - p)(N - p + 1)(N - p + 2)} \right] \tag{4.17}$$

which is based on a minimum average frequency variance.

- Rectangular window (ARB-R)

$$w_{p-1}[n] = 1 \tag{4.18}$$

The main advantages of Burg's method for estimating the parameters of the AR model are as follows [96]:

- It results in high frequency resolution

- It yields a stable AR model

- It is computationally efficient.

However, it has been shown that the Burg algorithm suffers from two major problems:

- line splitting, which is the occurrence of two or more closely–spaced peaks in an AR spectral estimate where only one should be present. This effect often occurs when either the signal-to-noise (SNR) is high, or the initial phase of sinusoidal components is some odd multiple of 45° or the time duration of the data sequence is such that sinusoidal components have an odd number of quarter cycles [105].

- bias in the positioning of spectral peaks with respect to their true frequency location [105, 106].

To overcome these problems, advanced signal processing techniques are implemented based on singular value decomposition (SVD) techniques. These approaches are designed to enhance desired signal components within data records.

4.6 SVD-based techniques

Modern digital signal processing is drifting away from classical approaches in which signals are invariably taken to be stationary and time-invariant. Classical analysis techniques often neglect the fact that for all practical purposes, the available measurements tend to be incomplete and are corrupted by noise. Modern digital signal processing is therefore faced with the problem of finding higher resolution and more accurate algorithms to extract the underlying signal parameters from the measurements. In this context, many important signal modelling and spectrum estimation problems have been solved robustly and accurately using the eigenvalues and eigenvectors of a covariance matrix or the singular value decomposition of a data matrix.

In this section the definition of SVD and a few comments relating to its properties are presented. There are three main reasons for using the SVD technique [107]:

- SVD is an appropriate linear algebraic device for approximating a measurement matrix by a low-rank matrix.

- SVD provides a natural way of spliting a matrix into dominant and subdominant subspaces.

- SVD is a useful tool for other kinds of decompositions, such as pseudo-inverse, Grammian, and matrix projections.

The theory of singular value decomposition states that any $m \times n$ matrix $\mathbf{R}$ of rank r, where $r \leq min(m, n)$ can be decomposed as

$$\mathbf{R} = \mathbf{U\Sigma V}^* \qquad (4.19)$$

where $\mathbf{U}$, $\mathbf{V}$ are $m \times n$ and $n \times n$ unitary matrices [1], and Σ is an $m \times n$ diagonal matrix [108]. An asteric is used to denote the complex conjugate transpose. The diagonal elements of Σ are ordered in a non-increasing order:

$$\sigma_1 \geq \sigma_2 \geq \cdots \geq \sigma_{min,(m,n)} \geq 0$$

These diagonal elements are the singular values of the matrix $\mathbf{R}$, i.e., the positive square roots of the eigenvalues of the matrices $\mathbf{R}^*\mathbf{R}$ or $\mathbf{RR}^*$. The columns of $\mathbf{U}$ and $\mathbf{V}$ are the eigenvectors of $\mathbf{RR}^*$ and $\mathbf{R}^*\mathbf{R}$, and they are called left and right singular vectors respectively. An important theorem related to SVD states that the unique $m \times n$ matrix of rank $p \leq$ rank $(\mathbf{R})$ which best approximates the $m \times n$ matrix, in the Frobenius norm sense[2], is given by

$$\mathbf{R}^{(\mathbf{p})} = \mathbf{U\Sigma_p V}^* \qquad (4.20)$$

where $\mathbf{U}$ and $\mathbf{V}$ are given in (4.19), and $\Sigma_\mathbf{p}$ is obtained from Σ by setting to zero all but its p largest singular values. The $\mathbf{R}^{(\mathbf{p})}$ matrix provides a 'cleaned up' estimate of lower rank signal components of the data.

The relative size of the error in approximating a matrix by a reduced rank p matrix is a important factor in selecting the order p. The *normalised* Forbenius norm of this approximation is given by

$$\rho(p) = \frac{\left\|\mathbf{R} - \mathbf{R}^{(\mathbf{p})}\right\|_F}{\|\mathbf{R}\|_F} = \sqrt{\frac{\sigma_{p+1}^2 + \sigma_{p+2}^2 + \cdots + \sigma_{p_e}^2}{\sigma_1^2 + \sigma_2^2 + \cdots + \sigma_{p_e^2}}} \qquad 1 \leq p \leq p_e \qquad (4.21)$$

in which '$\|.\|$' designates the standard matrix norm.

SVD distinguishes itself from the other decomposition algorithms because it is particularly effective in the presence of round-off errors of noisy data [110]. This feature arises

---

[1] The matrices (typed in upper case bold font) $\mathbf{U}$ and $\mathbf{V}$ are said to be unitary if $\mathbf{U}^{-1} = \mathbf{U}^*$ and $\mathbf{V}^{-1} = \mathbf{V}^*$

[2] The Frobenious norm of the $m \times n$ matrix difference $\mathbf{A}$-$\mathbf{B}$ is defined to be

$$\|\mathbf{A} - \mathbf{B}\| = \left[\sum_{i=1}^{m}\sum_{j=1}^{n}|a_{i,j} - b_{i,j}|^2\right]^{\frac{1}{2}}$$

because SVD techniques make use of the principal eigenvectors of $\mathbf{R^*R}$ and $\mathbf{RR^*}$ in solving least square problems which are generally more robust to the noise perturbations in the data. Therefore these methods obtain stable solutions to the normal equation [111].

The application of this method to different type of models is described in the following sections.

4.7 Sinusoid subspace identification

The algebric properties associated with sinusoidal modeling are best described by expressing forward and backward prediction relationships for the data $x[n]$, $1 \leq n \leq N$

$$x[n] + a_1 x[n-1] + \cdots + a_p x[n-p] \qquad p+1 \leq n \leq N$$

$$x^*[n] + a_1 x*[n-1] + \cdots + a_p x*[n-p] \qquad 1 \leq n \leq N-p$$

where $x^*[n]$ represents the conjugate of $x[n]$. However, in the case of PCG signal the data $x[n]$ are real valued, hence $x^*[n] = x[n]$. These two relationships can be expresed in their equivalent matrix format, that is

$$\mathbf{Xa} = \mathbf{0} \tag{4.22}$$

$$\mathbf{X} = \begin{bmatrix} \mathbf{X_T} \\ \mathbf{X_H} \end{bmatrix} \tag{4.23}$$

where $\mathbf{X_T}$ is the *(N-p)× (p+1)* Toeplitz matrix associated with the forward prediction filter (i.e. $x_T[i][j] = x(p+i+1+j)$), $\mathbf{X_H}$ is the *(N-p)× (p+1)* Hankel matrix associated with the backward prediction filter (i.e. $x_H[i][j] = x(p+i+1-j)$), while $\mathbf{a}$ is the vector solution[3]. To solve (4.22) an augmented SVD algorithm is applied [111],

$$\mathbf{a} = -\left[\mathbf{X_b^p}\right]^\dagger \mathbf{x_{b_1}^p} \tag{4.24}$$

---

[3]A lower case bold format represents the vector notation.

where † designates the pseudo matrix inverse operator while $\mathbf{x}_{\mathbf{b}_1}^{\mathbf{P}}$ and $\mathbf{X}_{\mathbf{b}}^{\mathbf{P}}$ are the first and remaining p_e columns, respectively, of the rank p approximation matrix $\mathbf{X}$. This augmented SVD algorithm achieves the full benefits of the rank p reduction data cleansing SVD operation since it includes the first column of $\mathbf{X}$ in the rank p approximation. The power spectrum is then calculated from:

$$P[f] = \frac{1}{\left|1 + \sum_{k=1}^{p} a[k]exp(-j2\pi fk)\right|^2} \qquad (4.25)$$

4.8   Autoregressive moving average modelling

The autoregressive moving average model (ARMA) assumes that a time series $x[n]$ can be modelled as the output of a filter containing p poles and q zeros:

$$x[n] = -\sum_{k=1}^{p} a[k]x[n-k] + \sum_{k=1}^{q} b[k]w[n-k] \qquad (4.26)$$

excited by a zero-mean, unit-variance, uncorrelated random data sequence (i.e. normalised white noise) $w[n]$ which is taken to be unobservable [99, 112].

The relationship of the ARMA parameters to the autocorrelation sequence is given by:

$$R_{xx}[l] = -\sum_{k=1}^{p} a[k]R_{xx}[l-k] + \sum_{k=1}^{q} b[k]R_{wx}[l-k] \qquad (4.27)$$

where $R_{wx} = E\left[w[n]x[n-k]^*\right]$ is the cross–correlation between the signal and noise, and $E[\cdot]$ is the statistical expectation operator. Note that R_{wx} must be zero for $k > 0$ since a future input to a causal, stable filter cannot affect the present output and $w[n]$ is white noise [99], therefore :

$$R_{xx}[l] = \begin{cases} -\sum_{k=1}^{p} a[k]R_{xx}[l-k] + \sum_{k=0}^{q} b[k]R_{wx}[l-k] & l = 0, \cdots, q \\ -\sum_{k=1}^{p} a[k]R_{xx}[l-k] & l = q+1, q+2, \cdots, M \end{cases} \qquad (4.28)$$

For $M = p+q$ these equations have been called the extended, or modified Yule–Walker (MYW) equations. The MYW are chosen since they show better performance than the maximum-likelihood realisation of other ARMA methods when poles of the model are very close to the unit circle [113], which is the case for heart sounds [23].

However, straightforward application of the MYW method can lead to poor performance, especially for short and noisy data records [113]. It has been observed by a number of researchers that significant improvements in the quality of the spectral estimates can be achieved by some variations of the basic method, such as increasing the number of MYW equations and the order of the estimated model [112–114]. Both these factors are of equal importance. The improvement in estimation accuracy results from the fact that there is valuable information in the high lag coefficients, which does not appear in the MYW equation. In this extended order approach it has been found that the resultant parameter estimates will be generally less sensitive to errors contained in the autocorrelation lag estimates than for the minimal ideal order choice of p [109]. Therefore, the set of linear equations for the extended order ARMA (p_e, q_e) model may be expressed in matrix form as follows,

$$\mathbf{R_{xx}a} = -\mathbf{r_{xx}} \tag{4.29}$$

where:

$$\mathbf{R_{xx}} = \begin{bmatrix} R_{xx}[q_e] & R_{xx}[q_e - 1] & \cdots & R_{xx}[q_e - p_e + 1] \\ R_{xx}[q_e + 1] & R_{xx}[q_e] & \cdots & R_{xx}[q_e - p_e + 2] \\ \vdots & \vdots & \cdots & \vdots \\ R_{xx}[q_e + m - 1] & R_{xx}[q_e + m - 2] & \cdots & R_{xx}[q_e - p_e + m] \end{bmatrix} \tag{4.30}$$

is the extended order autocorrelation matrix, and

$$\mathbf{a} = \begin{bmatrix} a[1] \\ a[2] \\ \vdots \\ a[p_e] \end{bmatrix}, \quad \mathbf{r_{xx}} = \begin{bmatrix} R_{xx}[q_e + 1] \\ R_{xx}[q_e + 2] \\ \vdots \\ R_{xx}[q_e + m] \end{bmatrix} \tag{4.31}$$

are respectively the model parameters and data vector, where p_e, and q_e are the extended order of the matrix. The choice of m is related directly to prior information about the spectral characteristics of the signal i.e. if it is known that the spectra contains sharp resonance or is broadband. It has been shown that statistical arguments exist for selecting $m \geq p$, especially when actual data points are available (and not autocorrelation lags) such as in the case of S1 and S2. Freidlander [113] has suggested that $m = 4\hat{p}$ is a good rule-of-thumb choice.

To solve (4.29) a technique based on SVD is used [112]. The SVD technique is applied in three different versions. In the first case the SVD technique is applied to the autocorrelation matrix, $\mathbf{R_{xx}}$, to approximate it with a p rank optimum approximation matrix $m \times p_e$, $\mathbf{R_{xx}^{(p)}}$. Once $\mathbf{R_{xx}^{(p)}}$ is computed, the parameters of the auto-regressive model can be found from [109]:

$$\mathbf{a} = - \left[\mathbf{R_{xx}^{p}} \right]^{\dagger} \mathbf{r_{xx}} = - \sum_{k=1}^{p} \frac{1}{\sigma_k} (\mathbf{v_k^*} \mathbf{r_{xx}}) \mathbf{v_k} \tag{4.32}$$

where $\left[\mathbf{R_{xx}^{p}} \right]^{\dagger}$ denotes the pseudoinverse of the matrix $\mathbf{R_{xx}^{(p)}}$, and the pairs $(\sigma_k, \mathbf{v_k})$ correspond to the p largest singular-value-characteristic-vector pairs associated with the SVD of the matrix $\mathbf{R_{xx}}$.

To eliminate the noise effects from the data vector, a simple variation of the above mentioned technique is used by working with the extended autocorrelation coefficient matrix $\mathbf{R_{xx}'}$ [112, 115] where $\mathbf{R_{xx}'} = [\mathbf{r_{xx}}, \mathbf{R_{xx}}]$ and then to compute the minimum norm solution

$$(\hat{\mathbf{R}}')_{xx}^{(p)} \begin{bmatrix} 1 \\ a \end{bmatrix} = \mathbf{0} \tag{4.33}$$

In this case SVD is applied to the extended order matrix $\mathbf{R_{xx}'}$ after which the p rank optimum approximation matrix $(\hat{\mathbf{R}}')_{xx}^{(p)}$ is decomposed into $(\hat{\mathbf{R}}')_{xx}^{(p)} = \left[\mathbf{r_1^p} \mid \mathbf{R_a^p} \right]$ where $\mathbf{r_1^p}$ is the leftmost $m \times 1$ column vector of $(\hat{\mathbf{R}}')_{xx}^{(p)}$ and $\mathbf{R_a^p}$ is a $m \times p_e$ matrix composed of the p_e rightmost $m \times 1$ column vectors of $(\hat{\mathbf{R}}')_{xx}^{(p)}$. In both cases mentioned above the size of the rank p approximation matrix obtained from the SVD technique is $m \times p_e$. The third ARMA algorithm has been implemented by reducing the dimension of the rank p approximation matrix to $p \times p$. This matrix is given by

$$\mathbf{R}_{xx}^{(p)} = \sum_{k=1}^{p_e-p+1} (\hat{\mathbf{R}}_k^{(p)})^* \hat{\mathbf{R}}_k^{(p)} \tag{4.34}$$

where $\hat{\mathbf{R}}_k^{(p)}$ are the submatrices of $(\hat{\mathbf{R}}')_{xx}^{(p)}$ composed of its columns from k to $p+k$. In the next section these three methods of computing the ARMA model are called respectively ARMA1, ARMA2 and ARMA3.

In order to complete ARMA modelling, it is necessary to determine the associated

moving average (MA) parameters of the model. There are a variety of procedures for achieving this [104, 112, 113]. However, if only a spectral estimate is desired, then there is no need to solve for the MA parameters, but only to determine the autocorrelation function, since

$$P_{MA}(f) = \Sigma_{m=-q}^{q} r_{xx} exp(-j2\pi fm) \tag{4.35}$$

Many contemporary MA-components estimators are based on utilising the forward and backward residual time–series associated with an ARMA time series. In our implementation the forward residual time series elements are computed from

$$r_f[n] = \sum_{k=0}^{p} \hat{a}[k]x[n-k] \qquad p+1 \le n \le N \tag{4.36}$$

where $\hat{a}[k]$ are the estimated AR parameters and $x[n]$ are the data points. Similarly, the backward residual components are generated using

$$r_b[n] = \sum_{k=0}^{p} \hat{a}_k^* x[n+k] \qquad 1 \le n \le N-p \tag{4.37}$$

After that, the following estimates of the residual first $q+1$ autocorrelation lags of the time series are generated from:

$$\hat{r}_{xx}[n] = \frac{1}{N-p-n} \sum_{k=1}^{N-p-n} \left[r_f[n+p+k]r_f^*[p+k] + r_b[n+k]r_b^*[k] \right]$$
$$0 \le n \le q \tag{4.38}$$

Taking the Fourier transform of these autocorrelation lags, the MA(q) spectral estimate components are obtained:

$$\left| \hat{B}_q(exp(-j\omega)) \right|^2 = \left| \sum_{n=-q}^{q} w[n]\hat{r}_{xx}[n]exp(-j\omega n) \right|^2 \tag{4.39}$$

in which $w[n]$ is a window sequence. In our particular case $w[n]$ is defined [112] as:

$$w[n] = \left(\frac{N - p - |n|}{N - p} \right) \left(\frac{q + 1 - |\,n\,|}{q + 1} \right) \tag{4.40}$$

which ensures positive-semidefiniteness of the $\hat{r}_{xx}[n]$ estimate and reduces the sidelobes. Finally, the overall ARMA spectral estimation is then given by

$$\hat{S}(f) = \frac{\left| \hat{B}_q(exp(-j2\pi f)) \right|^2}{\left| \hat{A}_p(exp(-j2\pi f)) \right|^2} \tag{4.41}$$

where $\hat{A}_p(exp(-j2\pi f))$ is :

$$\hat{A}_p(exp(-j2\pi f)) = \sum_{k=0}^{p} \hat{a}[k] exp(-j2\pi f k) \tag{4.42}$$

in which $\hat{a}[k]$ denotes the AR parameter estimates of the ARMA model.

The SVD method described above enhances the accuracy of the estimates from MYW equations. It does, however, increase the computational complexity of the overall estimation procedure. However, for SPCG where processing is often off-line this computational complexity is not important.

4.9   Prony's method

This method seeks to fit a *deterministic* exponential model to the data, in contrast to AR or ARMA methods that seek to fit a random model to the second–order data statistics. The model assumed in the modern Prony's method is a set of p exponentials of arbitrary amplitude, phase, frequency, and damping factor [104]. The discrete-time function is described by:

$$\hat{x}[n] = \sum_{m=1}^{p} h[m]z[m]^n \qquad n = 0, 1, 2, \cdots, N - 1 \tag{4.43}$$

where

$$
\begin{aligned}
h[m] &= A[m]exp(j\phi[m]) \\
z[m] &= exp\left[(d[m] + j2\pi f[m])\,\triangle t\right]
\end{aligned}
$$

$$\tag{4.44}$$

$A[m]$ is the amplitude, $\phi[m]$ is the phase in radians, $d[m]$ is the damping factor, $f[m]$ is the frequency in Hz, and $\triangle t$ represents the sample interval in seconds.

The main advantages of this method are as follows [104, 116]:

(i) It gives full parameterization of the signal spectrum: amplitude, phase and bandwidth information of the significant spectral components

(ii) It maintains linearity of each spectral peak height corresponding to its energy

(iii) The method does not produce sidelobes, which often appear in usual AR methods. The method extracts spectral parameters directly from the roots of the polynomial, but does not express the spectral distribution with the finite–ordered polynomial like other AR(MA) methods, which leads to sidelobes.

For the above reasons, Prony's method is useful for the quantitative analysis of heart sounds since it provides a complete parameterization of the resonant and damping characteristics of the heart-valve system. These parameters will reflect the mechanical and structural properties of this system.

However, Prony's original method has been found to be highly sensitive to additive measurement errors in the observed signal samples [115, 117]. To improve its performance many techniques have been suggested, which give good performance for reasonable signal-to-noise ratios (SNR) or specific characteristics of the signal [115, 116, 118]. However, these methods are not found to be very effective when the poles of the signal are close to the unit circle [119] or in the case of the direction finding problem [121].

To tackle these problems a new modified forward-backward overdetermined Prony's method (MFBPM) is introduced here. This approach uses (1) SVD of the augmented data matrix to reduce the effect of noise in both the observation vector and data matrix, (2) a modified procedure to estimate the position of signal poles and (3) an advanced method based on eigenvalue decomposition for computing the roots of the polynomials.

4.9.1   MFBPM algorithm

To decrease the sensitivity of the estimated parameters to the perturbation of data and reduce the numerical ill conditioning , the following overdetermined prediction equation

was set up using sampled data, $x[n]$, $0 \leq n \leq N - 1$, in both the backward and forward direction:

$$\mathbf{X_b b} = \mathbf{0} \quad \mathbf{X_f f} = \mathbf{0} \tag{4.45}$$

where $\mathbf{X_b}$ and $\mathbf{X_f}$ are the extended $(N - p_e) \times (p_e + 1)$ data matrices and p_e is the extended order of the matrices :

$$\begin{aligned} x_b(i,j) &= x(i + j - 2) \\ x_f(i,j) &= x(p_e + i - j) \end{aligned} \quad \left\{ \begin{aligned} &1 \leq i \leq N - p_e \\ &1 \leq j \leq p_e + 1 \end{aligned} \right. \tag{4.46}$$

and $\mathbf{b}$, and $\mathbf{f}$ are the $(p_e + 1)$ coefficient vectors in the backward and forward directions with elements $b[k]$ and $f[k]$ respectively. In practice the extended order, p_e, is chosen significantly larger than the true order of the system. The main reason for taking the data in both direction is to reduce the bias on the estimation of the damping factor [123]. The forward and backward matrices may be represented by their SVD [122]:

$$\mathbf{X_b} = \sum_{i=1}^{r} \sigma_k^b \mathbf{u}_k^b \mathbf{v}_k^{b*} \quad \left(\mathbf{X_f} = \sum_{i=1}^{r} \sigma_k^f \mathbf{u}_k^f \mathbf{v}_k^{f*} \right) \tag{4.47}$$

In this representation, the σ_k^b (σ_k^f) are positive *singular values* that are ordered in the monotonically decreasing fashion $\sigma_k^b \geq \sigma_{k+1}^b$, ($\sigma_k^f \geq \sigma_{k+1}^f$), the $\mathbf{u}_k^b$ ($\mathbf{u}_k^f$) and $\mathbf{v}_k^b$ ($\mathbf{v}_k^f$) are $(N - p_e) \times 1$ and $(p_e + 1) \times 1$ orthogonal *left* and *right singular vectors* respectively, of the $\mathbf{X_b}$ and $\mathbf{X_f}$ matrices and the integer r is the rank of $\mathbf{X_b}$ (both matrices $\mathbf{X_b}$ and $\mathbf{X_f}$ have the same rank).

In theory, if the signal is composed of only p sinusoids, the matrices $(\mathbf{X_b^T X_b})$ and $(\mathbf{X_f^T X_f})$, where T is the transpose operator, are of rank *2p* and calculation of their eigenvalues yields the value of p. In the case of externally recorded heart sounds, one can say that the part of the signal related to heart–valve movements contains a number of p exponentially damped sinusoids which lie in the amplitude range of 0 dB-M dB. To decide the level M (i.e. order p) one must use the characteristic of the eigenvalues (ρ_i) of the $\mathbf{X_b^T X_b}$ ($\mathbf{X_f^T X_f}$) which approach the squared amplitudes of each sinusoid when N and p_e approach infinity [118]. In this augmented SVD algorithm, the rank p approximation of the total data matrices $\mathbf{X_b}$ and $\mathbf{X_f}$ is first determined $(\mathbf{X_b^P}, \mathbf{X_f^P})$. It is well known that in the overdetermined case $(\mathbf{X_b}$ or $\mathbf{X_f})$ the matrix of rank p (where $p \leq r$) which lies closest to $\mathbf{X_b}(\mathbf{X_f})$ in the least squares sense is specified by [112,122]:

$$\mathbf{X_b^P} = \sum_{i=1}^{p} \sigma_k^b \mathbf{u_k^b} \mathbf{v_k^{b^*}} \quad \left(\mathbf{X_f^P} = \sum_{i=1}^{p} \sigma_k^f \mathbf{u_k^f} \mathbf{v_k^{f^*}} \right) \tag{4.48}$$

where only the p largest outer products $\sigma_k^b u_k^b v_k^{b^*}$ $(\sigma_k u_k^f v_k^{f^*})$ are retained in forming the closest rank p approximation. Finally, the related coefficient vectors are then specified by

$$\mathbf{b} = -\left[\mathbf{X_b^P}\right]^\dagger \mathbf{x_{b_1}^P} \quad \mathbf{f} = -\left[\mathbf{X_f^P}\right]^\dagger \mathbf{x_{f_1}^P} \tag{4.49}$$

where † designates the pseudo matrix inverse operator while $\mathbf{x_{b_1}^P}$ $(\mathbf{x_{f_1}^P})$ and $\mathbf{X_b^P}$ $(\mathbf{X_f^P})$ are the first and remaining p_e columns, respectively, of the rank p approximation matrices. The key point in the performance of Prony's method is the process of deciding the position of the poles which are related to the signal. In the backward direction case, it has been shown [115] that the poles of the signal can be separated from those introduced by noise (i.e. the norm of the signal roots is $[\lambda_i] \geq 1$). However, this method has a "hard failure" [119] when the number of roots outside the unit circle in the backward direction polynomial *B(z)*:

$$B(z) = \sum_{i=0}^{p_e} b[i] z^{p-i} \tag{4.50}$$

is not equal to p. This case occurs often when some of the roots of the *B(z)* are near the unit circle, or when the noise level is high. To combat this failure, the p largest norm roots [122] of the backward direction polynomial (*B(z)*) are searched for instead of the roots with norm $[\lambda_i] \geq 1$. Since the effect of noise tends to bias the roots of the forward polynomial *F(z)*:

$$F(z) = \sum_{i=0}^{p_e} f[i] z^{p-i} \tag{4.51}$$

in the opposite direction to those of *B(z)*, one can use the mean of the p largest norm roots in the backward direction with the p roots of the same frequency in the forward direction to estimate more accurately the real position of the signal poles [123]. Thus, these poles are estimated by

$$z[i] = \frac{Z_b^M[i] + z_f[i]}{2} \quad 1 \leq i \leq p \tag{4.52}$$

where

$$Z_b^M[i] = \begin{cases} \frac{1}{(z_b^l[i])^*} & |z_b^l[i]| \geq 1 \\ z_b^l[i] & |z_b^l[i]| < 1 \end{cases} \tag{4.53}$$

$z_b^l[i]$ are the p largest norm roots of *B(z)*, and $z_f[i]$ are the p roots of the *F(z)* which have the same frequency as the $z_b^l[i]$. This procedure has a great impact especially in those roots which are very close to the unit circle due to their volatile nature as a result of perturbation or machine round-off error.

However, it should be mentioned that the method used for computation of these roots (*B(z)*, *F(z)*) is also very important in the case of overdetermined systems because the order of the polynomials (p_e) is quite high which can cause divergence of the roots in practice [118, 124]. To combat this effect, a procedure is proposed based on eigenvalue decomposition of the system-matrix $\mathbf{A_b}(\mathbf{A_f})$ [125]:

$$A_b(i,j) = A_f(i,j) = \begin{cases} 1 & when \ j = i+1 \\ 0 & elsewhere \end{cases} \quad \begin{array}{l} 1 \leq j \leq p_e \\ 1 \leq i \leq p_e - 1 \end{array} \tag{4.54}$$

$$\begin{aligned} A_b(p,j) &= -b(j-1+p_e) \\ A_f(p,j) &= -f(j-1+p_e) \end{aligned} \quad \begin{cases} i = p_e \\ 1 \leq j \leq p_e \end{cases} \tag{4.55}$$

using a Hessenberg reduction and a balancing procedure to estimate $z_b[i]$ and $z_f[i]$ [124, 126]. This procedure is more computationally complicated compared with other methods such as Muller's or Laguerre's method [124], but it gives better results in terms of accurate estimation of the poles. Although computationally intense, this procedure is necessary for reducing the sensitivity of eigenvalues to small changes in the matrix elements and to rounding errors during the execution of the algorithm. These factors have a great impact especially in the case of the nonsymmetric matrices which is the case for $\mathbf{A_b}(\mathbf{A_f})$ [124]. However, it should be mentioned that this computational load is not a problem in off-line applications. With p roots computed from (4.52), a Vandermonde matrix [4] is created [104]:

---

[4] *Vandermonde* matrix: An $m \times n$ matrix whose elements are expressed in terms of powers of the n based parameters $x[1], x[2], \cdots, x[n]$; $v[i][j] = x[j]^{i-1}$ for $1 \leq i \leq m, 1 \leq j \leq n$.

$$\mathbf{Z} = \begin{bmatrix} 1 & 1 & \cdots & 1 \\ z_1^1 & z_2^1 & \cdots & z_p^1 \\ \vdots & \vdots & \cdots & \vdots \\ z_1^{N-1} & z_2^{N-1} & \cdots & z_p^{N-1} \end{bmatrix} \qquad (4.56)$$

and $\mathbf{h}$ the *time-independent* parameters (eq. 4.43) are estimated from the equation :

$$\mathbf{Zh} = \mathbf{x} \qquad (4.57)$$

where

$$\mathbf{h} = \begin{bmatrix} h_1 \\ h_2 \\ \vdots \\ h_p \end{bmatrix} \qquad \mathbf{x} = \begin{bmatrix} x[0] \\ x[2] \\ \vdots \\ x[N-1] \end{bmatrix} \qquad (4.58)$$

are a p dimension complex vector and an $N \times 1$ data vector respectively.

The amplitude $A[i]$, $\phi[i]$, damping factor $d[i]$, and frequency $f[i]$ are estimated from the $z[i]$ and $h[i]$ [104]:

$$\begin{aligned} A[i] &= |h[i]| \\ \phi[i] &= \tan^{-1}\left[\frac{\Im(h[i])}{\Re(h[i])}\right] \\ d[i] &= \frac{\ln[|z[i]|]}{\triangle t} \\ f[i] &= \frac{\tan^{-1}\left|\frac{\Im(z[i])}{\Re(z[i])}\right|}{2\pi \triangle t} \end{aligned} \qquad (4.59)$$

Although Prony's method normally terminates with the computation of above mentioned parameters, it is possible to calculate the spectrum. In our case the Prony's spectrum is calculated using the formula [99]:

$$\hat{S}_{Prony}[f] = \left|\hat{X}[f]\right|^2 \qquad (4.60)$$

where

$$\left|\hat{X}[f]\right| = \sum_{i=1}^{p} A[i] exp(j\phi[i]) \frac{2d[i]}{[d[i]^2 + (2\pi[f - f[m]])^2]} \qquad (4.61)$$

Two other advanced versions of Prony's method are also implemented in order to compare the performance of MFBPM when applied to S1 and S2: the modified backward Prony's method (MBPM) [126] (i.e. data in backward direction only and with p large norm ($z_b^M[i]$) roots) and forward-backward Prony's method (FBPM) based on the method proposed by Marple [104, 115] (data in forward and backward direction but only roots with norm $|\lambda[i]| \geq 1$ are used).

4.10   Model order selection criteria

One of the first problems associated with parametric methods is the selection of the proper model order p, i.e. the number of spectral components that are to be searched for. Although several criteria have been suggested, their performance seems to be very sensitive to the validity of the observation model and the characteristics of the real data. Since the best choice of the model order p is not known *a priori*, it is suggested [99, 104] that the final determination of a suitable model order is a subjective judgment in the analysis of actual data which originate from an unknown process. In this study, the performance of several criteria have been investigated for the analysis of S1 and S2. In the case of the ARB algorithm the four following criteria are used [99, 104]:

- Final prediction error (FPE),

$$FPE[p] = \hat{\sigma}_{wp} \left(\frac{N + p + 1}{N - p - 1} \right) \tag{4.62}$$

  where $\hat{\sigma}_{wp}$ is the estimated variance of the linear prediction error and N is the number of data samples. This criterion selects the order of the AR process so that the average error variance for one-step prediction is minimized.

- Akaike information criterion (AIC),

$$AIC[p] = N \ln \hat{\sigma}_{wp} + 2p \tag{4.63}$$

  In this case the model order is selected by minimising an information theoretic function.

- Criterion autoregressive transfer (CAT)

$$CAT[p] = \left(\frac{1}{N} \sum_{j=1}^{p} \gamma_j^{-1} \right) - \gamma_j^{-1} \tag{4.64}$$

where $\gamma_j = \left[\frac{N}{N-j}\right] \hat{\sigma}_{wj}$. The main idea behind this criterion is to select the model order p in which the estimate of the difference between mean-square-errors of the true prediction error filter and the estimated filter is minimised.

- Minimum description length (MDL)

$$MDL[p] = N \ln(\hat{\sigma_{wp}}) + p \ln(N) \tag{4.65}$$

In this criteria the model order is selected to be the one which yields the maximum posterior probability [127].

In the case of SVD-based methods, the validity of the relative distribution of eigenvalue magnitude and the consecutive relative eigenvalue magnitude (CRME) for deciding the order of the model is investigated [128]. In order to increase the stability of the matrix operation, tolerance to quantization, and to decrease the sensitivities to computational errors the SVD of the data matrix is used instead of the eigenvalue decomposition of the correlation matrix [129]. The relationship between the eigenvalue decomposition of the correlation matrix and SVD of the data matrix was described in section 4.6.

4.11   A numerical example

The performance of the above-mentioned algorithms is demonstrated by testing them on a synthetic signal, which has characteristics similar to those of heart sounds, namely:

$$x[n] = (0.98)^n \sin(0.123n) + (0.98)^n \sin(0.423n) + w[n] \quad n = 1, 2, .., 128 \tag{4.66}$$

where w[n] is white Gaussian noise. The criterion used for choosing the above time series was based on the fact that S1 and S2 are composed of transient sinusoidal signals of short duration and fast decaying amplitude, superimposed on a background of random noise [37, 132]. The signal to noise ratio (SNR) is defined as

$$SNR = 10 \log \left(\frac{\sum_{n=1}^{N} (x'[n])^2}{\sum_{n=1}^{N} (w[n])^2} \right) \tag{4.67}$$

where $N = 128$ and

$$x'[n] = (0.98)^n \sin(0.123n) + (0.98)^n \sin(0.423n) \quad n = 1, 2, \cdots, 128 \tag{4.68}$$

A percentage error, err, for the estimated frequency, $\hat{f_i}$, from the actual frequency, f_i, is calculated for all methods with different levels of SNR as follows:

$$err(\%) = \frac{\left| \hat{f_i} - f_i \right|}{f_i} \times 100 \qquad (4.69)$$

Table 4.1 summarises the results regarding the error in frequency estimation for each of these methods and Figure 4.2 shows the results achieved with the different methods.

Method	SNR(dB)	$f_1 = 0.01957$	$f_2 = 0.06732$	$err\ f_1\%$	$err\ f_2\%$
FFT	3.0	0.0155	0.07	20.82	3.9
ARB-O	3.0	0.0173	0.0661	11.6	1.8
ARB-H	3.0	0.0154	0.0665	21.0	1.14
ARB-B	3.0	0.0143	0.06715	26.95	0.25
ARB-R	3.0	0.0143	0.06718	26.95	0.2
SSI	3.0	0.0202	0.06755	3.1	0.33
ARMA1	3.0	0.0164	0.0689	16.22	0.23
ARMA2	3.0	0.0165	0.0689	15.7	0.23
ARMA3	3.0	-.-	0.0684	100.0	0.165
MFBP	3.0	0.0195	0.0674	0.38	0.1

Table 4.1:   Frequency error estimation for several algorithms applied to the signal shown in eq.(4.66)

From Figure 4.2 and Table 4.1 it can be seen that the FFT and ARB methods, regardless of the choice of window, perform badly in terms of frequency error. Moreover, both these methods suffer from the presence of spurious peaks as a result of noise and the large model order (p=20) in the case of ARB. For order less less than 20 the ARB method does not resolve the two peaks contained in the signal. Therefore, a much higher order was required to detect these two peaks. This consequently lead to spurious peaks in the estimated spectra. Regarding the impact of the window on the spectral performance of ARB, it is clear that ARB-O and ARB-H perform better than the two other windows. This improvement could be related to the efficiency computation of the first order coefficient in ARB-O and ARB-H [133]. From these results, it seems that the use of either the FFT or ARB methods would be an appropriate methods to investigate such classes of signals. However, in this chapter and the following one the FFT and ARB are used for comparison since they are the techniques commonly used to analyse spectral characteristics of S1 and S2 [26,27,30–32,42,62,67,74,79,80,90,134].
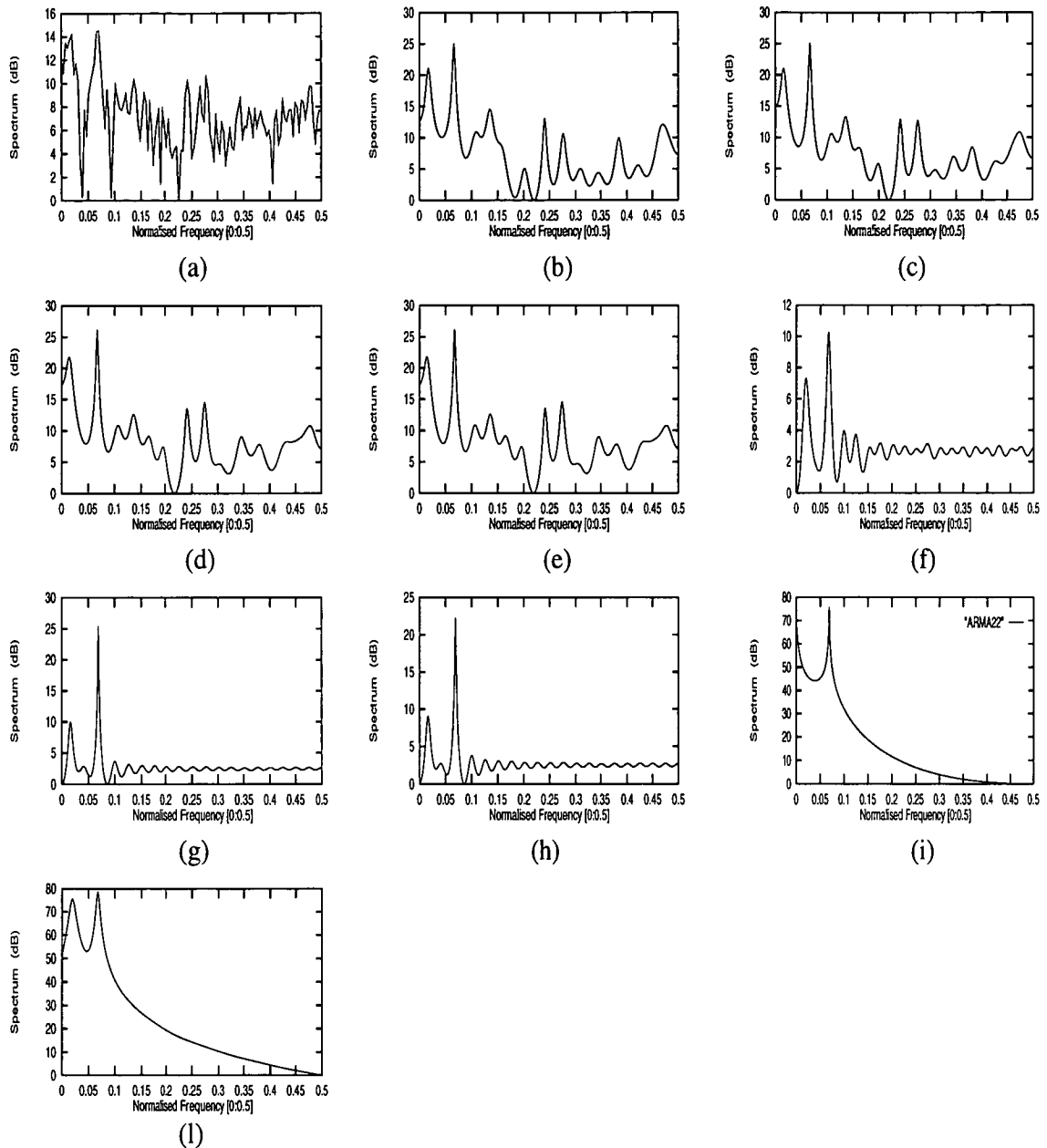
Figure 4.2:   Spectrum produced from several estimation algorithms when analysing the synthetic signal given in eq. (4.66); (a) FFT method, (b) ARB-O $(p = 20)$, (c) ARB-H $(p = 20)$, (d) ARB-B $(p = 20)$, (e) ARB-R $(p = 20)$, (f) SSI algorithm $(p = 4)$, (g) ARMA1 method $(p = q = 4)$, (h) ARMA2 method $(p = q = 4)$, (i) ARMA3 method $(p = q = 4)$,(l) Prony's spectrum $(p = 4)$.

A great improvement in spectral representation is obtained by the techniques based on the SVD method. These methods not only improve the resolution capabilities but they also increase the accuracy in frequency estimation. Amongst them the MFBPM

method gives the best results and the SSI method is the second best. Their superiority over ARMA methods can be explained by the model chosen as well as fact that in the case of SSI and Prony's method the data matrix is used rather than the covariance matrix. This is particularly important when one deals with short time signals [122].

Amongst the ARMA methods, ARMA1 and ARMA2 perform very similarly with a slight improvement in the case of ARMA2. This is related to the noise reduction in the data vector by using the augmented SVD method in this case. The ARMA3 method gives a very smoothed spectrum and even fails to detect the first peak.

Figure 4.3 shows the performance of model order criteria in the case of the synthesised signal simulated by eq. (4.66). Figures 4.3(a)-(d) represent the interesting portion of the normalised amplitude of FPE, AIC, CAT, and MDL respectively, plotted versus the model order. Theoretically the optimum model order of the model is determined
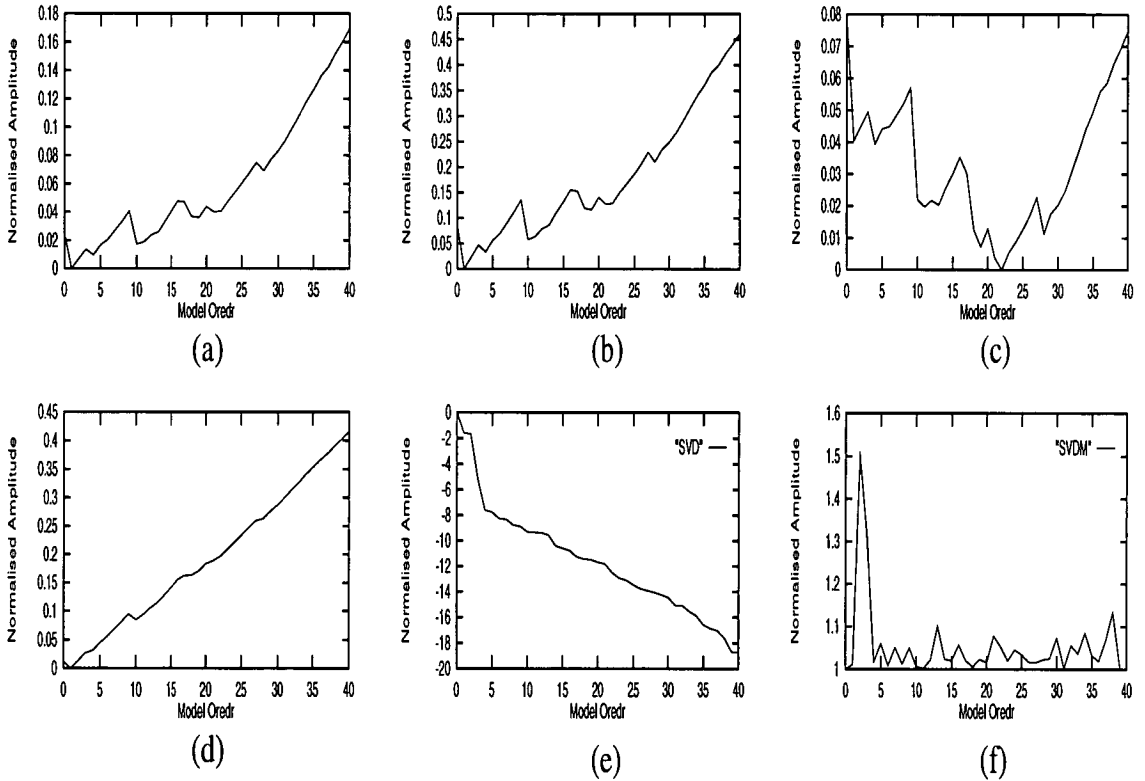
Figure 4.3:   Performance of several model order criteria when analysing the synthetic signal simulated by eq. (4.66); (a) FPE, (b) AIC, (c) CAT, (d) MDL, (e) distribution of eigenvalue magnitude, (f) CRME.

by the value of p at which the respective criterion (i.e. FPE, AIC, CAT, MDL) attains its minimum [99, 104]. However, this definition has been shown to underestimate the required model order in the case of purely harmonic components [99, 131]. Results

shown in Figure 4.3(a)-(d) support this fact. From Figures 4.3 (a), (b), and (d) it is clear that the minimum value for FPE, AIC and MDL underestimate the proper model order. All these three criteria return a model order equal to 2, whereas the actual model order should be four for the signal in hand (i.e. it has been shown that for a signal composed of m real sinusoids $2m$ coefficients are required to define the m poles in the generating system [130, 131]). However, Figures 4.3 (a), (b), and (d) show that the second minimum on the plot of FPE, AIC and MDL properly estimates the number of spectral components. This conclusion is not true for the case of the CAT criterion. From Figure 4.3(c) it is clear that the CAT criterion is unable to return an proper estimate for the number of spectral components contained in the signal.

On the contrary to the above mentioned criteria, criteria based on the distribution of eigenvalues represents an accurate means for estimating the proper model order. It is clear from Figure 4.3(e), and (f), which represent the distribution of the eigenvalues and the CRME factor, show that the required model order for analysing the signal in hand is four. In the case of Figure 4.3(e) a clear knee is present at $p = 4$ (note that in the case of real data matrices containing p signal components the rank of the matrix is $2p$). This knee is also associated with the biggest CRME ratio as well (Figure 4.3(f)). It must be said that the aboved-mentioned algorithms have been applied to other examples of simulated signals and very similar results were found. These results were presented in [135].

4.12 Summary and conclusion

This chapter has introduced the various methods investigated in this research for spectral analysis of first and second heart sounds. Four different parametric methods in several algorithms have been implemented. Amongst them the MFBPM obtains the best results and its superiority over other spectral analysis techniques has been demonstrated for the case of a synthetic signal similar to S1 and S2. This comparison is based on the assumption that S1 and S2 are decaying sinusoidal signals. From the results obtained, it was concluded that for the case of a synthetic signal almost all the methods based on the SVD technique perform better than conventional methods such as the FFT and ARB, which have been used widely to represent the spectral composition of S1 and S2. The only disadvantage of the SVD-based methods is their computational

complexity. However, bearing in mind that most processing is off-line and the required time for this processing is of the order of minutes, this disadvantage does not represent a major drawback for these methods.

Regarding the model order selection criteria, it appears that criteria based on the distribution of the eigenvalues of data matrix perform well in the case of simulated signals. However, these conclusions must be demonstrated for real heart sounds. The next chapter addresses this point.

Chapter 5

Application of Spectral Analysis Methods to PCG Signals

5.1 Introduction

Various authors have described the performance of spectral analysis methods in SPCG [10, 37, 57, 74, 76]. However, in most of these studies little attention has been paid to the performance of these methods in terms of the accurate representation of the overall spectral composition of the first and second heart sounds. This analysis is of crucial importance when one bears in mind the fact that a proper investigation of the origin of heart sounds or the diagnostic potential of the PCG method is entirely dependent on the performance of the method of spectral analysis used. Moreover, in the analysis of heart sounds, a definite relationship has not yet been established between the different spectral components in the externally-recorded PCG and the underlying system which generates the sounds. Therefore, one must investigate all the parameters of the sound spectrum and associate these with the known condition of the heart valve.

In this context, the better the method for representing the spectral characteristics of the SPCG signal, the more effective will be the classification procedure. The objective of this chapter is to investigate the performance of different spectral estimation techniques introduced in the last chapter when applied to the analysis of S1 and S2 and their ability to detect different frequency components associated with S1 and S2. Synthesised first and second heart sounds were generated to allow a rigorous comparison between all the methods of spectral analysis. The performance of spectral estimation techniques described in the previous chapter is investigated for S1 and S2 in terms of the overall spectral resolution rather than as others [10, 37, 75] have done which was to concentrate solely on certain spectral components.

5.2   Modelling of S1 and S2

To compare the performance of the spectral techniques, a synthesised signal is required which can be used as a reference signal. The synthesised signal is modelled as a linear combination of decaying sinusoids. This kind of model is selected because it is believed that it best represents the intrinsic properties of S1 and S2. The parameters of this synthesised signal are obtained using MFBPM based on a mean-least-square analysis in the time-domain. Since the recorded data are real-valued, the complex exponentials obtained from the MFBPM method occur in complex conjugate pairs [104]. Thus, only the positive frequency components are used for generating the synthesised signal:

$$\hat{s}[n] = \sum_{i=1}^{\frac{p}{2}} 2A[i] \exp\left(-nd[i]\right) \cos(2\pi f[i]n + \phi[i]) \quad 0 \le n \le N - 1 \tag{5.1}$$

Selection of the lower rank approximation p is the major problem in the performance of all the rank approximation algorithms when p is not known *a priori* (which is the case for real data such as PCG signals). In most of the signal processing applications of SVD, the model order p is defined based on theories of the distribution of singular values and a statistical significance test of the data matrix [128, 136]. However, all these tests are based on simulated data, therefore the model order is known *a priori*. Consequently, all effort is directed towards finding a relationship between the threshold bounds of the SVD distribution and their validity as a function of SNR, variance of the parameter estimation or other criteria. Although these criteria give good results in simulated cases, there is a big gap between the simulation experiments and real signals. In the proposed algorithm the best subset p out of the p_e exponential functions provided by the overdetermined matrices $\mathbf{X_b}$ and $\mathbf{X_f}$ is the one for which a linear combination of the p exponentials (5.1) best approximates the observed data in a normalised root-mean-square error (NMRSE) sense:

$$\text{NMRSE} = \left[\sum_{n=0}^{N-1} \frac{(s[n] - \hat{s}[n])^2}{s[n]^2}\right]^{\frac{1}{2}} \tag{5.2}$$

where $s[n]$ and $\hat{s}[n]$ are the real and synthesised signals respectively. The NMRSE is used because it is independent of empirical data size [137] and allows a comparison of results with other methods for modelling heart sounds [37, 75]. Afterwards, the relationship between this model order and the distribution of the singular values for the case of the PCG signals is derived.

The matching between the real signal and the synthesised one is also estimated by the normalised cross-correlation coefficient NCC which is defined for the case of zero shift between $s[n]$ and $\hat{s}[n]$ as

$$NCC = \frac{r_{s\hat{s}}[0]}{\sqrt{r_{ss}[0]r_{\hat{s}\hat{s}}[0]}};$$ (5.3)

where r represents the operation of correlation.

In all the cases, the objective is to maximise NCC and to minimise the NMRSE. In more than 200 sample cases obtained from the 150 subjects under examination the average value of NCC was 99.65% and the average value of NMRSE was 5.4%. As an example, Figure 5.1 and Figure 5.2 show the real and the synthetic signals for four different cases of S1 and S2. Table 5.2 and Table 5.3 give the model parameters governing the synthesised signals shown in Figure 5.1 and Figure 5.2 respectively. From Figure 5.1 and Figure 5.2 it can be seen that the real and synthesised signals are almost identical.
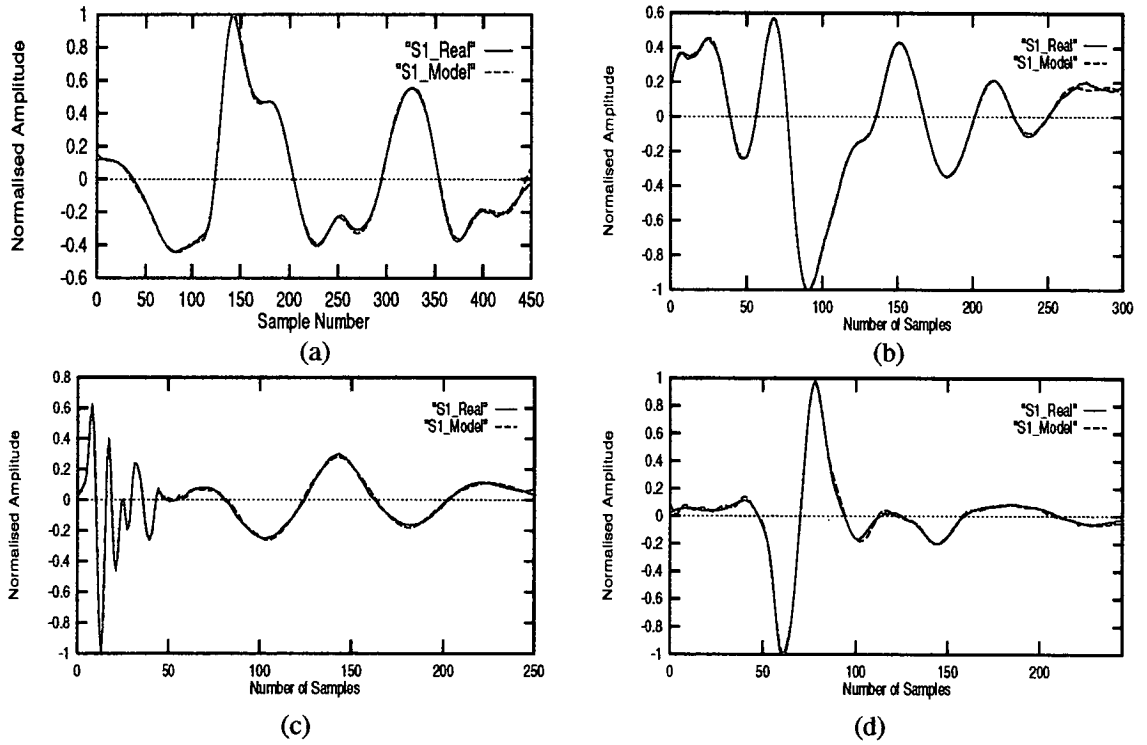
Figure 5.1:   Real (green line) and synthetic signals (blue line) of S1 for four different subjects: (a) a normal patient, (b) a patient with a dysfunctioning native mitral valve, (c) a patient with mechanical artificial heart valve, (d) a patient with bioprosthetic artificial heart valve.

(a)

(b)

(c)

(d)
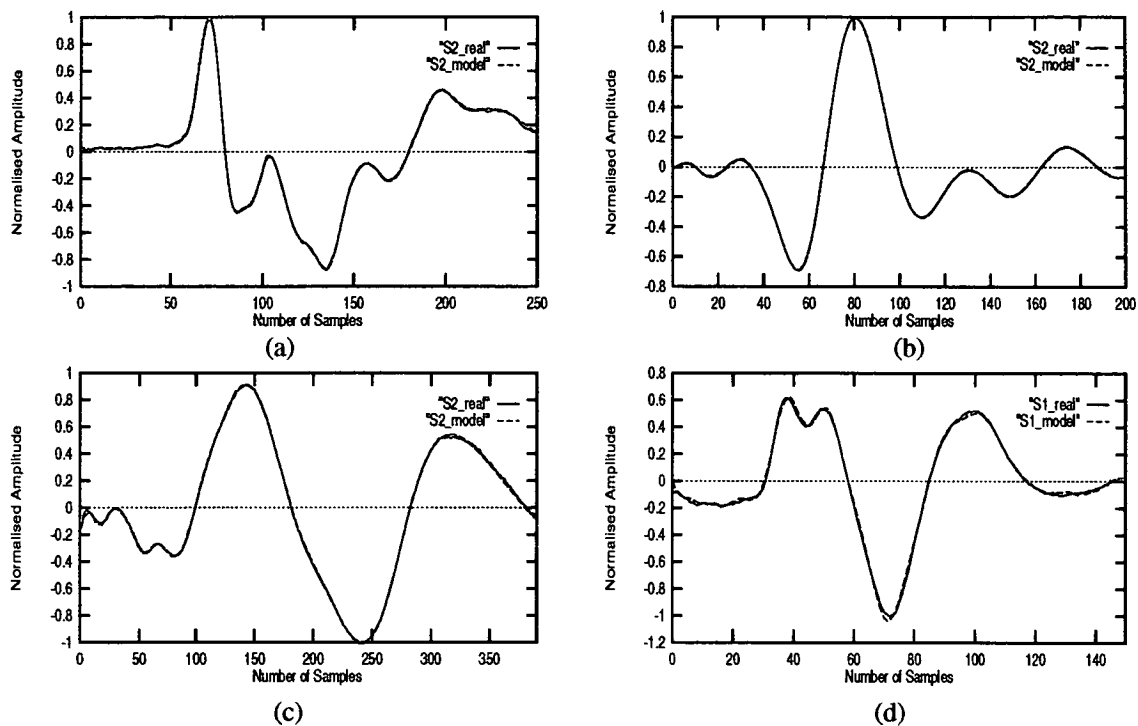
Figure 5.2:   Real (green line) and synthetic (blue line) signals of S2 for four different subjects: (a) a normal patient, (b) a patient with a dysfunctioning native aortic valve, (c) a patient with mechanical artificial heart valve, (d) a patient with bioprosthetic artificial heart valve.

Table 5.1 gives the characteristics of these signals.

	NCC%	NMRSE%	Duration ms.	No. of Comp.
Figure 5.1(a)	99.91	4.02	90	8
Figure 5.1(b)	99.95	2.95	60	7
Figure 5.1(c)	99.81	6.1	50	11
Figure 5.1(d)	99.90	4.43	110	11
Figure 5.2(a)	99.93	1.8	54	11
Figure 5.2(b)	99.98	1.17	40	8
Figure 5.2(c)	99.98	1.96	78	8
Figure 5.2(d)	99.87	4.49	80	7

Table 5.1:   Performance of the MFBPM for the signals shown in Figures 5.1 and 5.2. NCC is the normalised cross-correlation coefficient, NMRSE is the normalised-mean-square-error, and 'No. of Comp.' describes the optimum number of components in eq.(5.1) for the synthesised signal.

Comp	f[i] Hz	A[i]	d[i]	φ [i]
1	14.0	0.618	0.0065	5.198
2	31.1	1.0	0.001	1.51
3	56.6	0.212	0.00015	3.48
4	77.1	0.185	0.0009	1.31
5	96.02	0.481	0.006	3.347
6	122.5	0.452	0.01114	5.04
7	144.98	0.203	0.01	0.833
8	175.9	0.039	0.0048	2.51

(a)

Comp	f[i] Hz	A[i]	d[i]	φ[i]
1	10.7	0.847	0.0095	2.986
2	44.1	1.0	0.0089	5.699
3	70.47	0.608	0.0055	1.397
4	103.8	0.39	0.0047	5.412
5	129.9	0.603	0.014	2.354
6	177.6	0.241	0.0152	4.822
7	212.04	0.123	0.0124	0.37

(b)

Comp	f[i] Hz	A[i]	d[i]	φ[i]
1	18.9	0.006	0.009	3.546
2	56.46	0.115	0.001	3.99
3	81.9	0.085	0.0048	5.72
4	172.34	0.0026	0.0009	2.186
5	243.77	0.49	0.0068	5.26
6	323.99	0.073	0.011	5.74
7	357.0	0.688	0.042	3.88
8	469.6	0.135	0.044	0.64
9	588.03	1.0	0.102	1.7
10	755.25	0.329	0.072	4.05
11	1105.98	0.0255	0.042	3.88

(c)

Comp	f[i] Hz	A[i]	d[i]	φ[i]
1	20.38	0.183	0.007	2.19
2	39.43	1.84	0.033	4.77
3	49.94	2.15	0.031	1.17
4	71.48	0.95	0.0316	2.8
5	96.04	0.44	0.027	4.08
6	111.03	0.18	0.015	5.71
7	132.95	0.019	0.012	5.91
8	148.14	0.021	0.014	2.72
9	164.06	0.039	0.019	5.1
10	197.13	0.016	0.015	5.71
11	231.17	0.006	0.01	6.19

(d)

Table 5.2: Parameters for the components of the modelled signals shown in the four parts (a) to (d) of Figure 5.1; $f[i]$ frequency, $A[i]$ amplitude, $d[i]$ damping factor, and $\phi[i]$ phase of the synthesized signal.

Columns 1 and 2 give the NCC and the NMRSE between the real signals and the synthesised ones, whilst column three and four present the duration of the signal and the optimal number of the decayed sinusoids (p) to synthesise these signals respectively.

Results obtained by MFBPM are compared with MBPM and FBPM for all the cases. The improvement in accuracy in terms of the NMRSE of MFBPM is up to 10% compared with MBPM and up to 20% compared with FBPM. Table 5.4 summarises results

obtained from normal subjects with normally functioning native heart valves for recordings made in the mitral position (i.e. S1). From this table it is clear that MFBPM is always superior to both MBPM and FBPM. The main part of error in the FBPM comes from cases where there is a big difference between the order of the model (p) and the number of poles outside the unit circle.

Comp	f[i] Hz	A[i]	d[i]	$\phi[i]$
1	26.0	0.575	0.0045	0.627
2	41.0	1.0	0.02	3.197
3	103.0	0.031	0.002	6.05
4	120.0	0.285	0.0065	3.738
5	170.2	0.436	0.019	5.219
6	201.6	0.146	0.0014	1.24
7	245.0	0.2	0.024	5.68
8	279.2	0.019	0.02	1.34
9	337.0	0.363	0.0209	2.18
10	376.0	0.228	0.015	3.184
11	426.1	0.012	0.012	3.34

(b)

Comp	f[i] Hz	A[i]	d[i]	$\phi[i]$
1	38.31	0.51	0.015	4.27
2	68.03	1.0	0.022	0.53
3	108.28	0.494	0.012	2.88
4	167.08	0.162	0.031	4.24
5	224.49	0.0622	0.035	5.81
6	288.89	0.001	0.0044	1.59
7	363.95	0.001	0.009	5.01
8	430.22	0.004	0.025	3.83

(b)

Comp	f[i] Hz	A[i]	d[i]	$\phi[i]$
1	19.44	0.795	0.0005	5.13
2	31.69	1.0	0.001	1.72
3	60.84	0.28	0.0026	3.88
4	80.23	0.088	0.0034	4.46
5	111.17	0.354	0.01	4.75
6	144.25	0.317	0.019	0.86
7	238.26	0.004	0.003	5.74
8	265.07	0.041	0.017	5.26

(c)

Comp	f[i] Hz	A[i]	d[i]	$\phi[i]$
1	23.36	0.18	0.0029	5.76
2	38.39	0.32	0.004	2.32
3	57.64	0.11	0.007	4.17
4	84.57	0.096	0.014	4.59
5	122.69	0.107	0.0027	0.20
6	149.37	0.101	0.033	2.69
7	181.03	0.049	0.02	5.15

(d)

Table 5.3: Parameters for the components of the modelled signals shown in the four parts (a) to (d) of Figure 5.2; $f[i]$ frequency, $A[i]$ amplitude, $d[i]$ damping factor, and $\phi[i]$ phase of the synthesized signal.

The physiological explanation for this difference could be as follows; some of the frequency resonance modes of the externally recorded PCG signal are related to the oscil-

lation of the lung-thorax system. Amongst these, there are components related to the vibration of the lung-thorax structures very close to the area of recording. Therefore their damping factor is almost zero (i.e. poles of the signal lie on the unit circle). As a result of the extended order of the polynomial, and the perturbation of the matrices, it is always possible that their value fluctuates very close to the unit circle. FBPM therefore does not take into account cases when these poles move randomly inside the unit circle. In contrast to that, the MFBPM uses the p largest roots instead of the roots outside the unit circle. Hence, MFBPM is independent of motion in the polynomial roots.

	MFBPM		MBPM		FBPM	
	NCC%	NMRSE%	NCC%	NMRSE%	NCC%	NMRSE%
1	99.9	4.3	99.6	8.9	99.26	12.09
2	99.98	1.6	99.9	1.76	99.98	1.6
3	99.93	1.8	99.75	7.01	98.51	17.14
4	99.85	5.3	99.5	9.95	90.29	42.96
5	99.49	9.6	99.43	10.8	99.48	10.12
6	99.5	9.2	99.41	10.82	99.12	13.19
7	99.51	8.9	96.17	27.33	97.18	23.55
8	99.57	8.5	98.86	15.2	98.26	18.56
9	99.79	6.3	99.5	9.9	99.79	6.3
10	99.45	9.7	94.59	32.24	98.45	17.51
11	99.77	6.6	99.51	9.8	99.04	13.76
12	99.77	6.6	99.51	9.8	99.04	13.76
AVR	99.69	6.5	99.08	14.63	96.6	17.99

Table 5.4:   Performance of MFBPM, MBPM and FBPM in the cases of normal subjects for the S1. NCC is the normalised cross-correlation coefficient, NMRSE is the normalised-mean-square-error. The last row gives the average values for the corresponding parameters.

The improvement in accuracy of MFBPM compared with MBPM is related to the reduction of the bias in the estimation of the position of the signal poles, which results in a better estimation of the amplitude, phase and damping factor. Another factor which affects the performance of the algorithm is the extended order p_e. Table 5.5 describes the impact of the p_e parameter on the performance of the algorithm in the

case of a normal subject. Results obtained from all the other cases are very similar. It is found that the best results could be achieved when $0.4N \leq p_e \leq 0.45N$ where N is the data length. This finding is in accordance with what would be expected from these methods [138, 139]. For these values the matrices $\mathbf{X_b}$ and $\mathbf{X_f}$ are nearly square which makes them less sensitive to the statistical anomalies in the data being analysed than would be the case for lower orders [109, 138].

NMRSE as a function of p and $\frac{p_e}{N}$			
p	$\frac{p_e}{N}$		
	0.22	0.42	0.48
2	66.39	59.70	62.3
4	56.96	57.21	63.4
6	53.50	31.43	26.89
8	47.51	18.65	25.55
10	58.28	12.65	17.51
12	66.37	16.77	18.16
14	66.14	13.03	20.00
16	66.87	13.32	21.50
18	68.00	4.26	3.98
20	65.92	4.23	4.94
22	63.30	3.21	4.22
24	65.98	3.27	19.11
26	67.43	3.5	19.16
28	66.39	3.54	19.18
30	66.43	3.62	19.19

Table 5.5:   Performance of MFBPM in a case of S2 as a function of the extended order p_e in absolute range ($\frac{p_e}{N}$) for different model orders.

The deterioration in performance for $p_e \geq 0.45N$ could be explained by the higher order of the polynomials $(B(z)$ $(F(z))$. An overestimated degree of these polynomials (p_e) improves the accuracy of the position of the signal poles p [120, 121], however, for very high values of p_e their position may diverge in practice [118]. Thus, in all cases the extended order of $\mathbf{X_b}$ and $\mathbf{X_f}$ is selected to be in the interval $0.4N \leq p_e \leq 0.45N$.

Bearing in mind that S1 and S2 last for about 30-100 ms and that the lowest sampling rate used to record the PCG signal was 5 kHz, the above mentioned range of p_e parameter leads to an order, at least, greater than seventy for $B(z)$ and $F(z)$ polynomials. Consequently the method used to estimate the roots of $B(z)$ and $F(z)$ polynomials is of paramount importance in the general performance of MFBPM algorithm. To present the improvement that the eigen-value decomposition method (EVDM) gives over other classical methods, such as Laguerre's method (LM) applied elsewhere [118], to estimate the roots of $B(z)$ and $F(z)$ polynomials, three different examples are presented in Figures 5.3 to 5.6. In the case of LM, a algorithm presented in [124] was implemented.

Figure 5.3 and Figure 5.4 show the position of the polynomial roots estimated respectively by LM and EVDM method in the case of a synthetic signal composed of two damped sinusoids generated by (4.68).

(a)   (b)

Figure 5.3:   Location of the polynomial roots in the case of the synthesesid signal generated by (4.68) for extended order $p_e = 10$ using LM method; (a) estimated location of the polynomial roots in backward ($\Diamond$) and forward direction (+), (b) final location of signal poles.

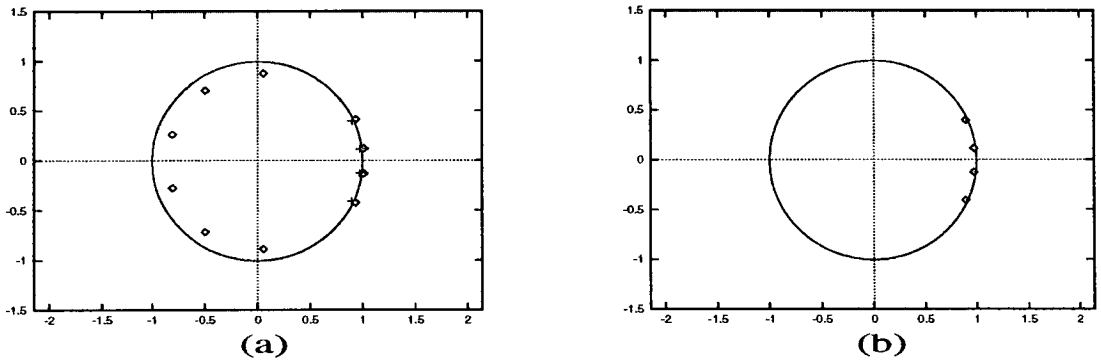
(a)   (b)
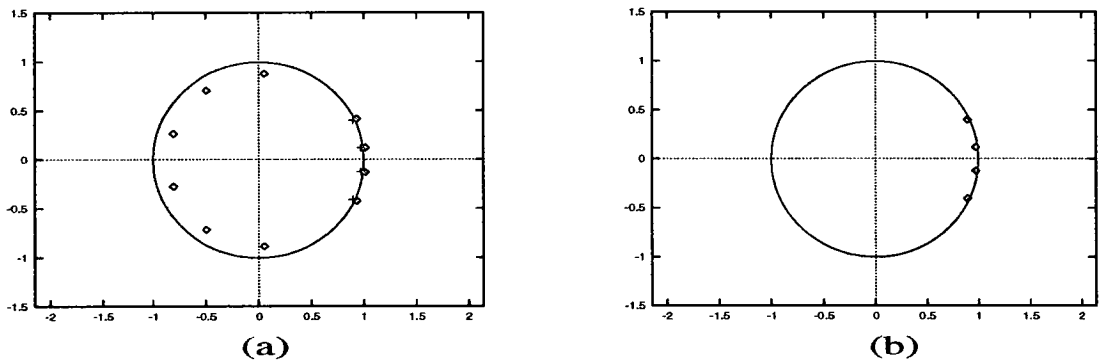
Figure 5.4:   Location of the polynomial roots in the case of the synthesesid signal generated by (4.68) for extended order $p_e = 10$ using EVDM method; (a) estimated location of the polynomial roots in backward ($\Diamond$) and in forward direction(+) , (b) final location of signal poles.

In both these cases the extended model order, p_e, has a moderate value (i.e. $p_e = 10$, note $p_e > 2p$). It is clear from Figure 5.3 and Figure 5.4 that both methods perform equally well in estimating the position of polynomial roots resulting in an excellent match between the synthetic signal and the modelled signal (i.e. in both cases NCC=100% and NMRSE=0). However, as the extended model order of the polynomial increases, the performance of LM methods deteriorate. Figure 5.5(a) and (b) give the performance of LM and EVDM methods respectivelly for the case of an extended order of $p_e = 18$. From Figure 5.5(a) it can be seen that the estimated roots diverge from their real position in the case of LM method, whereas EVDM still gives an accurate estimation of their location. In the case of the LM method the matching between synthetic signal and the modelled one drops to NCC=50%. The performance of the LM method further deteriorates as the order p_e is extended.

The performance of the LM method worsens in the case of heart sounds. Figure 5.6 gives the estimated root locations obtained using the LM method(Figure 5.6(a)) and EVDM ((Figure 5.6(b)) for the case of a signal modelled as a sum of eight damped sinusoids. The paramters of this synthesised signal were given in Table 5.3(b).

(a) (b)
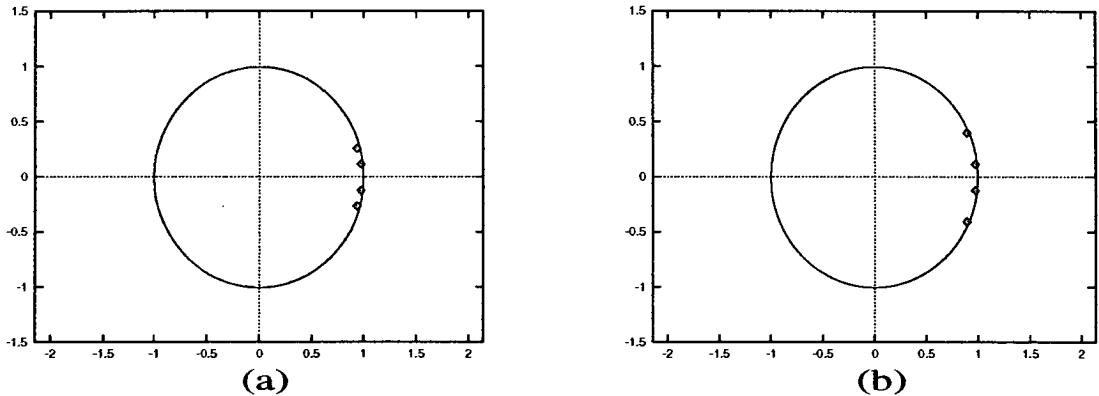
Figure 5.5:   Location of the estimated signal poles in the case of the synthesised signal generated by (4.68) for extended order $p_e = 18$; (a) using LM method, and (b) using EVDM method.

In this case the extended model order, p_e, is selected as 34. The algorithm based on EVDM obtains a very accurate matching between the synthesised signal and the modelled one (i.e. NCC=100%, NMRSE=0.0), whereas in the case when LM method is used the accuracy in the mathching is only 26%.
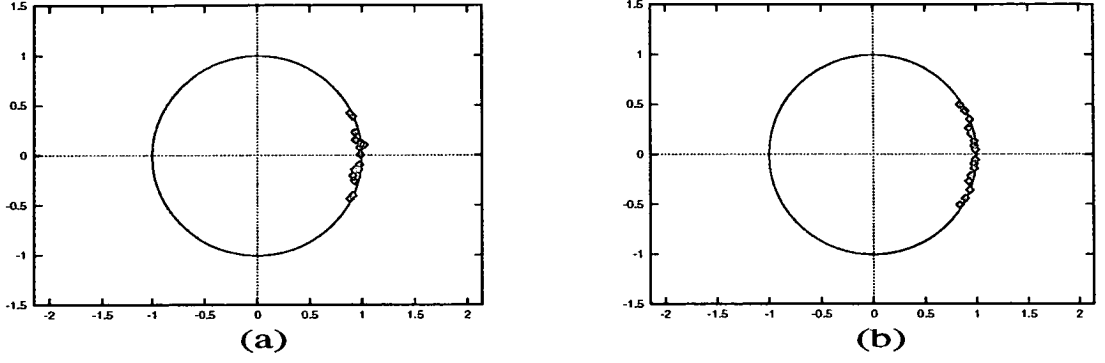
Figure 5.6: Location of the estimated signal poles in the case of a synthesised heart sound generated by (5.1) for extended order $p_e=34$; (a) using LM method, and (b) using EVDM method.

The reason for the poor performance of the LM method compared to EVDM is because of the nature of the PCG signal and the inability of LM method to estimate the location of polynomial roots in the case of high order ill-conditioned polynomials. S1 and S2 contain very close frequency components, which means that the polynomial roots are located very close to each other. Therefore conventional techniques such as the LM method are unable to converge to an accurate estimation. Instead, the roots are sprawled all over the complex plane. In this respect, the EVDM is a more robust technique, largely because of the fairly sophisticated convergence method embodied by the balancing technique used. However, it must be mentioned that the EVDM requires more computation than the LM method which results in an execution time which is a factor of 2 times slower in operation.

To examine the stability of the MFBPM algorithm the synthesised sounds have been remodelled. Results of this complimentary analysis shown that in all cases MFBPM produces a very stable estimation (i.e. NCC=100% and NMRSE=0.0) between the synthesised and remodelled signals.

Comparison of these results with those quoted in Cloutier's work [37,75] show that this method is 50% more accurate in modelling heart sounds in terms of NMRSE than method presented in [37,75]. In addition, MFBPM has the following advantages over those methods:

- It does not require *a priori* knowledge of the duration of S1 or S2.

- It does not need an initialisation for the phase parameter.

- It does not require an interactive procedure for adjusting the model parameters.

For all these reasons, it is proposed that MFBPM represents a very good method for modelling the S1 and S2. Furthermore, MFBPM provides a very accurate and stable estimator for a large variety of cases ranged from native heart valves to MPHV.

5.3 Performance of different spectral methods when applied to analysis of S1 and S2

To explain some of the important findings of this study, some examples of the performance of these spectral analysis methods are given for the signals in Figures 5.1 and 5.2. It must be said that other examples obtained from the remaining subjects give very similar results.

5.3.1 Performance of the FFT

Figure 5.7 represents the spectrum produced by the FFT in cases of signals shown respectively in Figure 5.2(a) for S2 in a healthy subject with native valve, and in Figure 5.1(b) for a subject with malfunctioning native valve. Figure 5.1(c) shows the spectrum for S1 in a normal subject with mechanical prosthetic heart valve in the mitral position.

(a) (b) (c)
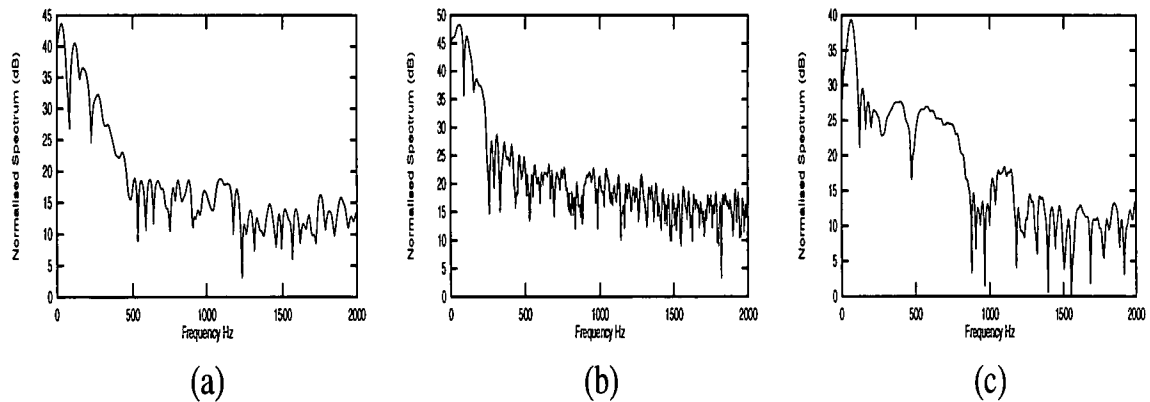
Figure 5.7: Performance of the FFT when applied to the analysis of the sounds shown in Figures 5.2(a), 5.1(b), and 5.1(c) respectively.

Comparing the spectrum produced by the FFT (i.e. Figure 5.7) with the spectral components contained in the respective signals (see Table 5.2 and Table 5.3), it is clear

that the FFT method does not have sufficient resolution to detect all the peaks in the respective signals. In almost all the cases spectral peaks have merged together in the power spectrum plot as a result of the poor resolution of the FFT.

5.3.2 Performance of AR estimator

In general, the ARB algorithm produces a representation of the envelope of the spectrum rather than a clear picture of the spectral components regardless of the choice of window. Figure 5.8 shows the spectrum produced when a ARB-H is applied for different model orders in the case of the S2 signal shown in Figure 5.2(a). For model order equal to the actual order (i.e. $p=22$, it has been shown that for a signal composed of m real sinusoids $2m$ coefficients are required to define the m poles in the generating system [130,131]) this method can detect only one or two of the largest amplitude spectral peaks of the signal spectrum (Figure 5.8(a)). This result is in agreement with previous work presented by Cloutier et al [37,75]. There is an improvement when the order is increased but this is also accompanied by spurious peaks, especially outside the signal frequency band (Figure 5.8(b)(c)). This result would be expected from this estimator especially when 'peaky' power spectra are being analysed [106].

The effect of the window choice was also investigated. Figure 5.9 shows the performance of four different windows for $p=50$. As was expected, the window function has an impact only on the variance of the spectral estimator. Amongst the three types of windows, the Hamming window was found to be the best regarding the variance for the detected peaks produced by this method. However, the performance of this method is so poor that it is not worthwhile improving its performance by optimising the window function.

(a) (b) (c)
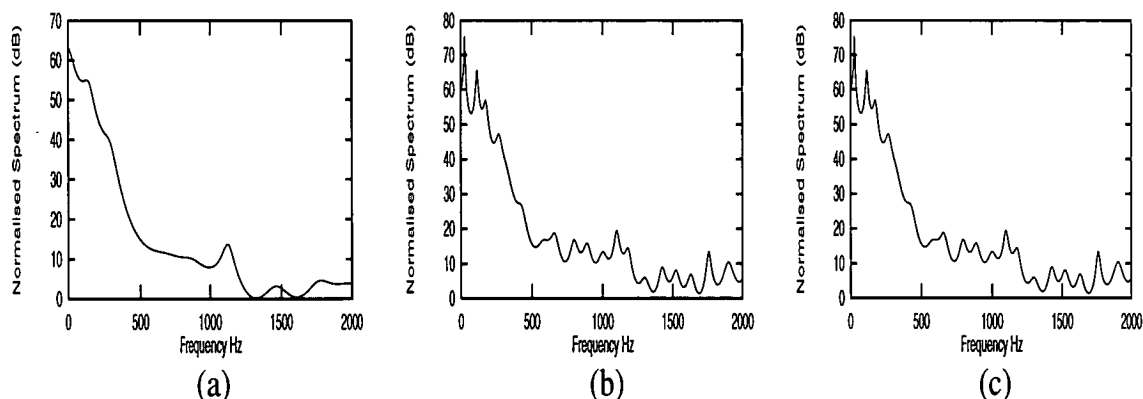
Figure 5.8:   Performance of ARB algorithm as a function of model order p using a Hamming window in the case of S2 signal shown in Figure 5.2(a), (a)$p = 22$, (b) $p = 50$, (c) $p = 80$.

(a)

(b)

(c)

(d)
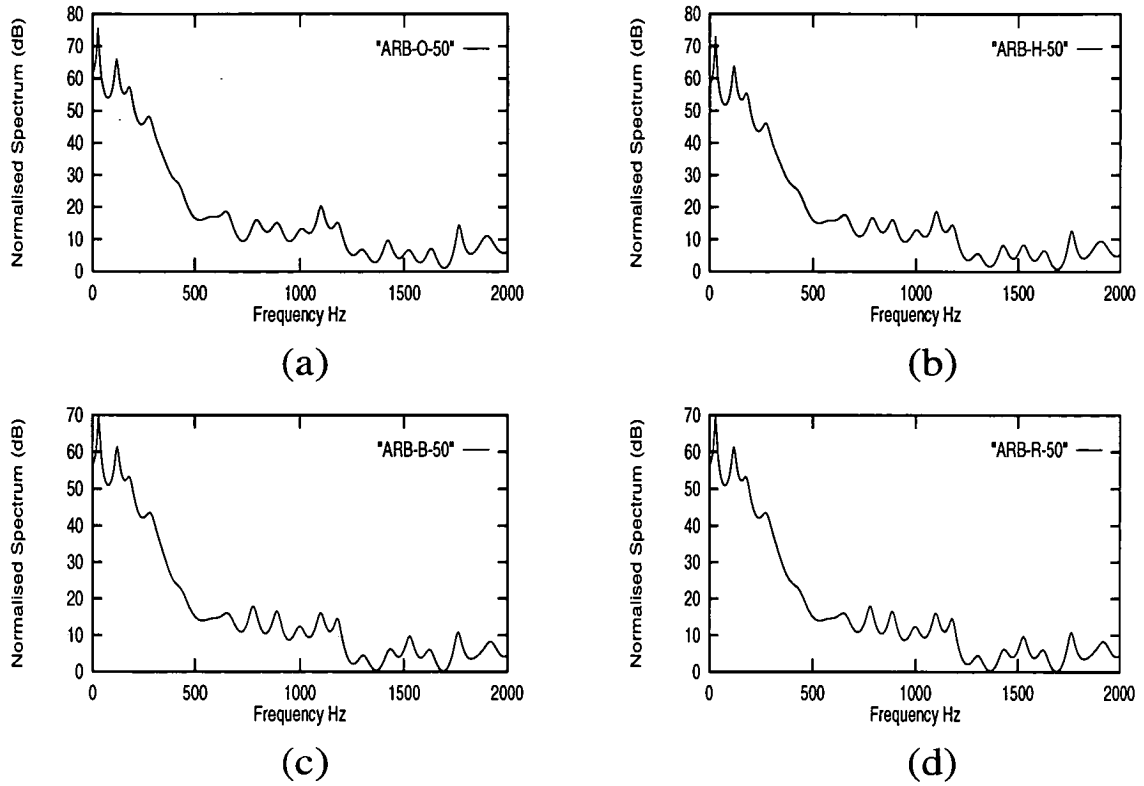
Figure 5.9:   Performance of ARB algorithm method for four different types of windows for order $p = 50$; (a) optimum, (b) Hamming, (c) Burg, and (d) rectangular window.

From the results obtained with the FFT and ARB based algorithm, it can be said that neither of these methods represent sufficiently accurately the spectral composition of S1 and S2.

These two conventional techniques, which are extensively used for analysing S1 and S2 [26, 27, 30–32, 42, 62, 67, 74, 79, 80, 90, 134] , do not extract the information specific to the resonance frequencies of the heart-valve system. Instead, they provide a global spectrum resulting from the summation of the various resonance modes of the sound in which the individual resonant frequencies are merged into a few dominant peaks (i.e. 3 to 4 peaks).

5.3.3   Performance of SVD-based techniques

A major improvement in spectral resolution has been found by employing SVD techniques compared with either the FFT or ARB algorithm. Power spectra produced by these methods for various signals are shown in Figures 5.10- 5.12. Table 5.6 gives the spectral peaks detected by certain of the methods outlined in the previous chapter when applied to the signal shown in the Figure 5.2(a). Performance of the ARMA3 is not

included in this table because it produces a very smooth spectra and cannot resolve most of the spectral peaks (Figure 5.11 (c)). In terms of spectral resolution, results obtained from all the other subjects are very similar.

Frequency Component(Hz)	Spectral Method			
	SSI	ARMA1	ARMA2	PSE
26.0	28.0	20.0	20.0	26.0
41.0	-.-	34.0	35.0	41.0
103.0	92.0	106.0	104.0	103.0
120.7	115.0	122.0	120.0	124.0
170.2	174.0	164.0	175.0	167.0
201.6	203.0	191.0	194.0	201.0
245.0	-.-	243.0	245.0	244.0
279.2	260.0	270.0	272.0	-.-
337.5	345.0	-.-	-.-	326.0
376.8	385.0	-.-	-.-	360.0
426.17	-.-	-.-	-.-	430.0

Table 5.6: Spectral peaks of the PSD produced by several parametric methods for the signal shown in Figure 5.2 (a). '-.-' represents a failure to detect the particular spectral peak.

Performance of SSI method

A significant improvement compared with ARB was found for the case of the SSI algorithm. Figure 5.10 presents the performance of this method in the case of signals shown respectively in Figure 5.2(a) , 5.1(b), and 5.1(c).

However, this method suffers from three main problems: (a) sometimes it is not able to detect peaks which are very close together (e.g. spectral components at 26 Hz and 41 Hz in Figure 5.10(a), 103 Hz and 129 Hz in Figure 5.10(b)), (b) it is not capable of detecting frequency components with relatively small amplitude (e.g. the peak at 426.17 Hz in Figure 5.10(a), the peaks at 755 Hz and 1105 Hz in Figure 5.10(c)), and (c) a relatively small degree of variance on the estimated spectral components (see the second column of Table 5.6). Moreover, the sharpness of peaks produced is not as good as is desired. Generally, however, this method performs much better than either the FFT, ARB or ARMA3 (Figure 5.11(c)).

(a) (b) (c)

Figure 5.10:   Performance of SSI algorithm in three different cases; (a) S2 shown in Figure 5.2(a), (b) S1 shown in Figure 5.1(b), and (c) S1 shown in Figure 5.1(c)

Performance of ARMA algorithms

Figure 5.11 illustrates the spectra produced by ARMA1, ARMA2, and ARMA3 for the signal shown in Figure 5.2 (a). It is clear from this figure, that the ARMA3 method gives the smoothest spectral estimation amongst all other methods. The performance of ARMA3 is in some extent very similar to spectra produced by ARB algorithms for model order equal to the real one in terms of spectral resolution (Figure 5.11(c)).

However, ARMA1 and ARMA2 methods perform much better than ARMA3 and other conventional techniques. ARMA1 and ARMA2 give very similar results for the variance of the spectral components detected. Generally ARMA2 tends to give a smaller error although in most of the cases the difference is negligible. Both these methods suffer to some extent from the same problems as the SSI algorithm. However, their performance is on the whole better than SSI.

(a) (b) (c)
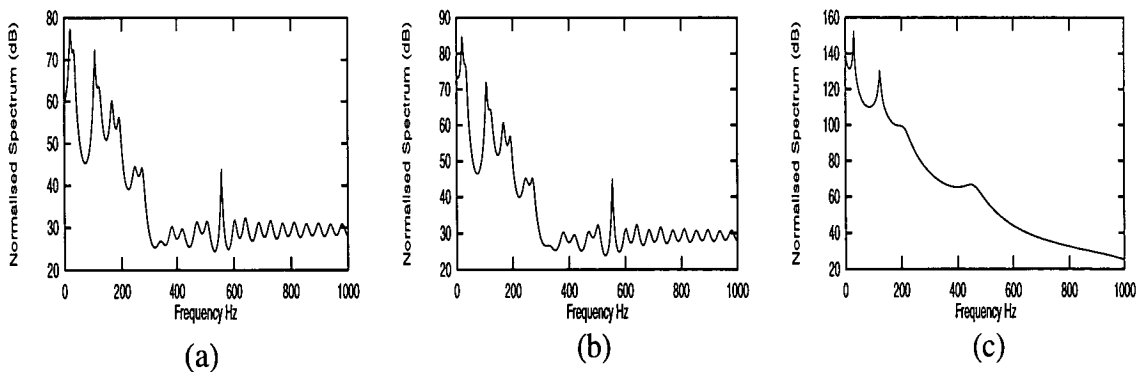
Figure 5.11:   Power spectrum produced by ARMA algorithms:(a) ARMA1, (b) ARMA2, (c)ARMA3 for the signal shown in Figure 5.2 (a).

80

Prony's spectral estimator (PSE)

Figure 5.12 shows the power spectrum produced by PSE for some of the signals shown in Figure 5.1 and Figure 5.2. The model parameters are estimated by using MFBPM and then the PSE is estimated using (4.61). The power spectrum produced by PSE gives the best spectral estimator in terms of resolution, variance, and clarity of the spectrum. In more than 90% of the cases it was able to produce clear and distinguishable peaks with very small variance. In contrast to other methods, which were not capable of detecting frequency components with relatively small amplitude, the power spectrum produced by PSE give an accurate estimation of them. For instance, the spectral peak at 1105 Hz (Figure 5.12(c)) and at 426 Hz (Figure 5.12(a)), which were not detected by the other methods, are now clearly apparent.

However, in some cases, the spectrum produced by this estimator still fails to detect all the components (e.g. the peak at 279 Hz in Figure 5.12(a)). This effect arises because the fast-decaying sinusoids have wide spectral peaks, and those close to each other are often identified as a merged power spectrum estimate.

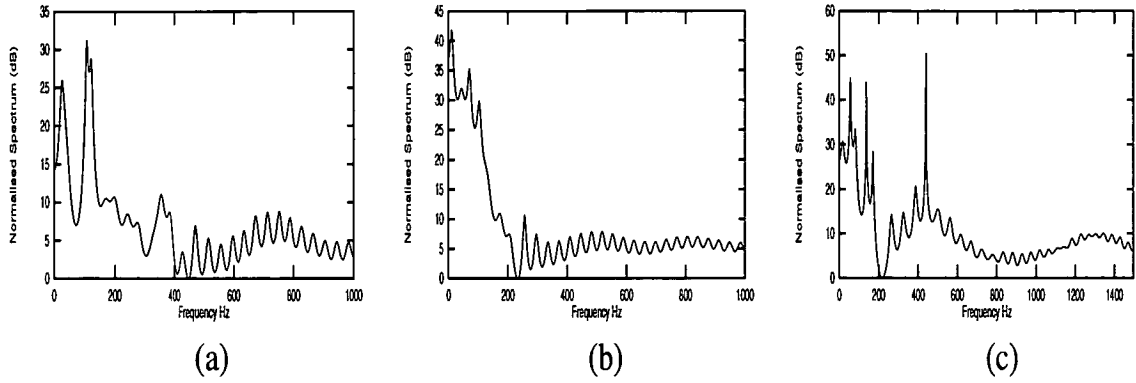(a)   (b)   (c)
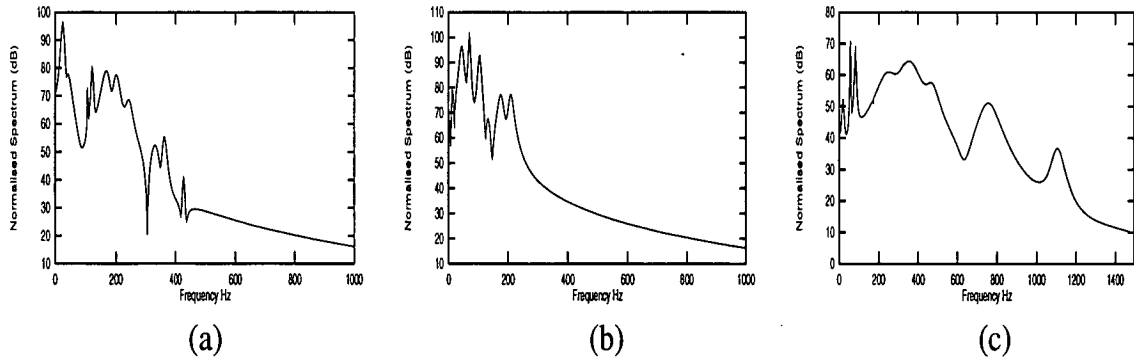
Figure 5.12:   Performance of PSE spectral estimator in three different cases; (a)S2 shown in Figure 5.2(a), (b) S1 shown in Figure 5.1(b), and (c) S1 shown in Figure 5.1(c)

Regarding the fact that the PSD, even in the case of Prony's method, does not produce a proper representation of the resonance frequencies of heart sounds and, as the final goal is to use the extracted parameters for automatic classification, it seems that it would be better to use the parametric description obtained directly from time-domain modelling of heart sounds. This conclusion is also supported by the fact that the power spectrum calculated by parametric methods is a linear operation based on the discrete Fourier transform of the respective coefficients. Thus, the amount of information is

the same, only the manner of representing it differs. Parameters obtained by time-domain modelling not only represent S1 and S2 with very high accuracy, but, also are obtainable without extra calculation necessary to obtain the spectrum or to extract heuristic characteristics from it.

5.4   Model order selection

Figures 5.13 and Figure 5.14 give the performance of the model order selection methods for the case of S2 (Figure 5.2(a)) and S1 (Figure 5.1(c)). In figures (a)-(d) the normalised amplitude of FPE, AIC, CAT, and MDL versus the model order is plotted, whereas figures (e) and (f) show the distribution of eigenvalues in dB scale and their CRME ratio for the respective signals. For all model order criteria the aim is to derive a relationship between their respective amplitude distribution and the actual model order of the signal. Table 5.7 gives the model order estimated by different criteria for the signals shown in Figures 5.1 and 5.2. The actual order is derived from time-domain modelling based on a mean-least-square criterion as described in section 5.2.

In most of the cases the FPE and AIC do not yield consistent estimates of the model order. Their performance is very similar because they are in fact asymptotically equivalent [140]. Amongst the four criteria, the CAT criterion performs the worst. In general it gives a very overestimated order. Regarding the MDL it appears to give the best estimate of the the actual order compared with the other three. These results confirm the theoretical findings given by Wax [127] for the case of real signals. Although this consistency in closeness between the real and estimated model order is high, MDL does not return the actual order in a considerable number of cases. This can be seen from the Table 5.7 where the performance of FPE, AIC, CAT, and MDL is given for the signal shown in Figures 5.1 and 5.2. Comparing column five with six, it is clear that the MDL identifies the proper order only in 50% of the cases. However, the estimated model order obtained using MDL is always closer to the actual model than those given by FPE, AIC, and CAT. From this table, it can also be clearly seen that CAT produces a vastly overestimated model order. It must be emphisesed that the conclusions drawn from Table 5.7 for FPE, AIC, CAT, and MDL criteria are also found in all the remainig patients studied in this thesis.

	FPE	AIC	CAT	MDL	Actual Order
Figure 5.1(a)	22	24	70	6	8
Figure 5.1(b)	6	6	40	7	7
Figure 5.1(c)	18	18	32	11	11
Figure 5.1(d)	8	6	45	6	11
Figure 5.2(a)	15	15	68	9	11
Figure 5.2(b)	3	8	12	8	8
Figure 5.2(c)	12	12	46	8	8
Figure 5.2(d)	9	9	10	8	7

Table 5.7:   Performance of the the model order selection criteria in the case of the signals shown in Figure (5.1 and 5.2); FPE, AIC, CAT, and MDL
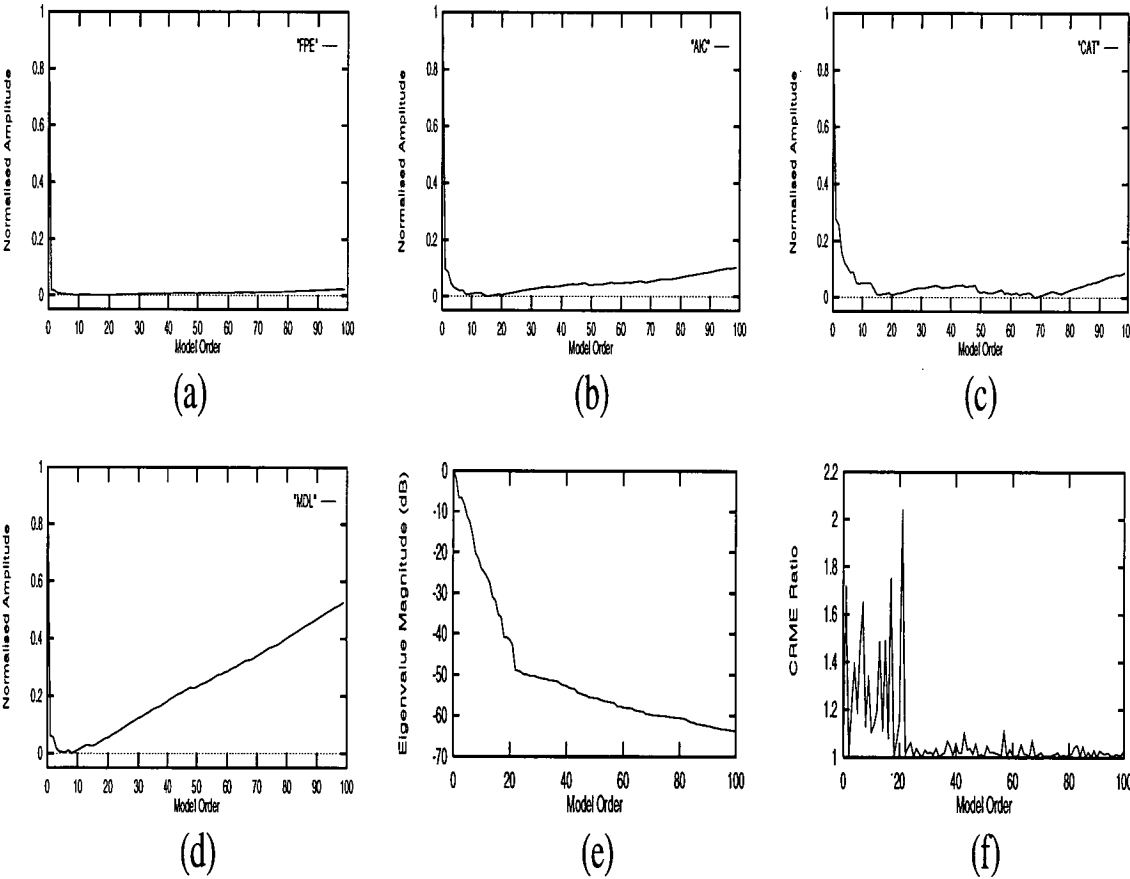
Figure 5.13:   The magnitude of several model order selection criteria for the case of the signal shown in Figure 5.2 (a) (i.e. S2); (a) FPE, (b) AIC, (c) CAT, (d) MDL, (e) eigenvalue magnitude, (f) CRME.
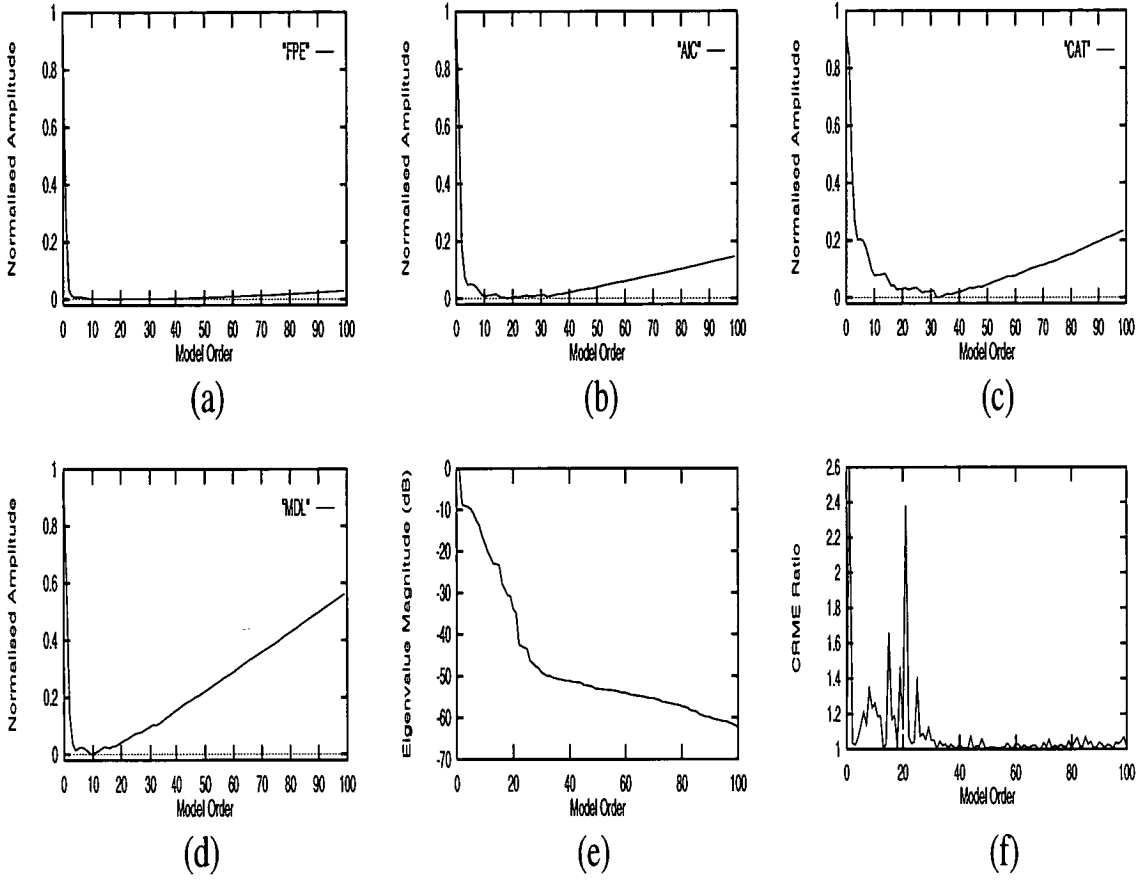
Figure 5.14: The magnitude of several model order selection criteria for the case of the signal shown in Figure 5.1 (c) (i.e. S1), (a) FPE, (b) AIC, (c) CAT, (d) MDL, (e) eigenvalue magnitude, and (f) CRME.

In contrast to the performance of FPE, AIC, CAT and MDL criteria, it can be said that criteria based on the distribution of eigenvalues produce a more consistent estimate of the correct model order. It should be observed that the knee on the plot of the eigenvalue magnitude (Figure 5.13 (e), 5.14 (e)) associated with the biggest CRME ratio, $(\frac{\sigma[i]}{\sigma[i+1]})$(Figures 5.13 (f), 5.14(f)) which lies in the region -40 dB to -60 dB can be used as a criterion for estimating the proper order of the model in the case of S1 and S2. From Figure 5.13 and 5.14 it can be seen that the rank of the matrix (in these cases it is 22) is exactly estimated from the CRME ratio (note that in the case of a real signal containing p components, the rank of the data matrix is $2p$ [104,115]). The wide range of the parameter M (-40 dB $\leq$ M $\leq$ -60 dB) is related to the individual characteristics of the lung-thorax system which differ from one subject to another.

It seems that the combination of the criteria based on the eigenvalue distribution with

the MDL criterion is the best method for estimating the proper order. This is because the MDL criterion asymptotically (as N, the length of data gets very large) provides the same information as the eigenvalues of the covariance matrix [140]. This finding simplifies the procedure of deciding the best subset p without searching over all possible subsets in the case of S1 and S2 sounds.

It must be said that the order of the model in analysing S1 and S2 is always greater than five and it varies from subject to subject. This can be explained by the fact that S1 and S2 are governed mainly by the interaction of heart-valve movement with the lung-thorax system. In this context the number of spectral components of these sounds will be decided by the geometric configuration of the heart valve, its material, and heart-valve interaction with blood masses and surrounding tissues [73]. Consequently, different subjects would have their own characteristics regarding the above mentioned factors, hence the model order, p, would be different. The differences between recording systems could be another factor in explaining the discrepancies observed between results presented in this work and those presented elsewhere [10, 38, 77]. For instance, the frequency response of the system used by Foale *et al.* [77] was linear with a rise of 6 dB per octave between 30 and 1000 Hz. Therefore, it is clear that our system emphasises much higher frequencies and covers a broader signal band.

These findings also suggest that S1 and S2 are more complicated than it was previously assumed [10, 26, 77] and further investigations are required in order to improve the understanding of physiological significance of these components.

5.5   Conclusion

The performance of several spectral estimation techniques applied to the analysis of S1 and S2 has been investigated for a wide variety of subjects including normal and malfunctioning native heart valves, bioprosthetic heart valves, and mechanical prosthetic heart valves. For all the cases, synthesised first or second heart sounds were generated using the MFBPM to allow a rigourous comparison between all the methods.

It was shown that the MFBPM is a highly stable technique for modelling S1 and S2 and performs more precisely than the modified backward Prony's method with an accuracy improvement of up to 10% and up to 20% when compared with the conventional

forward-backward Prony's method. This degree of improvement in modelling S1 and S2 is due to the procedure for estimating the position of the the signal poles, which effectively reduces the sensitivity of these parameters to perturbation and round-off errors, and bias reduction on the estimation of the damping factor as a result of taking the data in both forward and backward directions. Moreover, in contrast to previous techniques in modelling S1 and S2, the proposed procedure does not require a interactive procedure for initialisation and adjusting the model parameters.

In general, it was also found that all parametric methods based on the SVD technique produce a more accurate spectral representation than the conventional methods (i.e. FFT and ARB) in terms of spectral resolution. Among these, the PSE is the best. In this context, it must be said that the conclusions of previous work regarding the spectral composition of S1 and S2 obtained using the FFT and ARB algorithm are incomplete. This concern especially arises when these methods (i.e. FFT and ARB) are used to investigate the origin of the heart sounds. On the other hand, it must be said that although advanced spectral techniques based on SVD give a large improvement in spectral representation of S1 and S2 compared to FFT and ARB, none of spectra produced by them are able to resolve all components in all the cases with the proper accuracy. Based on this finding, it is proposed that time-domain modelling of heart sounds allows a more straightforward and direct parameterisation of their information than extracting heuristic features from a spectral representation. The parameters obtained from time-modelling provide a complete parameterisation of the resonance and damping factors of the heart-valve system. Moreover, the use of the parameters of a time-domain model can lead to an easier procedure for automatic classification of the PCG signal since it does not require the extra computation to obtain the power spectrum nor extraction of features from this spectrum.

It has also been observed that the proper model order can be properly estimated from the distribution of the magnitude of the eigenvalues and their CRME. It is proposed that, for the case of S1 and S2, the model order criterion can be defined as the biggest CRME ratio in the region -40 dB to -60 dB on the eigenvalue magnitude plot. This procedure was found empirically to be very effective in estimating the proper model order in a mean-least-square sense.

Chapter 6

Spectral Characteristics of PCG Signals

6.1 Introduction

It has been suggested that resonances in heart sound spectra, resulting from vibration of mitral or aortic valve leaflets may yield useful information regarding heart valve condition *in vivo* [132] . As was described in section 2.5, SPCG has been used extensively to diagnose different valvular heart malfunctions. However, the previously reported uses of the SPCG method [5,10,26–31,33,37,41,42,48,57,58,60,65,66,68,71,72,74,80] have not realised the full potential of the phonocardiography method in one of the most fundamental aspects of heart sound study namely, the overall impact of the lung-thorax and heart-valve system on the spectral composition of S1 and S2. Such an understanding would not only allow a better interpretation of the spectral components of the sounds, but would also facilitate their use in classification procedures aimed at monitoring the condition of the native or implanted prosthetic valve. In this context, the main objectives of this chapter are:

- To investigate the impact of heart-valve movements and the lung-thorax system on the spectral composition of the externally recorded phonocardiogram

- To investigate the impact of the prosthetic heart valve type on the overall spectral composition of PCG signal

- To investigate whether or not there is a difference in the spectral composition of the PCG signal between normal and malfunctioning cases for the same prosthetic heart valve.

All the results presented here are obtained using MFBPM. This method is applied not only because its performance in representing heart sounds is superior to other methods, but it also gives a full parameterisation of the signal in terms of the amplitude, frequency, phase and damping factor, which are not available from other techniques such as FFT, AR or ARMA.

6.2 Signal parameters

In this work, results are presented in the form of average values rather than single instances. This allows for more consistency in the interpretation of the results and reduces the individual variances of the lung-thorax system from subject to subject. Five parameters are used in this respect for each class of subjects:

- The spectral distribution coefficient, F_K, which is defined as the number of spectral components in four subbands $K \in \{A,B,C,D\}$ of the overall spectrum where:

  A: 10-120 Hz (low frequency band),

  B: 120-250 Hz (medium frequency band),

  C: 250-400 Hz (high frequency band),

  D: $\geq$ 400 Hz (very high frequency band).

  This partition of the frequency spectrum is based on the results presented in previous work in this area [30, 31, 38] and matches as closely as possible the individual bandwidth of significance of the different physiological events in the cardiac system [26]. Although there are indications that frequency components beyond 400 Hz are very rare in the case of native valves, a specific subband is dedicated to these components to investigate properly that part of the spectrum where the content due to mechanical prosthetic heart valves is believed to be substantial [67,90]. However, a straightforward comparison of the results presented here with other works will prove difficult because of the differences in the PCG recording systems and the spectral analysis techniques used to analyse the signal.

- Normalised amplitude distribution coefficient W_K defined as:

$$W_K = \frac{\sum_{j \subset K} A[j]}{\sum_{i=1}^{p/2} A[i]}, \tag{6.1}$$

where $K \in \{$ A,B,C,D$\}$ and j denotes the spectral components in each band.

- A normalised energy distribution coefficient, E_K defined as:

$$E_K = \frac{\sum_{j \subset K} E[j]}{\sum_{i=1}^{p/2} E[i]},$$

(6.2)

where $E[j]$ is the energy of each spectral component contained in the signal.

- The average frequency of the largest amplitude component for each group of patients $f_{A_{max}}^{AV}$ defined as:

$$f_{A_{max}}^{AV} = \frac{\sum_{i=1}^{i=N} f_{A_{max}}[i]}{N},$$

(6.3)

where N represents the number of cases in the respective group under examination.

- The average frequency of the largest energy component for each group of patients $f_{E_{max}}^{AV}$ defined as:

$$f_{E_{max}}^{AV} = \frac{\sum_{i=1}^{i=N} f_{E_{max}}[i]}{N}$$

(6.4)

The fluctuation of the above mentioned coefficients is measured by calculating the standard deviation, σ, for each case. The five parameters used to describe the composition of PCG signals represents the main characteristics, such as the distribution of energy, amplitudes and the number of frequency components contained in the signal. They will also help to identify where in the frequency band the main contribution of heart-valve movement occurs for the case of externally recorded PCG.

6.3 Difference in spectra before and after mechanical heart valve implantation

Although it is generally accepted that the lung-thorax system represents an important factor in determining the intensity and frequency distribution of externally recorded heart sounds, its precise relationship with the number of frequency components and their respective energy has yet to be established.

To investigate the impact of the lung-thorax and heart-valve system on the spectral composition of the externally recorded PCG, thirty patients were recorded one day

before and four to six days after mechanical heart valve implantation. Half of these patients were to have a replacement mitral valve and the other half were to have a replacement aortic valve. In all the cases, patients with a malfunctioning native valve were to receive a mechanical prosthetic heart valve. The information regarding these two groups of patients is described in appendix A.

6.3.1   Model of the system

In this study the PCG signal is modelled as the interaction between the heart-valve system as a whole (i.e. myocardium tissues, adjacent vessels and the contained blood) with the lung-thorax system. The exciting source of the overall system is presumed to be the heart-valve system as a whole rather than any separate part of it, because of the uncertainties regarding the origin of the heart sound and the fact that a damaged heart valve affects the functioning of the heart as a whole. Figure 6.1 shows the model chosen.
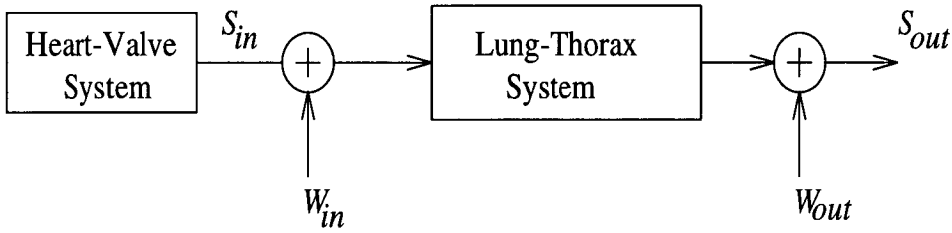
Figure 6.1:   Model of the externally recorded PCG signals.

In this model S_{in} represents the exciting source signal generated by the vibration of the heart-valve system. W_{in} is the internal noise which is a composite of respiratory sounds and thoracic muscular activity. W_{out} is the output noise which contains the effect of the ambient noise and instrumentation noise. Thus, the externally recorded PCG, S_{out}, can be seen to be a combination of the desired signal (S_{in}), superimposed noise ($W = W_{in} + W_{out}$) and the effect of the lung-thorax system. However, it is assumed that a part of the superimposed noise which consists of thoracic muscular activity, ambient noise and instrumentation noise is non-coherent with the heart sound signal [141]. Thus its effect can be diminished by taking the coherent time-average of several cardiac cycles, which may also be helpful in circumventing the difficulties caused by the beat-to-beat variation of heart sounds as was described in chapter 3. The effect of respiratory sounds is reduced by recording the PCG signal on the so-

called auscultatory areas, namely: the second right interspace, often called the **aortic** area and the cardioapex or the **mitral** area during apnea. In these areas the heart valve movements are assumed to be the "primary" source of the externally recorded PCG [132]. These assumptions lead to the conclusion that the interaction between heart-valve system and the lung-thorax system is the primary origin of the externally recorded PCG.

In our study the same patients have been recorded one day before and five to six days after implantation of a MPHV. Studying the model of Figure 6.1, S_{in} will therefore be the only input which has substantially changed as a result of surgery. It must be said that inevitable minor changes would be expected even in the lung-thorax system. However, Durand *et. al.* [142] have shown that a period of two weeks would be sufficient for the lung-thorax system to recover in the case of dogs, with even more severe surgery. Thus, all the major changes in the spectrum can be related to the S_{in} parameter.

A group of twelve normal healthy subjects were also recorded to compare the effect of a degenerated native heart valve. This group was of approximately the same age as the other patients. Comparison of the spectral composition in this latter case with cases before surgery (i.e. patients who were to have a MPHV implanted as a result of native valve disease) allows a better understanding of the impact of the native valve on the overall spectrum of the externally recorded PCG. However, it must be said that the individual differences in the properties of the lung-thorax system between the normal subject and those with malfunctioning native valves make it difficult to perform a straightforward comparison between these two groups in terms of the absolute position of spectral components.

6.3.2 Spectral characteristics of the first heart sound

It is widely accepted that the first heart sound (S1) is associated with atrioventricular valve closure [26, 132] although it is unlikely that mitral valve closure is the sole cause of this sound. It is now believed that S1 is caused by the abrupt decceleration of blood due to valve closure [30, 132]. Thus, it would be useful to identify the impact of the condition of the mitral valve on the spectral composition of S1. Table 6.1 gives the average values of F_K, W_K, and E_K coefficients for the cases of: normal subjects, patients before surgery, and patients after surgery. Table 6.2 presents the standard

deviation, for all these parameters.

	F_K coefficients			
	10-120 Hz	120-250 Hz	250-400 Hz	$\geq$ 400 Hz
Normal Subject	3.6	2.15	0.84	0.1
Before Surgery	3.53	2.15	0.69	0.0
After Surgery	3.61	1.92	1.38	4.23

(a)

	W_K coefficients			
	10-120 Hz	120-250 Hz	250-400 Hz	$\geq$ 400 Hz
Normal Subject	69.47%	26.15%	4.36%	0.017%
Before Surgery	90.55%	7.54%	1.908%	0.0%
After Surgery	61.32%	17.36%	5.12%	16.62%

(b)

	E_K coefficients			
	10-120 Hz	120-250 Hz	250-400 Hz	$\geq$ 400 Hz
Normal Subject	96.08%	3.89%	0.0074%	0.0001018%
Before Surgery	99.78%	0.17%	0.0043%	0.0%
After Surgery	95.96%	2.05%	1.49%	0.48%

(c)

Table 6.1: The average values of (a) F_K, the spectral distribution coefficient, (b) W_K, normalised amplitude distribution coefficient, and (c) E_K, normalised energy distribution coefficient for each subband of the spectrum for S1.

Comparison of the normal cases with cases before surgery shows that the number of frequency components and the relative distribution of the energy (Table 6.1 (a),(c)) are almost independent of the condition of the native mitral valve. However, there is a big difference in the distribution of the normalised amplitude coefficient. The difference in the distribution of the W_K and E_K parameters suggests that while the amplitude of frequency components is related straightforwardly to the condition of exciting source (i.e. S_{in}), the E_K parameters are mostly governed by the damping factor, which is

σ	Normal subjects	Before surgery	After surgery
σ_{F_A}	0.78	0.552	0.7
σ_{F_B}	0.78	0.86	0.64
σ_{F_C}	0.79	1.19	0.8
σ_{F_D}	0.65	-.-	3.58
σ_{W_A}	26.0	26.63	24.0
σ_{W_B}	20.9	20.95	12.2
σ_{W_C}	7.08	7.14	8.4
σ_{W_D}	0.0001	-.-	16.48
σ_{E_A}	8.19	0.47	6.53
σ_{E_B}	8.25	0.47	3.89
σ_{E_C}	0.0024	0.016	4.3
σ_{E_D}	0.0003	-.-	1.2

Table 6.2: Estimated standard deviation of F_K, W_K, and E_K coefficients in the four subbands A, B, C, D for the first heart sound.'-.-' represents a nonmeasurable parameter.

determined by characteristics of the lung-thorax system. This explains the fact that big changes of the W_K parameters are reflected in small changes in the signal energy domain (i.e. differences of more than 20% of W_K parameters are scaled to only 3% for E_K parameters (Table 6.1(b) (c)).

The primary role that the lung-thorax system plays in determining the spectral composition of S1 is also supported by the value found for the frequency of the biggest amplitude component for the normal and malfunctioning cases of native mitral heart valves. Table 6.3 gives the average frequency of the largest amplitude component for all three groups.

	$f_{A_{max}}^{AV}$
Normal subjects	59.93 Hz
Before surgery	33.02 Hz
After surgery	115.88 Hz

(a)

	$f_{E_{max}}^{AV}$
Normal subjects	35.450 Hz
Before surgery	31.04 Hz
After surgery	31.45 Hz

(b)

Table 6.3: The average values of $f_{A_{max}}^{AV}$ (a), and $f_{E_{max}}^{AV}$ (b) for the first heart sound, S1.

σ	Normal subjects	Before surgery	After surgery
$\sigma_{f_{A_{max}}^{AV}}$	65.0	17.0	53.12
$\sigma_{f_{E_{max}}^{AV}}$	20.77	14.0	11.0

Table 6.4: The estimated standard deviation of $f_{A_{max}}^{AV}$ and $f_{E_{max}}^{AV}$ for the first heart sound S1.

It is clear that in both the normal patients and the abnormal patients before surgery the values of $f_{A_{max}}^{AV}$ and $f_{E_{max}}^{AV}$ are well below 120 Hz, which is the upper limit of the subband A. Additionally, the standard deviations of $f_{A_{max}}^{AV}$ and $f_{E_{max}}^{AV}$ are quite high, which suggests a strong dependance on the individual lung-thorax sizes.

In terms of the average number of components per subband, F_K, it can be said that they are largely independent of the condition of the native mitral valve. This finding suggests that the number of frequency components contained in S1 and their relative energy for the case of native heart valves, are mostly dependent on the vibrating resonance characteristics of the lung-thorax system excited by the heart-valve vibration, rather than the exciting source itself. The amplitude of frequency components, however, is a better estimator of the condition of the native mitral valve.

This conclusion is also supported by the examination of heart sounds in the case of patients before and after a MPHV was implanted. In respect of the frequency of the largest amplitude component, it can be said that, even in the case of patients with a mechanical prosthesis, this component lies in subband A. The fact that $f_{A_{max}}^{AV}$ =115.88 Hz (i.e. almost twice as large as the normal case and three times larger than the malfunctioning case) shows the importance of regarding the system as a whole heart-valve system rather than the valve itself. It also underlines the interaction between heart-valve vibration and the lung-thorax system has on the spectral composition of the externally recorded S1. Table 6.3 shows that $f_{A_{max}}^{AV}$ for the same patient after surgery is 3.5 times greater than before surgery. This finding clearly shows the impact that heart-valve movement has on the amplitude distribution of the spectral components in the first heart sound S1.

The direct relationship between heart valve type and the amplitudes of the spectral components of the externally recorded PCG can clearly be seen from Table 6.1. This table shows that there are only minor differences between the F_K and E_K parameters below 400 Hz. However, the distribution of W_K is entirely different. The effect of the lung-thorax system becomes more evident from the values of F_K, W_K, and E_K in the subband D. It is well known that the closure of the MPHV generates high frequency components as a result of their structure [144], and this is reflected in the composition of the F_D and W_D parameters. However, as a result of high attenuations of the lung-thorax system in this part of the spectrum [38], and the very short duration of these components (i.e. high damping factor), only 0.48% of the total energy is concentrated

in the D subband (Table 6.1 (c)). To illustrate this effect a closure sound of a mitral prosthesis is shown in Figure 6.2.

Comp.	$f[i]$ Hz	$A[i]$	$d[i]$	$\phi[i]$
1	124	0.099	0.02	1.13
2	659	0.217	0.018	1.99
3	951	0.318	0.123	4.26
4	1194	0.093	0.09	0.03
5	1488	0.072	0.072	1.19

(c)
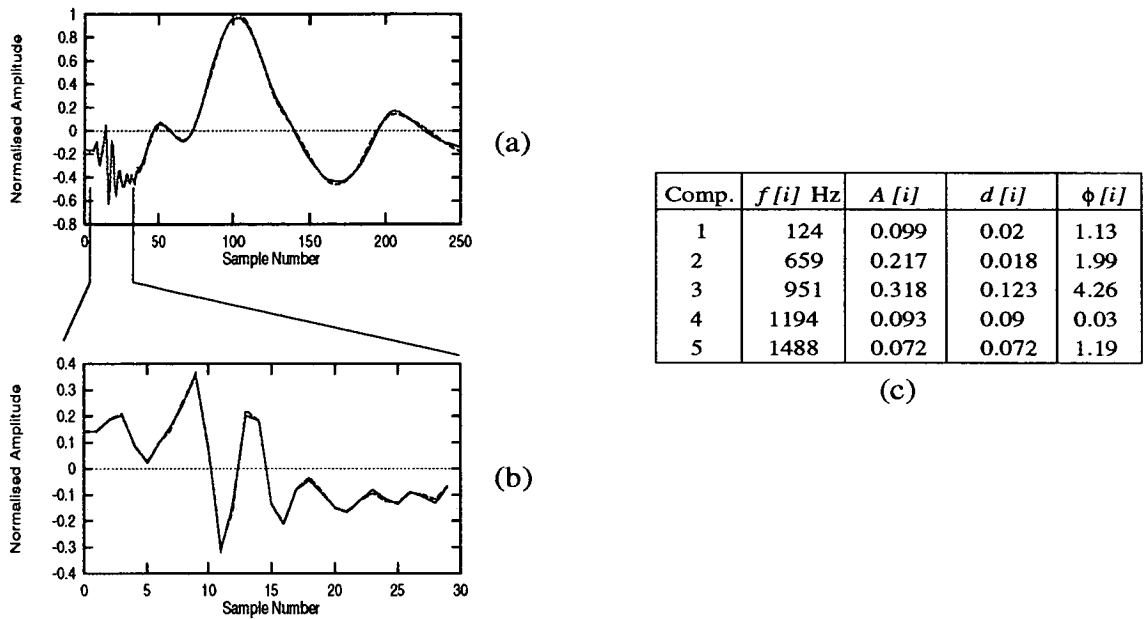
Figure 6.2:   Closure sound of a mitral mechanical prosthesis; (a) full S1, (b) that part of S1 related to the closure of the mitral mechanical prosthesis, and (c) the parameters of the synthesised signal for part (b). In both cases the actual signal is represented by a green line and the synthetic signal by a blue line (the difference is negligible). The patient has a 19 mm Carbomedics prosthetic valve.

Figure 6.2 (a) shows the complete S1 (50 ms synthesised as the sum of twelve damped sinusoids) and its synthesised signal(blue line). Figure 6.2(b) gives that part of the signal which is related to the closure of the mechanical prosthesis (6 ms) and its synthesised signal (blue line). The parameters of the signal in Figure 6.2 (b) are shown in Figure 6.2 (c). It is obvious from this case that the frequencies above 400 Hz appear at the moment of closure of the MPHV. From Figure 6.2 (c) it can be seen that the major component is at 951 Hz. This component could be related to the sound of the valve closure since its time duration is the smallest of all components (its damping factor (0.123) is the greatest of all the other damping factors). However, there are three other components above 400 Hz which occur during this very short time interval. Two of them (659 Hz and 1488 Hz) are widely spread from the highest energy component (951 Hz) and their damping factors are more than one order less than the damping factor of the 951 Hz component. Since these components are longer in duration than the

principal component at 915 Hz, these components could be related to the interaction between the closure of the prosthetic heart valve with the higher vibrating modes of the lung-thorax system. This argument is also supported by the distribution of the σ_F parameter. From Table 6.2 it can be seen that σ_{F_D} has the largest value of the other σ_F parameters, which suggests that the number of these components depends upon the lung-thorax size of the patients and the type of MPHV. The existence of a low frequency component (100-150 Hz) with one of the lowest amplitudes at the moment of MPHV closure is another important finding. Since similar findings are present from all the patients with an implanted mitral prosthesis regardless of the type of valve, sex and age of the patients, it can be said that this component is related either to the vortex shedding of the blood around the prosthetic valve [47] or to the vibration of muscular chords previously associated with the orifice of the native valve which are still present after prosthetic valve implantation.

6.3.3 Spectral characteristics of second heart sound

The relationship of aortic and pulmonary valve closure with the second heart sound (S2) is now widely accepted [132]. In general S2 is shorter in duration than S1 and has higher frequency components. Table 6.5 gives the average values for the F_K, W_K, and E_K coefficients for S2 for the cases of: normal subjects, patients before surgery, and patients after surgery. Table 6.6 gives the standard deviation of these coefficients.

From Table 6.5 it can be seen that the conclusions drawn for the impact of the lung-thorax system in the case of S1 remains valid for S2. It can be seen that the distribution of F_k and E_k parameter below 400 Hz is almost the same for all three groups of the patients. However, the difference in the distribution of the W_k parameter is more obvious. The attenuating effect of the lung-thorax system above 400 Hz is clear from Table 6.5(b) and Table 6.5(c).

Regarding the $f^{AV}_{A_{max}}$ and $f^{EV}_{A_{max}}$ parameters it is clear that they lie in subband A for all three cases, which supports the assertion that the main contributor to the externally recorded PCG is the lung-thorax system as a whole rather than the heart valve itself. Table 6.7 gives the values of $f^{AV}_{A_{max}}$ and $f^{AV}_{E_{max}}$ for S2 in the three different patient groups.

	F_K coefficients			
	10-120 Hz	120-250 Hz	250-400 Hz	$\geq$ 400 Hz
Normal subject	3.0	2.77	1.72	0.27
Before surgery	3.2	2.4	1.26	0.26
After surgery	3.53	2.46	1.53	1.4

(a)

	W_K coefficients			
	10-120 Hz	120-250 Hz	250-400 Hz	$\geq$ 400 Hz
Normal subject	69.45%	23.96%	6.128%	0.1%
Before surgery	74.14%	23.68%	2.04%	0.03%
After surgery	78.44%	15.93%	4.91%	0.69%

(b)

	E_K coefficients			
	10-120 Hz	120-250 Hz	250-400 Hz	$\geq$ 400 Hz
Normal subject	98.55%	1.39%	0.0345%	0.000068%
Before surgery	98.46%	1.48%	0.042%	0.000317%
After surgery	98.01%	1.95%	0.031%	0.00299%

(c)

Table 6.5:   The average values of (a) F_K, the spectral distribution coefficient, (b) W_K, normalised amplitude distribution coefficient, and (c) E_K, normalised energy distribution coefficient for each of the four subbands of the spectrum for S2.

σ	Normal subjects	Before surgery	After surgery
σ_{F_A}	0.1	0.63	0.76
σ_{F_B}	0.95	0.78	0.54
σ_{F_C}	0.87	1.05	1.19
σ_{F_D}	0.78	0.85	0.85
σ_{W_A}	12.0	19.0	16.25
σ_{W_B}	11.4	17.52	15.77
σ_{W_C}	5.56	2.39	4.35
σ_{W_D}	0.23	0.38	1.17
σ_{E_A}	2.46	2.99	4.63
σ_{E_B}	2.46	2.95	4.38
σ_{E_C}	0.068	0.107	0.047
σ_{E_D}	0.0002	0.003	0.0016

Table 6.6:   The estimated standart deviation of F_K, W_K, E_K coefficients in the case of S2.

97

	$f^{AV}_{A_{max}}$
Normal subjects	82.36 Hz
Before surgery	62.96 Hz
After surgery	75.43 Hz

(a)

	$f^{AV}_{E_{max}}$
Normal subjects	35.00 Hz
Before surgery	40.36 Hz
After surgery	35.13 Hz

(b)

Table 6.7:   The average value of $f^{AV}_{A_{max}}$ (a), and $f^{AV}_{E_{max}}$ (b) in the case of S2.

σ	Normal subjects	Before surgery	After surgery
$\sigma_{f^{AV}_{A_{max}}}$	40.0	44.8	30.36
$\sigma_{f^{AV}_{E_{max}}}$	14.4	30.86	20.0

Table 6.8:   The estimated standard deviation of $f^{AV}_{A_{max}}$ and $f^{AV}_{E_{max}}$ in the case of S2.

6.3.4   Difference in spectral components between S1 and S2

Comparison of Table 6.1 and Table 6.5 for cases of native valves shows that S1 and S2 contain approximately the same number of spectral components throughout the spectrum. However, S2 has a greater F_k in the frequencies over 250 Hz than S1. In terms of the overall differences between normal and malfunctioning native mitral valves, it can be said the amplitudes of spectral peaks in the subband B are most affected by the condition of the mitral valve. There is a clear difference in the W_B coefficient between both cases (26.15% in the case of normal subjects, and only 7.54% in the cases before surgery). This conclusion is also supported by the value of the W_B and coefficient in the region 120-250 Hz for recordings after MPHV implantation. The normalised amplitude distribution coefficient is 17.36% in this case, which is approximately 10% less than the normal native mitral valve case and 10% more than the case before surgery. This important finding suggests that the amplitudes of spectral components between 120-250 Hz are more related to the closure of the native mitral valve and, as the valve deteriorates, these amplitudes decrease. In the case of S2 it is the amplitude of the subband C components which are affected by the condition of the aortic valve (i.e. a difference of 4.2% in W_C was found).

Another difference between S1 and S2 can be seen in terms of the $f^{AV}_{A_{max}}$ parameter. From Table 6.3 and Table 6.7 it is clear that this parameter is greater in the case of S2 for native valves regardless of their condition. This finding still supports the suggestion

that the amplitudes of spectral components are a better estimator for the condition of heart valves than the distribution of energy or the number of frequency components. This argument can also be supported by the values of $f_{E_{max}}^{AV}$ for all the three groups of patients. From Table 6.3 and Table 6.7 it can be said that this parameter is independent not only of the condition of the heart valve, but it also does not appear to be affected by the type of heart valve.

A clear difference in the distribution of F_D, W_D, and E_D between S1 and S2 can also be seen from Table 6.1 and Table 6.5 in the case of MPHV for frequencies beyond 400 Hz. From these tables it can be said that the number of components and their relative energy above 400 Hz in the case of S2 is not as high as S1. This can be explained by the longer transmission path of the aortic closure sounds from the aortic valve to the 'aortic' area than the distance from the mitral valve to the 'mitral' area. Thus the sound related to the mechanical closure of the aortic prosthesis has to travel a longer path and hence suffers higher attenuation as a result of the low-pass characteristic of the lung-thorax tissues.

The difference in spectral composition of S1 and S2 above 400 Hz between native heart valves and MPHV proves that the mechanical prosthesis is responsible for these components in both S1 and S2. The change in these components has been investigated for four malfunctioning (leaky) cases of the mechanical prosthesis which were subsequently replaced or repaired. Figure 6.3 depicts the spectrum for one of them. It is clear that there are no predominant peaks above 400 Hz and a large part of the energy is concentrated between 250 and 400 Hz.
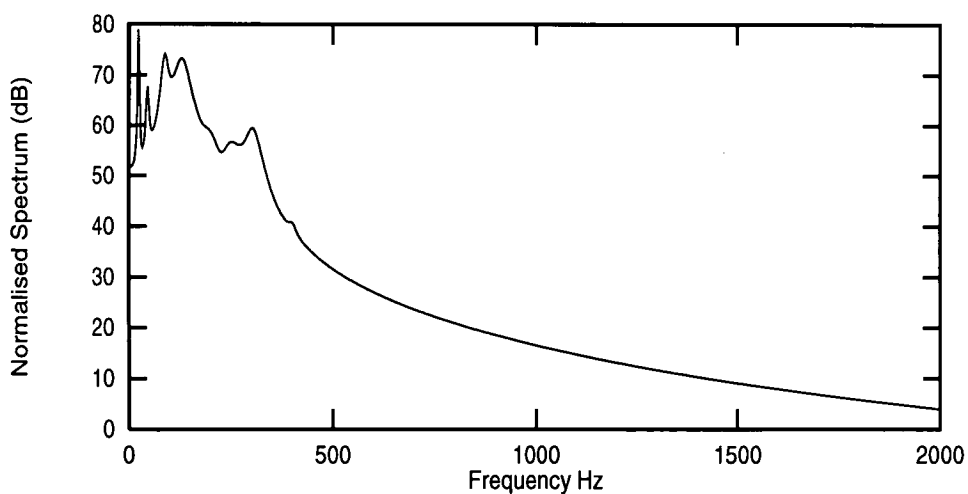

Figure 6.3:   Spectrum of S2 in a patient with a leaky valve in the aortic position.

6.4 The impact of prosthetic heart valve type on the spectral composition of S1 and S2

Several studies *in vitro* have been conducted to investigate the spectral characteristics, loudness, and the impact of mechanical construction on the characteristics of several MPHV [65, 134]. Although studies *in vitro* can give a clear picture of the relative loudness and the frequency content of MPHV sounds, they neglect an important factor in the spectral composition of these valves – the impact of the lung-thorax system on the overall observed spectrum at the chest surface generated by the closing click of MPHV. It has been shown by Durand [38] and Yoganathan [30] that the lung-thorax system behaves like a low-pass filter for frequencies above 100 Hz for the second heart sound (S2). Moreover, they have found that the graph of sound attenuation through the lung-thorax system varies as a function of frequency. Therefore, it can be said that the lung-thorax system has a non-linear transfer characteristic in different regions of the frequency spectrum which may cause distortion, or even changes in the intensity of sounds produced by the opening or closing of a MPHV. It was also shown in the previous section that the lung-thorax system plays a very important role even in the total number of frequency components of the externally recorded PCG.

In this context, studies *in vivo* are of crucial importance as they relate directly to the daily functioning of MPHV. Furthermore, the *in vivo* technique can be used to improve the design and mechanical construction of these valves by investigating the differences in spectral composition between the different types of valves and the impact of particular elements in their design and construction on the overall spectrum of the valve closing sounds.

The aim of the following two subsections is to investigate the impact of the mechanical prosthetic heart valve construction on the spectral characteristics of the closing sounds produced by these valves in both *mitral* and *aortic* position. The spectral composition of *in vivo* closing sounds produced by different mechanical prosthetic heart valves such as monostrut Bjork-Shiley (MBSH), Carbomedics (CRB), and Starr-Edwards (SE) are investigated. More than one hundred recordings were carried out for fifty-three different patients with a MPHV implanted in the mitral or the aortic position. The information concerning the type of MPHV, sex, and age of all these patients is given in appendix A.

From the results obtained with the air-coupled microphone it was observed that the number of frequency components above 2 kHz was negligible. In eight of the 53 patients, only one component was found beyond 2 kHz. These components always had the smallest amplitudes among all the frequency components. Figure 6.4 shows the real and modelled signal for four different recordings. Two of these recordings were obtained using the *contact* microphone (Figure 6.4(a)(c)) and the remaining two with the *air-coupled* microphone (Figure 6.4(b)(d)). The model parameters for the signal shown in Figure 6.4(a) and (b) are presented in Table 6.9.
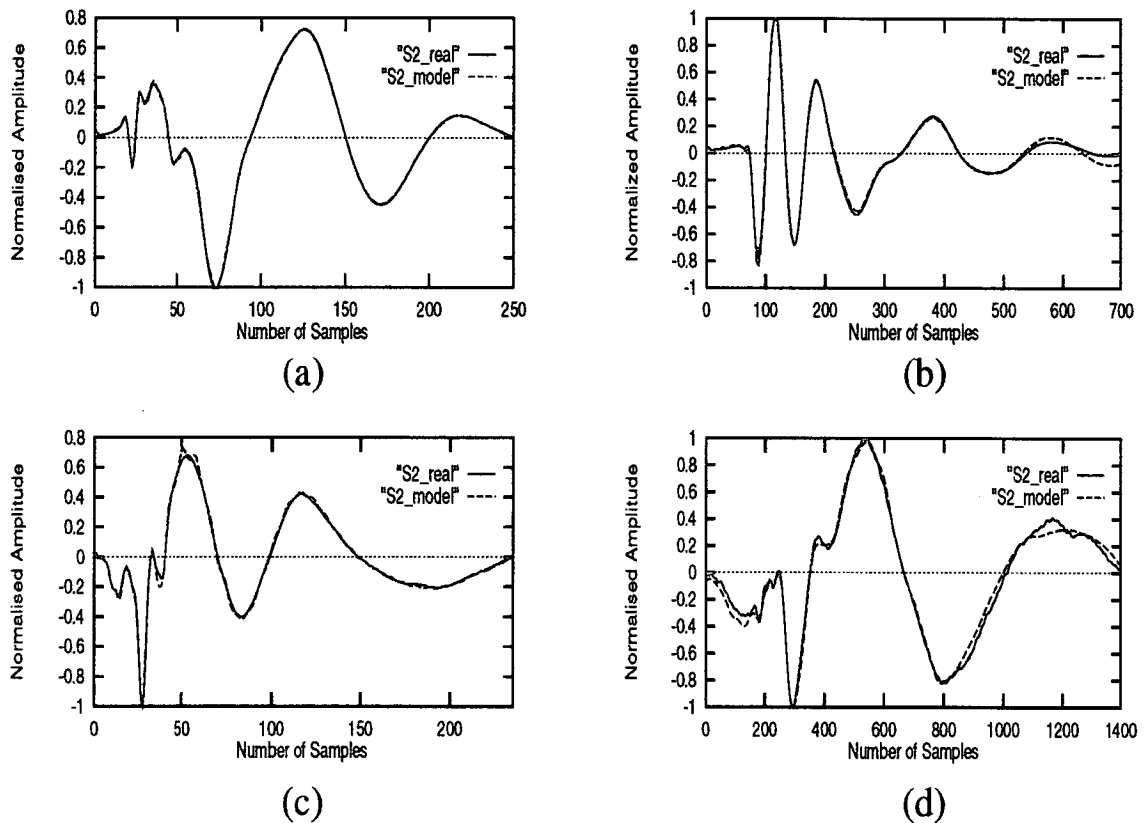
Figure 6.4: Actual (green line) and synthetic (blue line) signals of S2 for four different recordings: (a) a patient with MBSH valve recorded with contact microphone (actual and synthesised signal indistinguishable), (b) a patient with a MBSH valve recorded with an air-coupled microphone, (c) a patient with a Carbomedics valve recorded with a contact microphone, (d) the same patient shown in (c) recorded with an air-coupled microphone.

It can be seen from Table 6.9(b) that there are no frequency components above 2 kHz in the case of the S2 recorded using the *air-coupled* microphone. Similar findings were also shown in [68,92]. This finding suggests that even though the spectral components

of the recording *in vitro* could extend up to or beyond 10 kHz, the energy of these components *in vivo* is very small as a result of the low-pass filtering characteristic of the lung-thorax system. As the main part of the energy of closing sounds produced by the MBSH, CRB and SE valves was found to be below 2 kHz, the following results are presented from the recordings carried out with the Hewlett-Packard microphone.

Comp	$f[i]$ Hz	$A[i]$	$d[i]$	$\phi[i]$
1	31.3	0.735	0.0153	3.167
2	53.7	1.0	0.0117	5.75
3	81.9	0.077	0.008	6.06
4	118.0	0.859	0.337	0.07
5	160.4	0.74	0.038	1.664
6	192.4	0.037	0.018	6.047
7	222.9	0.226	0.03	3.129
8	327.5	0.065	0.04	2.84
9	405.0	0.0064	0.049	6.068
10	569.0	0.07	0.053	4.19
11	676.4	0.07	0.053	4.19
12	820.1	0.027	0.045	0.401
13	1009.9	0.01	0.0028	1.575
14	1199.6	0.0045	0.0203	1.775

(a)

Comp	$f[i]$ Hz	$A[i]$	$d[i]$	$\phi[i]$
1	55.8	0.12	0.012	1.086
2	99.9	0.05	0.002	2.66
3	210.5	0.22	0.011	1.025
4	260.7	0.025	0.003	0.76
5	286.8	1.0	0.032	3.57
6	361.6	0.492	0.021	6.25
7	537.8	0.128	0.031	0.809
8	739.8	0.0084	0.004	1.11
9	769.0	0.0175	0.019	1.96
10	1107.7	0.043	0.012	1.38
11	1262.2	0.0025	0.01	2.85

(b)

Table 6.9: Parameters of the modelled signals shown in Figure 6.4(a) and (b); $f[i]$ frequency, $A[i]$ amplitude, $d[i]$ damping factor, and $\phi[i]$ phase of the synthesised signal.

6.4.1 Differences in spectral composition between monostruct Bjork-Shiley and Carbomedics valves implanted in the aortic position

Table 6.10 presents the average values of F_K, W_K, and E_K obtained from two groups of patients with normally functioning valves. Table 6.11 gives the standard deviation parameter for each of these coefficients.

From Table 6.10, it can be said that similar conclusions can easily be demonstrated for the MBSH and CRB valves about the impact of the lung-thorax system on the spectral composition of S2 with those mentioned in the previous section. From Table 6.10 it can be seen that large differences in amplitude distribution are reflected in smaller changes in the energy domain. This once again suggests that the amplitudes of spectral components are more related to the condition and type of heart valve than the other parameters of spectral composition in the case of externally recorded PCG.

	F_K coefficients			
	10-120 Hz	120-250 Hz	250-400 Hz	$\geq$ 400 Hz
MBSH Valves	3.33	2.83	2.05	4.5
CRB Valves	3.78	2.71	2.07	1.78

(a)

	W_K coefficients			
	10-120 Hz	120-250 Hz	250-400 Hz	$\geq$ 400 Hz
MBSH Valves	50.14%	29.14%	11.16%	9.28%
CRB Valves	70.47%	16.69%	10.708%	2.09%

(b)

	E_K coefficients			
	10-120 Hz	120-250 Hz	250-400 Hz	$\geq$ 400 Hz
MBSH Valves	83.67%	10.41%	1.274%	4.646%
CRB Valves	96.97%	2.64%	0.354%	0.035%

(c)

Table 6.10:   The average values of (a) F_K, spectral distribution coefficients, (b) W_K, normalised amplitude distribution coefficients, and (c) E_K normalised energy distribution coefficients for the patients with MBSH and CRB valve in the aortic position.

From these results it can be seen that the difference in the number of frequency components between patients with Bjork-Shiley and Carbomedics implants below 400 Hz is quite small. However, there is a big difference in the number of frequency components above 400 Hz (there are in fact three times as many in the case of the MBSH valve). In terms of the relative energy distribution, it can be said that differences are more obvious below 120 Hz, where a 15% increase in relative energy is present for the case of the Carbomedics valve. However, in relative terms, the MBSH valve has much more energy above 400 Hz than the CRB valve (i.e. in subband D). This conclusion is very important when one bears in mind the characteristics of the human auditory system [143]. Since the discriminatory power of the auditory system is up to three orders

σ	MBSH valve	CAR valve
σ_{F_A}	0.57	1.01
σ_{F_B}	0.685	1.028
σ_{F_C}	0.787	1.03
σ_{F_D}	2.79	2.075
σ_{W_A}	22.38	22.0
σ_{W_B}	15.53	11.19
σ_{W_C}	13.51	12.65
σ_{W_D}	3.7	3.6
σ_{E_A}	23.5	4.37
σ_{E_B}	14.49	4.29
σ_{E_C}	2.93	0.63
σ_{E_D}	20.67	0.119

Table 6.11: The estimated standard deviation of F_K, W_k, and E_K coefficients in the case of MBSH and CRB valves implanted in the aortic position.

of magnitude higher between 400 Hz and 2 kHz than for sounds in the range between 20-120 Hz [25], it is this part of the total energy which disturbs the patient most. This finding suggest that one of the reasons why the Carbomedics valve is quieter than the MBSH valve [51, 144] is due to the fact that the main part of energy emitted by the closing sound *in vivo* is below 120 Hz where the dynamic sensitivity of the human ear is poor.

The frequency of the largest amplitude and energy spectral components was also investigated. Table 6.12 presents this information for those values and Table 6.13 gives their respective standard deviation.

	$f_{A_{max}}^{AV}$
MBSH valve	129.49 Hz
CRB valve	92.35 Hz

(a)

	$f_{E_{max}}^{AV}$
MBSH valve	79.53 Hz
CRB valve	42.99 Hz

(b)

Table 6.12: The average values of $f_{A_{max}}^{AV}$ (a), and $f_{E_{max}}^{AV}$ (b) in the case of patients with MBSH and CRB valves implanted in the aortic position.

Studying Table 6.12 it can be said that the value of $f_{A_{max}}^{AV}$ for these two groups is slightly greater than for the cases of native valves, especially in the case of the MBSH valve. On the other hand, it is clear that these frequencies are well below the frequency ranges that could be related to closure of the MPHV. This finding further suggests that the main component of S2 is related to the interaction of the lung-thorax system

σ	MBSH valve	CRB valve
$\sigma_{f^{AV}_{A_{max}}}$	96.75	25.0
$\sigma_{f^{AV}_{E_{max}}}$	91.49	47.85

Table 6.13:   The estimated standard deviation of $f^{AV}_{A_{max}}$ and $f^{AV}_{E_{max}}$ in the case of patients with MBSH and CRB valves implanted in the aortic position.

with the heart-MPHV rather than the closure of the MPHV itself. The large values of $\sigma_{f^{AV}_{A_{max}}}$ and $\sigma_{f^{AV}_{E_{max}}}$ also emphasise the differences in lung-thorax sizes between subjects on the spectral composition of the externally recorded heart sounds. These results also suggest that although the type of the MPHV has most impact beyond 400 Hz it also affects the remainder of the spectrum. Since there are no reasons to believe that frequencies beyond 400 Hz are generated by other factors [132] than the MPHV or its interaction with the lung-thorax system, it can be proposed that these components are related to the condition of the MPHV. From the preliminary results obtained from the four malfunctioning cases, it has been found that components above 400 Hz disappear or shift down in frequency to the lower regions of the spectrum when the valve is dysfunctioning. Figure 6.5 shows the spectrum of two different patients recorded 24 hours before the leaky valve was replaced.

It is clear from Figure 6.5 that there are no predominant peaks above 300 Hz and a large part of the energy is concentrated in subband C between 250 and 400 Hz. These results support the findings of Durand [79]. Durand found that the low frequency region of the opening sound of MPHV contains useful information regarding the integrity of the MPHV.
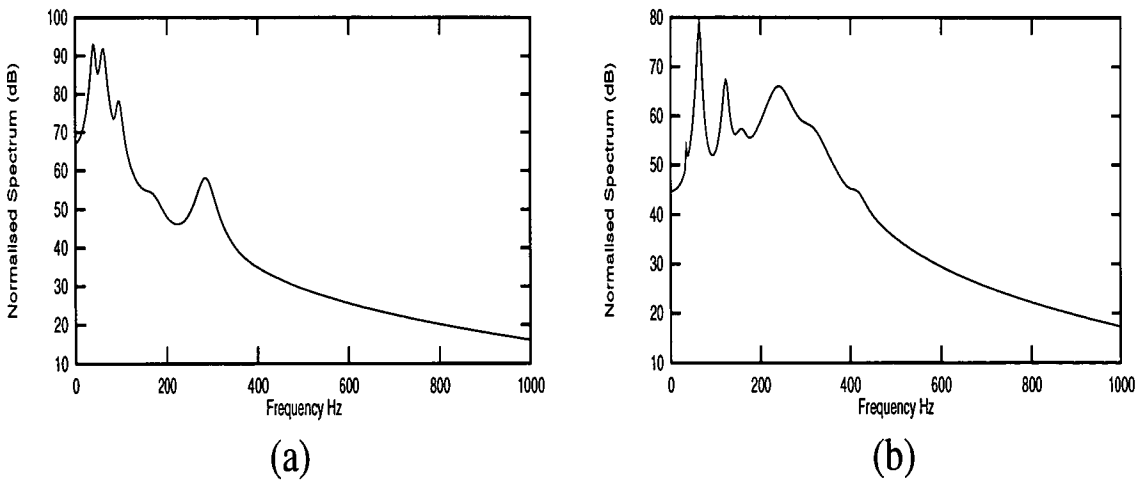

(a)   (b)

Figure 6.5:   Spectra of S2 for two different subjects with a leaky valve in the aortic position: (a) patient with 23mm CRB valve, (b) patient with 23mm MBSH valve.

6.4.2 Differences in spectral composition between monostruct Bjork-Shiley and Starr-Edwards valves implanted in the mitral position

In contrast to the previous case, there are clear differences in spectral composition of the closing click between SE and BSHM mechanical prosthetic heart valves in the *mitral* position. Figure 6.6 shows the real and modelled signal for a case of a SE valve and MBSH valve implanted in the *mitral* position. The respective parameters of these two modelled signals are given in Table 6.14. Table 6.15 presents the average values obtained from these two groups of patients. The standard deviation of these parameters is given in Table 6.20.

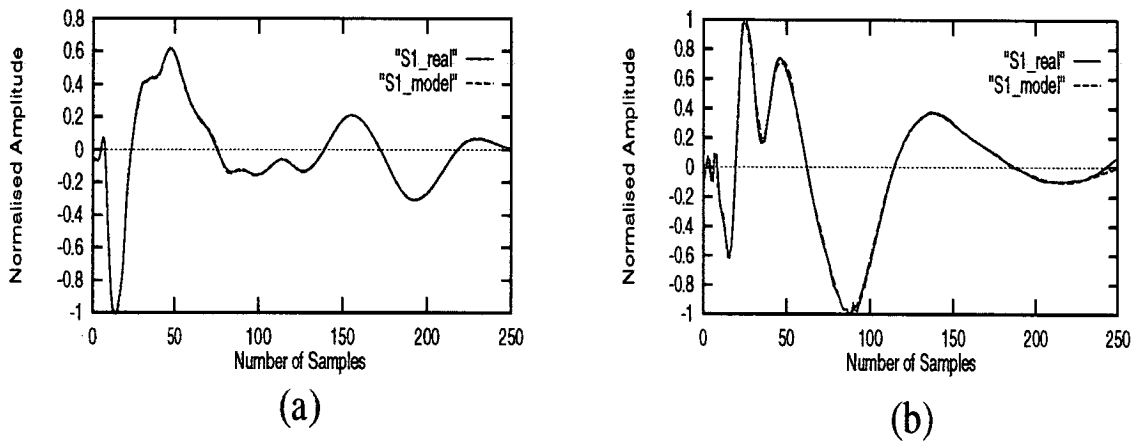(a)   (b)

Figure 6.6:   Actual (green line) and synthetic (blue line) signals of S1 for two different recordings: (a) patient with SE valve , (b) patient with a MBSH valve

Comp	f[i] Hz	A[i]	d[i]	φ[i]
1	10.88	0.4	0.0077	1.68
2	52.52	0.569	0.0045	4.27
3	85.64	0.358	0.0047	2.94
4	127.5	1.0	0.029	2.15
5	159.8	0.654	0.028	3.17
6	189.25	0.159	0.022	4.56
7	232.7	0.51	0.029	5.93
8	318.7	0.69	0.047	4.27
9	345.86	0.59	0.046	6.03
10	711.7	0.296	0.09	1.33
11	1131.1	0.036	0.038	3.46
12	1393.7	0.019	0.061	0.39
13	1687.3	0.01	0.35	4.88

(a)

Comp	f[i] Hz	A[i]	d[i]	φ[i]
1	37.04	0.373	0.01	0.86
2	69.74	1.0	0.029	2.9
3	80.36	0.599	0.034	5.6
4	157.85	0.127	0.054	3.34
5	205.41	0.13	0.038	1.21
6	298.78	0.2	0.074	4.24
7	521.31	0.024	0.037	5.41
8	669.56	0.005	0.032	0.55
9	976.61	0.014	0.037	4.55
10	1336.6	0.0019	0.024	3.24

(b)

Table 6.14:   Parameters of the modelled signals shown in Figure 6.6. $f[i]$ frequency, $A[i]$ amplitude, $d[i]$ damping factor, and $\phi[i]$ phase of the synthesised signal.

	F_K coefficients			
	10-120 Hz	120-250 Hz	250-400 Hz	$\geq$ 400 Hz
MBSH valves	3.75	2.75	1.5	4.25
SE valves	2.44	2.55	2.0	6.88

(a)

	W_K coefficients			
	10-120 Hz	120-250 Hz	250-400 Hz	$\geq$ 400 Hz
MBSH valves	74.06%	15.15%	6.68%	4.06%
SE valves	22.79%	39.51%	23.23%	18.67%

(b)

	E_K coefficients			
	10-120 Hz	120-250 Hz	250-400 Hz	$\geq$ 400 Hz
MBSH valve	97.315%	2.55%	0.123%	0.00127%
SE valve	65.14%	31.28%	1.85%	1.668%

(c)

Table 6.15: The average values of (a) F_K, the spectral distribution coefficient , (b) W_K, normalised amplitude distribution coefficient, and (c) E_K, normalised energy distribution coefficients for the patients with Bjork-Shiley(MBSH) and Starr-Edwards(SE) valves in the mitral position.

There is a clear difference of the energy and amplitude distributions within the respective subbands between these two cases. A different pattern is also found for the spectral distribution coefficient, especially beyond 400 Hz. These findings suggest that the there is a strong relationship between the spectral composition of externally recorded PCG and the type of mechanical prosthetic heart valve. As was described in chapter 2, SE and MBSH valves have completely different mechanical structure and geometrical configurations, hence the differences in the spectral composition of their respective closing sounds. However, the importance of the lung-thorax system on the externally recorded PCG can still be distinguished even in this case. From Table 6.15(b) and Table 6.15(c) it can be seen that very large differences in amplitude distribution are reflected in a

smaller scale in the energy distribution. It can be seen that differences of 52%, 17% and 14% in the W_K coefficient are scaled down to 30%, 1.7% and 1.6% in the case of the E_K parameter, respectively.

σ	MBSH valve	SE valve
σ_{F_A}	0.48	0.68
σ_{F_B}	0.66	0.83
σ_{F_C}	0.5	0.47
σ_{W_A}	6.33	12.46
σ_{W_B}	7.9	20.75
σ_{W_C}	2.86	16.4
σ_{W_D}	5.3	17.53
σ_{E_A}	3.5	31.8
σ_{E_B}	3.59	29.95
σ_{E_C}	0.146	2.53
σ_{E_D}	0.0013	2.57

Table 6.16: The estimated standard deviation of F_K, W_K, and E_K coefficients in the case of MBSH and SE valves implanted in the mitral position.

The difference in the number of components, amplitude, and energy distributions between these two types of valve above 400 Hz is an important discovery of this investigation. From Table 6.15(b), it is clear that the SE valve has 18.76% of the total amplitude distribution above 400 Hz which, in relative terms, is four times larger than the value of W_D for MBSH in this subband. This difference is also reflected in a higher respective energy in the case of SE than MBSH valves. As was described in subsection 6.4.1 this part of the spectrum disturbs the patient most because of the dynamic sensitivity of the human auditory system. However, various authors have found that in absolute terms the MBSH valve is much louder than the SE valve [51,72]. Our results suggest that the loudness of functioning of the mechanical prosthetic heart valves *in vivo* is strongly related to the material of construction of the mechanical prosthetic valve and their mode of vibration. These results agree with other work on mechanical prosthesis [67,72].

Table 6.17 and Table 6.18 gives the values of $f^{AV}_{A_{max}}$, $f^{AV}_{E_{max}}$ and their standard deviation, respectively.

	$f_{A_{max}}^{AV}$
MBSH valve	83.57 Hz
SE valve	247.88 Hz

(a)

	$f_{E_{max}}^{AV}$
MBSH valve	43.64 Hz
SE valve	81.04 Hz

(b)

Table 6.17: The average value of (a) $f_{A_{max}}^{AV}$ and (b) $f_{E_{max}}^{AV}$ coefficients in the case of patients with MBSH and SE valve implanted in the mitral position.

σ	MBSH valve	SE valve
$\sigma_{f_{A_{max}}^{AV}}$	15.53	175.74
$\sigma_{f_{E_{max}}^{AV}}$	20.3	50.99

Table 6.18: Standard deviation for parameters in the case of S1.

The value of $f_{A_{max}}^{AV} = 247.88$ Hz, which is greater than 120 Hz (i.e. subband A), provides a distinction between SE prosthetic heart valves and all the other cases. However, bearing in mind the greater value of $\sigma_{f_{A_{max}}^{AV}}$ in this case, compared to other groups of patients, it may be suggested than this inconsistency might be caused by poor statistical properties of the data in this group patient.

6.5 Differences in spectral composition between normal and malfunctioning Carpentier-Edwards bioprosthetic heart valves in the aortic position

In a practical sense, the ultimate goal of spectral PCG is to properly diagnose different cardiac diseases especially those related to malfunctioning of either native heart valves or prosthetic heart valves. In this context, a large amount of interest has been shown in using the spectral characteristics of the PCG signal for detecting the malfunctioning of bioprosthetic heart valves. This procedure includes two main steps:

- to investigate whether or not there is a difference in spectral composition between normal and malfunctioning cases of prosthetic valves

- to extract feature parameters which can be used in a classification procedure.

This section is concerned with the first step of the above mentioned procedure for the case of normal and malfunctioning Carpentier-Edward (C-E) bioprosthetic heart valves implanted in the *aortic* position. Twenty-six patients with C-E valves were recorded for this purpose. Fourteen of them had a normally functioning (NF) C-E valves and the remaining twelve had malfunctioning (MF) ones, which included a leaky or stiffening bioprosthesis. The information regarding these patients is given in appendix A. Table 6.19 and Table 6.20 give the distribution of F_K, W_K and E_K coefficients and their standard deviations, respectively.

	F_k coefficients			
	10-120 Hz	120-250 Hz	250-400 Hz	$\geq$ 400 Hz
NF	3.85	2.85	1.21	1.14
MF	4.09	2.63	0.0	0.0

(a)

	W_K coefficients			
	10-120 Hz	120-250 Hz	250-400 Hz	$\geq$ 400 Hz
NF	76.04%	20.78%	2.75%	0.356%
MF	83.57%	16.377%	0.0%	0.0%

(b)

	E_K coefficients			
	10-120 Hz	120-250 Hz	250-400 Hz	$\geq$ 400 Hz
NF	97.88%	2.088%	0.02%	0.00036%
MF	98.875%	1.125%	0.0%	0.0%

(c)

Table 6.19: Average values of (a) F_K, spectral distribution coefficient, (b) W_K, normalised amplitude distribution coefficient, and (c) E_K normalised energy distribution coefficient for patients with normal (NF) and malfunctioning (MF) Carpenter-Edwards valves in the aortic position.

From Table 6.19 it can be said that the main difference between normal and malfunctioning cases occurs in the frequencies above 250 Hz. Comparing Table 6.19 with Table 6.5 it can be said that the pattern of energy and amplitude distribution in the case of native heart valves and C-E bioprosthetic heart valves implanted in the aortic

position is very similar. In both cases the major part of the total energy, (98%), is concentrated in subband A. It also appears that as the heart valve degenerates the amplitudes of spectral components in the subband A rise.

σ	NF valve	MF valve
σ_{F_A}	1.11	0.66
σ_{F_B}	0.94	0.72
σ_{F_C}	0.92	-.-
σ_{F_D}	1.02	-.-
σ_{W_A}	10.34	18.0
σ_{W_B}	9.1	17.89
σ_{W_C}	2.36	-.-
σ_{W_D}	0.42	-.-
σ_{E_A}	4.062	2.99
σ_{E_B}	4.06	2.99
σ_{E_C}	0.18	-.-
σ_{E_D}	0.00079	-.-

Table 6.20: The estimated standard deviation of F_K, W_K and E_K coefficients in the case of C-E valves implanted in the aortic position.'-.-' represents a nonmeasurable parameter.

The only difference is the amount by which the difference between normal and malfunctioning cases occur respectively. It seems that in the case of C-E bioprosthesis there is a greater amount of difference in the W_K coefficient between normal and malfunctioning cases in the frequency subband A than the native valve. However, the major difference in relative terms between normal and malfunctioning groups in both cases occurs in frequencies above 250 Hz. The similarity between these cases can be explained by their similarity in material construction: a native valve consists of human tissue, whereas the C-E valve in made of biological tissue with structural characteristics approaching those of natural valves. Therefore, the dynamic behaviour of these valves, which is believed to be the exiting source of the vibrating lung-thorax system, have similar characteristics.

The similarity between C-E and native heart valves in the aortic position is also supported by the values of the $f_{A_{max}}^{AV}$ and $f_{E_{max}}^{AV}$ parameters. Table 6.21(a) and Table 6.21(b) give the values of $f_{A_{max}}^{AV}$ and $f_{E_{max}}^{AV}$ parameters for the normal and malfunctioning cases

of C-E valves. The standard deviations of these parameters are presented in Table 6.22. Comparing Table 6.21 with Table 6.7 it is clear that in both native heart valves and C-E valves the value of $f^{AV}_{A_{max}}$ is greater for normally functioning valves and moves downwards in frequency in the case of a malfunctioning valve. In both cases the value of these parameters are located in the subbband A, which still supports the argument that the main part of the energy in the case of S2 is related to the interaction of the heart valve with the lung-thorax system rather than the valve itself.

	$f^{AV}_{A_{max}}$
NF valve	76.0 Hz
MF valve	53.0 Hz

(a)

	$f^{AV}_{E_{max}}$
NF valve	45.94 Hz
MF valve	28.09 Hz

(b)

Table 6.21: The average values of (a) $f^{AV}_{A_{max}}$, and (b) $f^{AV}_{E_{max}}$ in the case of a C-E valve implanted in the aortic position.

σ	NF valve	MF valve
$\sigma_{f^{AV}_{A_{max}}}$	40.97	37.72
$\sigma_{f^{AV}_{E_{max}}}$	26.52	13.06

Table 6.22: The estimated standard deviation of $f^{AV}_{A_{max}}$ and $f^{AV}_{E_{max}}$ in the case of a Carpentier-Edwards valve implanted in the aortic position.

From Table 6.19(b) it can be said that high frequency resonance components above 250 Hz disappear in the malfunctioning case of the C-E valve. This result disagrees with previous investigations presented elsewhere [20,32]. It is believed that this disagreement is due to the fact that in those studies the signal is processed using either the FFT or AR modelling with a fixed model order. As it was shown in the previous chapter, these two standard methods are not only inappropriate for representing S1 or S2 in terms of spectral resolution but, moreover, they produce spurious peaks especially outside the frequency band contained in the signal.

Results obtained using MFBPM show that the model order varies not only from subject to subject but even between two classes as well (i.e. normally and malfunctioning cases). As was described in section 5.4, there are a variety of factors that effect the differences in the model order. In this sense, the results presented here indicate the importance that the spectral analysis method has in the analysis of S1 and S2, and the criteria for

deciding the proper model order. Analysing S1 or S2 recorded from different subjects with the same model order means that either spurious peaks will be present in their spectral representation or some information will be missed when an underestimated model order is selected.

6.6   Summary and conclusion

The spectral composition of first and second heart sounds has been investigated for a large variety of subjects with native heart valves, prosthetic heart valves and bioprosthetic heart valves.
From the overall results, it can be concluded that the spectral composition of S1 and S2 depends on the interaction between the heart-valve movement and the response of the lung-thorax system. Although the number of frequency components and their relative energy is less dependent on the condition of the native heart valves, the relative distribution of the amplitude levels is strongly related to functioning of the valve. It seems that the number of spectral components and their frequency is more dependent on the resonance modes of the lung-thorax system excited by the movement of the overall heart-valve system.

With regard to mechanical prosthetic valves, it was found that the main part of the energy of the closing sounds *in vivo* is located below 2 kHz, although the *in vitro* analysis of these sounds show higher frequency components. This finding supports the theory that the lung-thorax system behaves as a low-pass filter. It was also found that the closure of the mechanical prosthetic heart valves either in the mitral or aortic position has more effects on the number of components and the energy of the signal above 400 Hz. The impact of the mechanical construction on the spectral composition was also investigated and clear differences were found especially between SE and BSHM valves. This finding emphasises the strong relationship between the construction of a mechanical valve and its spectral composition.

Clear differences in terms of the amplitudes of spectral composition of S1 and S2 were found between normal and malfunctioning cases for respective patient groups. In the case of S1 for native heart valves, the frequency band 120-250 Hz is most affected by diseases of the native mitral valve, whilst in the case of the dysfunctioning native aortic

valve it is the 250-400 Hz band which is more affected.

Although the lower part of the spectrum (i.e. up to 2 kHz) was investigated for the case of mechanical prosthetic heart valves, a clear difference was found between normal and malfunctioning cases. From preliminary results in some malfunctioning cases of mechanical prosthesis it was found that there is a large drop in the amplitudes of spectral components above 400 Hz. These results show that even with a sampling rate of 5 kHz the condition of these valve types can be monitored. The advantage of this relatively low sampling rate is that it substantially reduces the computational time and the requirements for data storage compared with the very high sampling-rate used in other studies [72].

In the case of Carpentier-Edwards bioprosthetic heart valves, the spectrum above 250 Hz was effected by the condition of the valves in the aortic condition. A similar pattern was found for C-E bioprosthetic heart valves and native heart valves in the aortic position. This is believed to be a result of their similarities in material of heart valve construction.

In general, all these results suggest that although the spectral composition of S1 and S2 is more complicated than previously found, there is a relationship between the condition of the heart valve and the spectral composition of the externally recorded PCG, especially in terms of the amplitudes of spectral components. In this sense the spectral analysis of S1 and S2 can potentially be used as a diagnostic method for detecting the malfunction of either prosthetic heart valves or native heart valves. This task is addressed in the next chapter.

Chapter 7

Classification of Normal and Malfuntioning Carpentier-Edwards Bioprosthetic Valves Implanted in the Aortic Position

7.1 Introduction

In a practical sense, the ultimate goal of PCG techniques is to properly diagnose different cardiac valvular diseases. In this context, a large amount of interest has been shown in using SPCG and pattern recognition techniques as a combined tool for automatic detection of malfunctioning bioprosthetic heart valves [10,76,78,145]. The principal task is to find a reliable, noninvasive, and repeatable technique to evaluate bioprosthetic valve integrity.

This procedure can be considered as a two stage process: (a) a feature input vector is extracted from the analysis of the PCG signal, and (b) a classification technique is applied to that input feature vector in order to provide a meaningful categorisation of the information of the data. The success of this procedure depends on the geometric properties of the pattern classes under consideration and on the characteristics of the algorithm employed for the respective task.

The purpose of this chapter is to describe the design, training, and testing of an adaptive single layer perceptron for the classification of C-E bioprosthetic heart valves implanted in the aortic position.

7.2 Adaptive single layer perception

The single layer perceptron (SLP) is a simple form of neural network used for the classification of a special type of patterns which can be considered linear [146]. This model allows classification of an input into one of two classes. Figure 7.1 shows the basic model of a SLP.
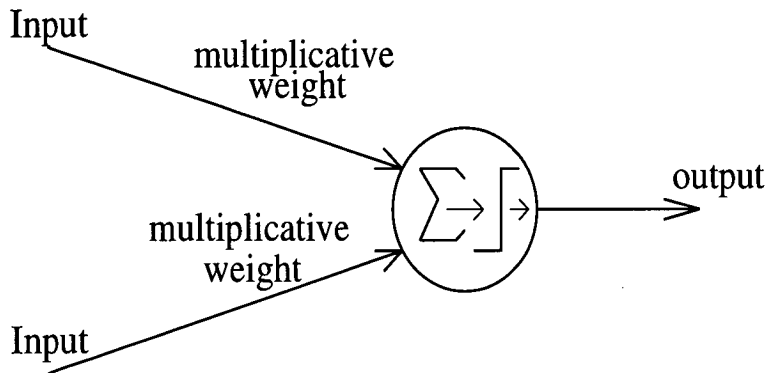

Figure 7.1:   Outline of a basic SLP model.

The SLP performs a weighted sum of its inputs, compares this to some internal threshold level, and produces an output only if the threshold is exceeded. It has been shown that if the inputs presented from two classes are separable (i.e. they fall on the opposite sides of a hyperplane), then the SLP training procedure converges and positions the decision boundaries between the two classes.

The decision regions formed by a SLP are similar to those formed by maximum likelihood Gaussian classifiers which make the assumption that the inputs are uncorrelated and distributions for different classes differ only in mean values [146]. However, there are some differences [147], namely:

- The SLP model is more robust than a Gaussian classifier because it makes no assumptions concerning the shape of the underlying distributions.

- The SLP convergence algorithm is both adaptive and simple to implement and

does not require storage of any more information than the weights and the threshold, whereas, the maximum-likelihood Gaussian classifier is fixed. The Gaussian classifier can be made adaptive, but at the expense of increase storage required and more complex computations.

For the above mentioned reasons an adaptive SLP model is applied to classification of normal and malfunctioning classes of C-E bioprosthetic valves.

As was mentioned earlier, the first step of any classification technique is the selection of features for the respective patterns. The objective of this stage is to identify discriminant pattern vectors such that the normal and malfunctioning prosthetic heart valves occupy different regions in the feature space. It is clear from Table 6.19 that high frequency components above 250 Hz disappear in the malfunctioning case of Carpentier-Edwards valve. However, from Table 6.20 it is clear that σ_{F_C} and σ_{F_D} have approximatly the same value as F_C and F_D, respectively. Therefore, this single feature is very volotile to be used as a discriminant characteristic between normal and malfunctioning valves. As the amplitudes of frequency components correlate better with the condition of the heart valve, the amplitudes of the three highest frequency components (i.e. $A_{fmax}, A_{fmax-1}, A_{fmax-2}$) contained in S2 were selected as the feature input vector of the SLP. The selection of this range of amplitudes is based on the fact that cardiologists use the auscultation as a diagnostic method to evaluate the condition of the valve. Bearing in mind that the human auditory system is more sensitive to the intensity of frequencies above 200 Hz [143], it seems that the amplitude of these components are the most likely components to be evaluated by cardiologists. It must be said that the number of frequency components contained in S2 for all the cases of C-E bioprosthetic valves was greater than five. Therefore it is always possible to obtain the required number of input parameters from the modelling procedure of S2.

It should be mentioned that prior to analysis, S2 sounds were normalised with respect to their maximum amplitude. This normalization removes any bias generated by the differences in sound intensity observed between recordings from different patients. Table 7.1 gives the amplitude of the three highest frequency components for the cases of normal and malfunctioning C-E bioprosthetic valves.

Patient's	Normally functioning valves		
Code	$A[f_{max}]$	$A[f_{max-1}]$	$A[f_{max-2}]$
P1CENA	0.089	0.042	0.019
P2CENA	0.0133	0.0078	0.096
P3CENA	0.036	0.0168	0.079
P4CENA	0.00079	0.00871	0.071
P5CENA	0.0026	0.0067	0.056
P6CENA	0.0052	0.0195	0.098
P7CENA	0.0082	0.007	0.067
P8CENA	0.000691	0.0158	0.00127
P9CENA	0.00658	0.0039	0.0185
P10CENA	0.0044	0.0029	0.013
P11CENA	0.00605	0.01877	0.0104
P12CENA	0.00093	0.0102	0.026
P13CENA	0.0065	0.0088	0.0351
P14CENA	0.01053	0.0119	0.1121

(a)

Patient's	Abnormally functioning valves		
Code	$A[f_{max}]$	$A[f_{max-1}]$	$A[f_{max-2}]$
P1CEMA	0.0088	0.022	0.127
P2CEMA	0.01045	0.098	0.1415
P3CEMA	0.042	0.0155	0.116
P4CEMA	0.086	0.11	0.072
P5CEMA	0.0098	0.043	0.133
P6CEMA	0.062	0.133	0.396
P7CEMA	0.1176	0.181	0.82
P8CEMA	0.1691	0.047	0.0243
P9CEMA	0.042	0.165	0.031
P10CEMA	0.0026	0.0173	0.336
P11CEMA	0.0041	0.144	0.2911
P12CEMA	0.0224	0.061	0.137

(b)

Table 7.1:   Amplitude of the three highest frequency components for (a) patients with normally functioning C-E valve and (b) malfunctioning C-E valve (records of appendix A).

The structure of the adaptive SLP model used to classify the two classes of C-E bioprosthetic valves implanted in the aortic position is given in Figure 7.2. This structure consists of three inputs, a bias input element (X_0), the threshold device, and the desired response. Denoting the output as y, one can write

$$y = F_h \left[\sum_{i=0}^{i=3} w_i[k] x_i[k] \right] \tag{7.1}$$

where F_h is the Heaviside function defined as

$$F_h[s] = \begin{cases} +1 & \text{if } s > 0 \\ 0 & \text{if } s \leq 0 \end{cases} \tag{7.2}$$
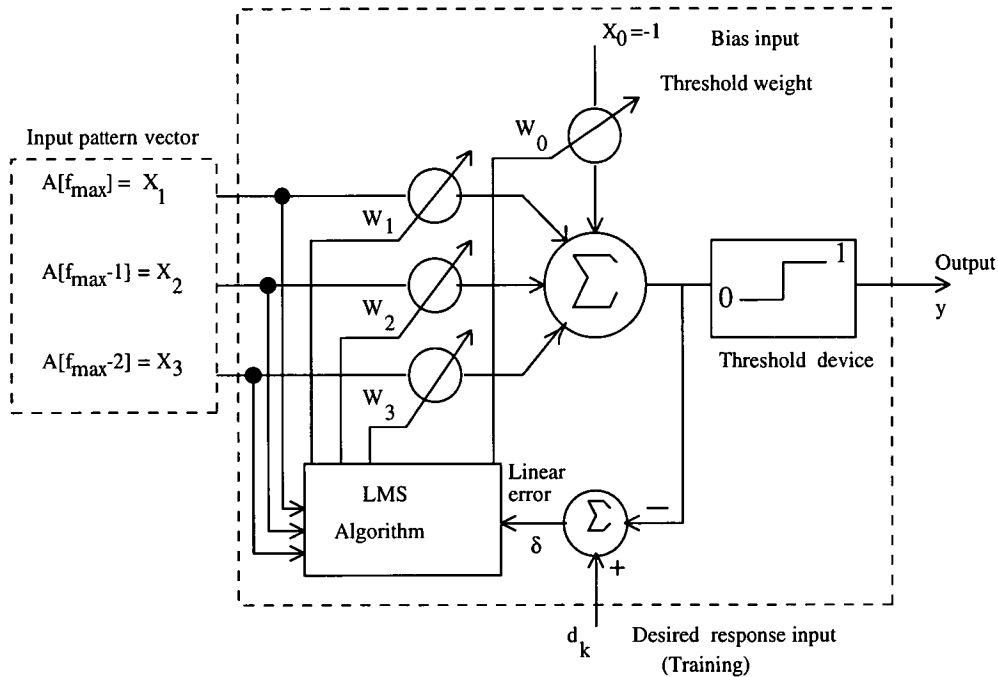
Figure 7.2: Schematic representation of SLP used for classifying normally functioning (NF) and malfunctions (MF) classes of C-E valves in the aortic position.

It must be noted that the biased input is included as an extra input of the model and its effect is merely to shift the decision boundary away from the origin [148].

There are several learning rules for the SLP. All the training methods specify an initial set of weights and modify the weights of the network in order that the output response to the input patterns is as close as possible to their desired response. An adaptive

119

learning process based on the least mean square (LMS) algorithm is applied to adjust the weights in the problem at hand. This learning rule is commonly known as the Widrow-Hoff delta rule [147]. The LMS learning algorithm minimises the mean square error between the desired output of the SLP and the actual output over the training set so that the actual response of the SLP approaches the target response. The linear error ($\delta_k[n]$), defined as the difference between the desired response $d_k[n]$ and the actual response of the model, $y_k[n]$, during the presentation k, is calculated by:

$$\delta_k[n] = d_k[n] - y_k[n] \tag{7.3}$$

Thus, according to the delta rule the adjustment $\triangle w_k[n]$ made to the weight w_k at time n is given by;

$$\triangle w_k[n] = \eta[n]\delta_k[n]x_k[n] \tag{7.4}$$

In this equation $\eta[n]$ is a positive gain term that lies in the range $0 \leq \eta[n] \leq 1$. This parameter is adjusted in order to control the convergence rate. In the model described in this chapter a fixed increment adaptive rule was applied (i.e. $\eta[n] = \eta$).

The weight vector of the SLP is then updated in accordance with the following rule:

$$w_k[n+1] = w_k[n] + \eta\delta_k x_k[n] \tag{7.5}$$

$$d[t] = \begin{cases} +1 & \text{if input comes from class MF} \\ 0 & \text{if input comes from class NF} \end{cases} \tag{7.6}$$

The basic idea behind this procedure is to make large changes in the weights when the actual response of the SLP is a long way from the desired value, whilst altering them only slightly when the weighed sum is close to that required to give the correct solution. This learning procedure can then be summarised as follows:

(i). Set the weight vector to zero. Then perform the following steps for time $n = 1, 2, 3, \cdots$

(ii). Calculate the actual output by taking the threshold value of the weighted sum of the inputs (7.1).

(iii). Alter the weight vector of the SLP based on the LMS algorithm.

(iv). Increment the time n and repeat step (ii) and (iii) until the desired response is obtained.

7.3 Functional classification of bioprosthetic valves

During the learning process approximately half of the patients were used, seven with normally functioning C-E bioprosthetic valves and six with a malfunctioning one. Connection weights were estimated using the procedure described in the previous section. The weight coefficients returned from the training procedure were: $w_0 = 1$, $w_1 = 6.5$, $w_2 = 6.2$, $w_3 = 7.6$.

The network was then tested on the remaining thirteen patients. The performance of the classifier was then evaluated by computing the percentage of correct classifications CC, false positives FP, and false negatives FN by using:

$$CC = 100 \times \frac{(TP + TN)}{N}\% \tag{7.7}$$

$$FP = 100 \times \frac{FPR}{TN + FP}\% \tag{7.8}$$

$$FN = 100 \times \frac{FNR}{TN + FP}\% \tag{7.9}$$

where TP is the number of true positives, FPR is the number of false positive results, TN is the number of true negative results, FNR is the number of false negative results, and N is the total number of trials.

Results show that in all the cases the SLP performed correctly (CC = 100%) classifying the patients into their respective classes.

Since the model consists of four weights, the separating boundary between the two classes will be a plane in three dimensional space. The equation of this plane depends on the connection weights and the threshold and is given by:

$$Z w_3 + Y w_2 + X w_1 + X_0 w_0 = 0 \tag{7.10}$$

The four weights determine the slopes, intercepts and the sides of the separating plane dividing the two classes. Figure 7.3 shows the position of this plane in a three dimensional space.
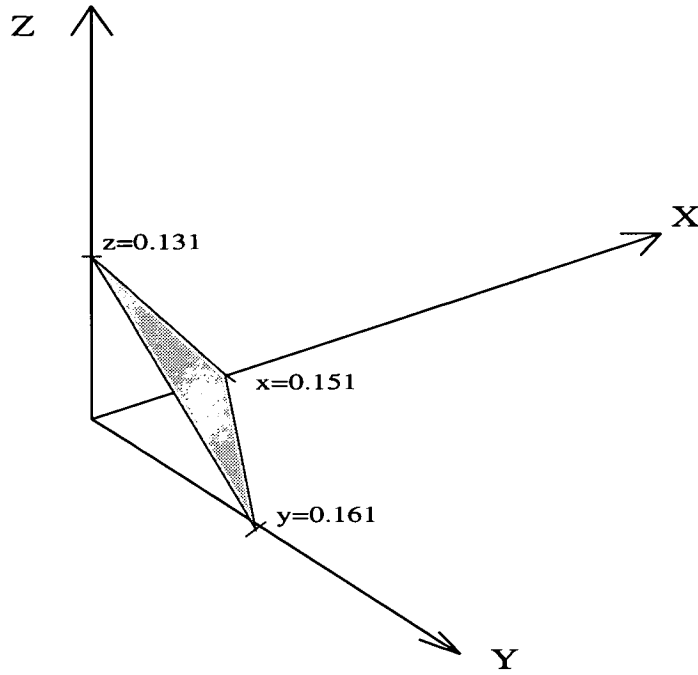
Figure 7.3:   Separating plane in pattern space.

In their latest study, Durand *et al* [76] evaluated the diagnostic performance of two spectral techniques (i.e. the FFT and AR modelling) combined with two classifiers (Bayes and nearest neighbour) in order to classify normal and malfunctioning bioprosthetic valves implanted in the aortic position for the case of forty-seven patients using the leave-one-out method. Here the network is trained on 46 records and then the 47th is tested to see in which class it lies. This is then repeated by leaving out each record in turn. Their results shown an 87% correct classification when an Hanning or Hamming window was applied to the data. In the case when an input feature vector was extracted form AR modelling the performance of the classifier dropped to 81%. By comparing Durand's results with those presented here, it can easily be seen that the adaptive SPL and improved spectral analyser used in this research clearly out performs those techniques in terms of the correct classification. Moreover, the SLP is simpler to implement. The improvement in terms of correct classification achieved by the method described in this chapter is believed to be mostly related to the accurate representation of the S2 characteristics by MFBPM. The classification technique adopted is also more than the earlier leave-one-out method. As was shown in section 5.3 the FFT and AR modelling do not provide accurate representation of S1 and S2. Therefore, it is most likely that spurious information will have been included in the input feature vectors when these methods were used to extract parameters from the spectral analysis of S2.

This is thought to be the cause of the deterioration in the performance of the classification technique. This conclusion is also supported by comparing our results with those presented by Guo *et al* [145]. In this latter case, a three-layer feed-forward back-propagation neural network was used to classify bioprosthetic valve sounds in the aortic position. Their results provided an 85% correct classification using spectral features obtained by the FFT, and 89% when AR modelling coefficients were used. Although a three-layer perceptron is a more complex and powerful model than the linear classifier described here, the results presented by Guo *et al* do not provide a significant improvement when compared with the results presented by Durand *et al* [76]. This fact emphasises the importance of the spectral analysis method applied to the analysis of S1 and S2 which has a direct impact upon feature extraction, the first stage of the classification procedure.

Although results obtained by the adaptive SLP in the evaluation of normal and malfunctioning C-E bioprosthetic valves are very good, it must be said that further investigation is required in order to validate the clinical use of the method. In this respect, a greater population is needed.

7.4 Conclusion

The performance of an adaptive SLP neural network for classifying the normal and malfunctioning Carpentier-Edwards bioprosthetic valves implanted in the aortic position was investigated for the case of twenty-six patients. The input features for the respective patterns were obtained from the modelling of second heart sounds by MF-BPM.

Results show that for the patient population this method classifies 100% correctly the normal and malfunctioning cases of C-E bioprosthetic valves implanted in the aortic position. It is believed that this high accuracy in correct classification can mostly be attributed to the accurate representation of the information contained in S2 by MF-BPM. However, a larger population is needed in order to validate the clinical use of the method.

Chapter 8

Conclusions

8.1 Introduction

The objective of the research described in this thesis was to investigate the feasibility of spectral phonocardiography as a method for automatic classification of normal and malfunctioning prosthetic heart valves. To achieve this objective, a three step approach was employed. Firstly, the performance of several spectral analysis techniques was investigated in order to establish the best method for representing the heart sounds produced during the closure of heart valves in vivo. Secondly, the relationship between the spectral composition of the externally recorded heart sounds and the condition of the heart valve was examined in order to assess the diagnostic potential of these methods. Finally, a methodology based on a combination a spectral analysis and a neural network classifier was applied in an effort to distinguish the normal and malfunctioning cases of Carpentier-Edwards bioprosthetic heart valves.

The following sections summarise the methods used in this research for the acquisition, conditioning, processing, and analysis of the phonocardiographic signal. The conclusions and achievements of the research are also given. The final section proposes possible extensions to the research detailed in the thesis.

8.2 Achievements

Chapter 2 introduced the area of spectral phonocardiography by first discussing the origin of the heart sounds. This chapter also provided the background material for the thesis by reviewing previous work done in this area with regard to the spectral

composition of first and second heart sounds and the monitoring of the condition of prosthetic heart valves in vivo.

The development of a data-acquisition system for recording phonocardiographic signals in a large variety of subjects, including native and prosthetic heart valves, was described in chapter 3. The design of the data-acquisition system was based on a number of significant hardware, software and ergonomic requirements to ensure high-quality reproduction of phonocardiographic signals. A two-channel system was designed to capture the PCG signal after a review of the spectral characteristics of sounds associated with the closure of native heart valves, bioprosthetic heart valves, mechanical prosthetic heart valves, and the characteristics of phonocardiographic transducers. The first recording channel, which has a frequency response from 500 Hz to 2 kHz, was used to record sounds produced by native and bioprosthetic heart valves. The second recording channel, which has a frequency bandwidth from 50 Hz to 10 kHz, was used to record the higher frequencies generated by the operation of mechanical prosthetic heart valves. The acquisition system comprised an Elonex LT-320X laptop personal computer, an analogue-to-digital convertor-42 input/output expansion card, two different types of microphone and analogue conditioning circuitry. The breakdown of the population of subjects used in this thesis was also presented in this chapter. Details of each subject are given in appendix A. It must be emphasised that a database of more than 150 different subjects now exists in the Department of Electrical Engineering at the University of Edinburgh, which provides an excellent opportunity for further research in this area.

Chapter 3 also considered the preprocessing of phonocardiographic signals in order to extract a ensemble first and second heart sound from the overall length of the recorded PCG signal. A semi-automatic heart sound extraction technique based on coherent averaging was implemented for this purpose. This technique makes use of the time relationship between the events in the ECG and PCG signals in order to detect the beginning of each cardiac circle. The time alignment of sounds included in the ensemble first and second heart sounds was then achieved using a cross-correlation method.

Chapter 4 introduced the spectral analysis methods investigated in this research for analysis of first and second heart sounds. Algorithms considered for frequency analysis of valvular closing sounds were: the FFT, the autoregressive Burg algorithm with four different types of weighting function, the original uniform Burg function, a Hamming taper function, an "optimum" parabolic weighting function, and a rectangular

window; sinusoidal signal identification, which is a data-block autoregressive modelling technique; several algorithms for autoregressive moving average modelling; and Prony's method. In addition, chapter 4 presented a modified forward-backward overdetermined Prony's method that represents more precisely in terms of the mean-least-square error the first and second heart sounds than other versions of Prony's method. Chapter 4 also introduced methods for determining the appropriate number of modelling coefficients, *i.e.* the model order, used by the parametric spectral estimation techniques. This is a very important issue, as the performance of parametric spectral methods is dependent on the criteria used to decide the proper model order. Model order criteria considered in this research were: final prediction error, Akaike information criterion, criterion autoregressive transfer, minimum description length, and methods based on the distribution and the consecutive relative ratio of the eigenvalue magnitudes of data matrix.

Chapter 5 investigated the performance of different spectral techniques when applied to the analysis of first and second heart sounds. This comparison is made possible by generating a synthesised first and second heart sound for each subject. The synthesised first and second heart sounds were generated based on the modified Prony's method. This method is used because it is believed that it best matches the characteristics of the underlying generating system. The matching between the real and synthesised sounds was estimated by the root-mean-square error and the normalised cross-correlation coefficient. Results obtained from more than 150 patients prove that the proposed modified forward-backward overdetermined Prony's algorithm outperforms the previous versions of the Prony's method in modelling the first and second heart sounds. The degree of improvement achieved with the proposed algorithm is due to the independence of the algorithm to the motion in the polynomial roots and the robustness of the mathematical procedure for estimating the position of signal poles. Furthermore, in contrast to previous techniques for modelling first and second heart sounds, the proposed procedure does not require an interactive procedure for initialisation and adjusting the model parameters.

From a signal processing perspective, it was found that all parametric methods based on singular value decomposition produced more accurate spectral representation than the conventional methods (*i.e.* the FFT and AR Burg algorithm). For the latter methods, it was found that both the FFT and AR Burg algorithm did not have sufficient resolution to detect all the spectral components contained in the first and second heart

sounds. Therefore, the extraction of the resonant frequencies of heart sounds from the spectrum produced by these two methods is very difficult, if not impossible. With regard to advanced parametric methods based on the SVD method, it can be said that, even though they outperform the conventional techniques in terms of spectral resolution, none of them was able to detect all the spectral components in all the cases with the required accuracy. This effect is due to the fact that fast-decaying sinusoids have wide spectral peaks, and those close to each other are often merged in the power spectrum analyser display. In this context, it is proposed that the parameters obtained from the time-modelling of heart sounds allow a more direct and accurate approach for presenting the information contained in the sounds from the closure of heart valves. In addition, the use of these parameters for automatic classification of PCG signals can lead to a reduced computational overhead.

A dynamic criterion based on the range of eigenvalue magnitudes and their consecutive relative ratio has also been proposed to choose the model order for the case of first and second heart sounds. This criterion can be defined as the biggest consecutive ratio of the eigenvalues in the region -40 dB to -60 dB on the ordered eigenvalue magnitude plot of the data matrix. It was observed that the model order varies from subject to subject which underlines the impact that the lung-thorax system has in the case of externally recorded PCG signals. This is an important point which has not been addressed in any of the previous published works in this field.

Summarising the conclusions reached in chapter 5, it can be stated that previous investigations of the spectral composition of first and second heart sounds can now be considered incomplete. This is not only because in most of the cases the analysis was performed by using the FFT or AR Burg algorithm, but when a more advanced parametric method was applied, a constant model order was used throughout the population under investigation. The research presented in this thesis suggests that the model order needs to be adjusted to suit particular data records in order to optimise the spectral analysis procedure. Thus, further research in this area is now necessary to investigate the origin of the heart sounds and for better understanding of the underlying signal generation process.

Chapter 6 investigated the relationship between the spectral composition of the externally recorded PCG signal and the condition of the heart valves. Firstly, the impact that heart-valve movement and the lung-thorax systems has on the heart sound spec-

tral composition was derived by investigating the same patients one day and four to six days after mechanical heart valve implantation. Secondly, the spectral characteristics of closing sounds produced by several types of prosthetic heart valves was also investigated.

It was found that the spectral composition of first and second heart sounds depends on the interaction between the heart-valve movement and the characteristics of the lung-thorax system. It was shown that the relative distribution of the amplitudes of spectral components is strongly related to the functioning of the heart valves, whereas the number of frequency components and their relative energy in more governed by the lung-thorax system.

In the case of mechanical prosthetic heart valves, it was found that the main part of the energy of the closing sounds was located below 2 kHz which supports the theory that the lung-thorax system behaves like a low-pass filter. A strong relationship was also found between the type of mechanical prosthetic heart valve and the distribution of the amplitudes of the spectral components contained in the first and second heart sounds. These results suggest that there is a clear correlation between the mechanical construction and the material of the mechanical prosthetic heart valve and the relative level of loudness generated during the closure of the prosthesis. This conclusion is also supported by the similarities found in the spectral composition of native and bioprosthetic heart valves.

Clear differences in terms of the amplitudes of the spectral composition were also found between normal and malfunctioning cases for respective patient groups. From preliminary results obtained in some cases of mechanical prosthetic malfunction, it was found that most of the differences between normal and malfunctioning cases occur in frequency components above 400 Hz. In the case of Carpentier-Edwards bioprosthesis, the spectrum above 250 Hz is mostly affected by the condition of the bioprosthetic valve.

Chapter 7 described the design, training and testing of an adaptive single layer perceptron for the classification of Carpentier-Edwards bioprosthetic heart valves implanted in the aortic position. It was found that for the patient population examined in this case a 100% correct classification was achieved. However, for practical assessment of the method it is suggested that a larger population is needed.

The objective of the research in this thesis has been to examine whether the spectral analysis of the closing sounds produced by prosthetic heart valves can be used as a diagnostic method. The proposition of this thesis is that when the appropriate methods are used to analyse these sounds, this objective can be meet with a high degree of success. Results in the case of Carpentier-Edwards bioprosthetic valves demonstrate the diagnostic potential of frequency analysis as an alternative physiological measurement technique, capable of assisting physicians in their post-operative assessment of prosthetic heart valves. Furthermore, the use of appropriate methods could lead to improved understanding of the underlying system that generates heart sounds. However, it must be emphasised that each type of valve has it own characteristics, hence the success of this method required specific consideration of the combination of frequency analysis with the subsequent pattern recognition methods.

8.3 Future work

A prototype system based on the combination of advanced signal processing methods with neural networks, for the processing and analysis of sounds produced by the operation of Carpentier-Edwards bioprosthetic heart valves is now operational. For this system to be more comprehensively tested, and its routine clinical value assessed, there is a requirement for a larger database of patients to be examined. It would also be of interest to investigate the feasibility of this method for all the other prosthetic heart valves. This would require recordings from many valve types and sizes, possibly obtained in consecutive time intervals since implantation of the valve. This procedure would lead to the investigation of how operational characteristics of the prosthetic heart valve change as a function of time. This could help therefore to detect prosthetic heart valve malfunction at an early stage.

The next stage then would be the real-time implementation of the algorithms. With the availability of high-speed digital signal processing chips, it would be possible to undertake a recording followed by a real-time analysis of the acquired phonocardiographic signal. This would lead to a more general system which could be used along side other traditional post-operative techniques such as echocardigraphy, with one method providing supplementary information to the other.

From a medical point of view, a more substantial extension to the research presented in this thesis, would be:

- The combination of esophageal heart sounds recording with the externally recorded phonocardiographic signal. From 1985 to 1988, a series of papers by Chin *et al.* [157] and Vermarien *et al.* [158] emphasised the diagnostic potential of esophageal phonocardiography for studying the origin of the first heart sound components. It would be of interest to investigate the frequency response of the transmission paths by comparing the signal morphology and its spectra in the case of esophageal and externally recorded phonocardiographic signal from the chest.

- Multi-site thoracic recordings.
  By significantly increasing the number of simultaneous recording sites, it could be of diagnostic use to investigate the radiation pattern of valve sounds across the thorax. This would provide useful information about the chronology of propagation of heart valve sound waves and source localisation, direction of sound radiation, and distribution of modal frequencies on the thorax.

The research reported in this thesis has shown that advanced parametric spectral analysis techniques can give better understanding of the generating system which produces heart sounds and proposes some answers regarding the controversies remaining on the genesis of heart sounds. However, there are many questions which remain unanswered regarding the stationarity, time-varying characteristics and nonlinear properties of heart sounds, as far as signal processing theory is concerned. In this context, it would certainly be worthwhile applying other signal processing techniques such as higher-order spectral analysis (HOSA) [149] or time-frequency methods (TFM) [150, 151].

There are three main motivations in using HOSA for analysing sounds produced by mechanical prostheses: (a) to suppress additive Gaussian noise, (b) to reconstruct the phase response of signals and/or the system, which is not available in second-order statistical spectral estimation methods such as ARMA and AR methods, (c) to detect and characterise nonlinearities in these sounds [152]. These characteristics of HOSA become very attractive when one bears in mind the nonlinear characteristics of the lung-thorax system, the dynamic vibration modes of mechanical prostheses [153] and the complexity of the cardiac system.

Other approaches such as TFM methods [150, 151] are also useful in the analysis of the non-stationary PCG signal. Barry [154] and Wood [151] have shown that muscle and heart sounds have a varying modal frequency which is due to changes in muscle stiffness during cardiac contraction. The usefulness of such methods when applied to the analysis of heart sounds has also been shown by Bentley [155] and Durand [156]. Based on these findings, it would be of diagnostic use to analyse the time variation of the dynamic properties of heart sounds when a prosthetic heart valve was implanted over the full time extent of the heart-beat rather than on a per sound basis as is done presently. However, bearing in mind the limitations of TFM methods, the presence of spurious information and poor frequency resolution, it would be useful to combine TFM methods with advanced parametric methods in order to obtain an optimal solution with respect to frequency resolution and the temporal extent of the dynamic events.

References

[1] P. J. Walter (Ed), "Quality of Life After Open Heart Surgery", *Kluwer Academic Publishers*, 1992.

[2] E. Braunwald, "Heart Disease: A Textbook of Cardiovascular Medicine, ISBN 0721630979, *W. B. Saunders Company*, 1992.

[3] R. E. Challis and R. I. Kitney, " Biomedical Signal Processing (in four parts), "Part 3: The Power Spectrum and Coherence Function", *Med.& Biol. Eng. & Comput.*, Vol. 29, pp. 225-241, May 1991.

[4] A. Baykal, Y. Z. Ider and H. Koymen, "Energy Distribution of the Resonance Components of PCG Signals on the Surface of the Chest". *IEEE Ann. Conference of the Eng. in Med. & Biol. Society*(EMBS), Vol. 2, No 2, pp. 576-557, 1990.

[5] A. H. Sabbagh, "Clotted Bjork–Shiley Mitral Valve Prostheses: Early Detection and Surgical Management", In *Cardiovascular Research Center Bulletin*, Vol. 21, No 4, pp. 100-107, 1983.

[6] L. Czinege, R. Urbanics and Z. Farkas, "Multi-Channel EEG Activity Correlation Analysis to Detect the Onset of Cerebral Ischemia", *Proc. of the 16th IEEE Ann. Conf. on EMBS*, Vol. 2, pp. 1230-1232, Baltimore Nov. 1994.

[7] A. Cohen and D. Landsberg, "Analysis and Automatic Classification of Breath Sounds", *IEEE Trans. on BME*, Vol 31, No. 9, pp. 585-590, Sept. 1984.

[8] V. Goncharoff, J. E. Jacobs and D. W. Cugell, "Wideband Acoustic Transmission of Human Lungs", *Med.& Biol. Eng. & Comput.*, Vol. 27, pp. 513-519, Sept. 1989.

[9] R. J. Triolo and M. Lawrence, "An Automated Method for Describing Muscle Fatige", *Proc. of the 16th IEEE Ann. Conf. on EMBS*, Vol. 1, pp. 337-339, Baltimore Nov. 1994.

[10] T. H. Joo, J. H. McClellan, R. A. Foale, G. S. Myers and R. S. Lees, "Pole-Zero Modelling and Classification of Phonocardiograms" *IEEE Trans. on BME*, Vol. 30, No. 2, pp. 110-118, Feb. 1983.

[11] R. J. Dobrow, J. B. Calatayud, S. Abraham and C. A. Caceres, "A Study of Physician Variation in Heart-Sounds Interpretation", *Annals of Medicine*, Vol. 33, pp. 305-311, 1964.

[12] J. S. Butterworth and E. H. Reppert, "Auscultatory Acumen in the General medical Population", *Journal of the Am. Medical Association*, Vol. 174, pp. 114-118, 1960.

[13] H. Feigenbaum, "Electrorardiography", *Heart Disease: A Textbook of Cardiovascular Medicine*, Vol. 1, Third Edition, E. Braunwald (Ed.), W. B. Saunders Company, pp. 83-88, 1988.

[14] J. N. Schapira, R. P. Martin, R. E. R. E. Fowles, H. Rakowski, E. B. Stinson, J. W. French, N. E. Shumway, and R. L. Popp, "Two Dimentional Echocardiography Assessment of PAtients with Biprosthetic Valves", *American Journal of Cardiology*, Vol. 43, pp. 510-519, March 1979.

[15] H. S. Rosman, M. Alam, J. B. Lakier, S. R. Kemp, H. N. Sabbah, D. J. Magilligan and P. D. Stein, "Utility of Physical Examination and Nonivasive Tests in the Diagnosis of Degeneration of Porcine Bioprosthetic Valves in the Mitral Position" *America Journal Noninvasive Cardiology*, Vol. 2, pp. 48-51, 1988.

[16] A. F. White, R. E. Dinsmore and M. J. Buckley, "Cineradiographic Evaluation of Prosthetic Cardiac Valves", *Circulation*, Vol. 48, pp. 882-889, 1973.

[17] D.W. Soubank, A. P. Yoganathan, E. C. Harrison and W. H. Corcoran, " A Quantitative Method for the *In Vitro* Study of Sounds Produced by Prosthetic Aortic Heart Valves (In three parts)", *Med.& Biol. Eng. & Comput.*, Vol. 22, pp. 32-55, Jan. 1984.

[18] A. Leatham, "Auscultation of the Heart and Phonocardiography", *J. & A.Churchill*, pp. 1-86, 1970.

[19] G. J. Leech and A. Leatham, "Correlation of Heart Sounds and Valve Motions", In "Evaluation of Cardiac Function by Echocardiography", W. Bleifeld, S. Effert,

P. Hanrath, D. Mathey (Eds.), *Springer–Verlag* Berlin Heidelberg New York, pp. 89–94, 1980.

[20] L-G. Durand, J. Genest and R Guardo, "Modelling of the Transfer Function of the Heart-Thorax Acoustic System in Dogs", *IEEE Trans. on BME*, Vol 32, No. 8, pp. 592-601, Aug. 1985.

[21] J. Verburgh and E. Van Vollenhoven, "Phonocardiograhpy: Physical and Technical Aspects and Clinical Uses", In Non-Invasive Physiological Measurements, P. Rolfe (Ed.), *Academic Press*, pp. 214–259, 1979.

[22] M. Akay, J. L. Semmlow,W. Levkowitz, M. D. Bauer and J. B. Kostis, "Detection of Coronary Occlusions Using Autoregressive Modelling of Diastolic Heart Sounds" *IEEE Trans. on BME-37*, No 4, pp. 366-373, April 1990.

[23] Y. M. Akay, M. Akay, W. Levkowitz, J. L. Semmlow and J. B. Kostis, "Noninvasive Acoustical Detection of Coronary Artery Disease: A Comparative Study of Signal Processing Methods", *IEEE Trans. on BME*, Vol. 40, No. 6, pp. 571-578, June 1993.

[24] P. J. Arnott, G. W. Pfeiffer and M. E. Tavel, "Spectral Analysis of Heart Sounds: Relationship Between Some Physical Characteristics and Frequency Spectra of First and Second Heart Sounds in Normals and Hypertensives", *Journal of Biomedical Eng.*, Vol. 6, pp. 121-128, April 1984.

[25] R. Beyar, Sh. Welkowitz, Sh. Braun and Y. Palti , "Heart–Sound Processing by Average and Variance Calculation- Physiologic Basic and Clinical Implications". *IEEE Trans. on BME*, Vol. 31, No 9, pp. 591–596, Sept. 1984.

[26] T. C. Hearn and J. Mazumdar, "Use of the Phonocardiogram for the Noninvasive Study of the Mitral Valve", *Australasian Physical Sciences in Medicine*. Vol 2-2, No. 79, pp. 96–101, Feb. 1979.

[27] A. Iwata, N. Suzumura and K. Ikegaya, "Pattern Classification of the Phonocardiogram Using Linear Prediction Analysis" , *Med. & Biol. Eng.& Comput.*, Vol. 15, pp. 407-412, July 1977.

[28] A. Iwata, N. Ishii and N. Suzumura, "Algorithm for Detecting the First and Second Heart Sound by Spectral Tracking", *Med, & Biol. Eng. & Comput.*, Vol. 18, pp. 19-26, Jan. 1980.

[29] A. Iwata, N. Ishii, N. Suzumura and K. Ikegaya, "Automatic Classification of the Phonocardiogram: I. Investigation for Several Factors of the Algorithm", *Automedica*, Vol. 3, pp. 165-173, 1980.

[30] A. P. Yoganathan, R. Gupta, F. E .Udwaidia, J. W. Miller, W. H. Corcoran, R. Sarma, J. L. Johnson and R. J. Bing, "Use of the Fast Fourier Transform in the Frequency Analysis of the First Heart Sound in Normal Man", *Med & Bio. Eng*, Vol. 14, pp. 69-73, Jan. 1976.

[31] A. P. Yoganathan, R. Gupta, F. E. Udwaidia and W. H. Corcoran, "Use of the Fast Fourier Transform in the Frequency Analysis of the Second Heart Sound in Normal Man", *Med & Bio. Eng*, Vol. 14, pp. 455-459, July 1976.

[32] P. D. Stein, H. N. Sabbah, J. B. Lakier and D. J. Magilligan, "Frequency of the First Heart Sound in the Assessment of Stiffening of the Mitral Bioprosthetic Valves", *Circulation*, Vol. 63, No, 1, pp. 200-203, 1981.

[33] M. K. A. Dayem and E. B. Raftery, "Mechanisms of Production of Heart Sounds Based on Records of Sounds After Valve Replacement", *The Amer. Journal of Cardiology*, Vol. 18, pp. 837-843, Dec. 1966.

[34] A. A. Luisada, "The Sounds of the Normal Heart", *Warren H. Green*, Inc., St. Louise, Missouri, U.S.A. 1972.

[35] A. Leatham and G. Leech, "Auscultation of the Heart", In The Heart, J. W. Hurst(Ed.), pp. 203-249, 1982.

[36] O. Orias, "The Genesis of Heart Sounds", *The New England Journal of Medicine*, Vol. 241, No. 20, pp. 763-769, Nov. 1949.

[37] G. Cloutier, M. C. Gernier, R. Guardo and L. G. Durand ," Spectral Analysis of Closing Sounds Produced by Ionescu-Shiley Bioprosthetic Aortic Heart Valves, Part 1: Optimal Number of Poles and Zeros for Parametric Spectral Analysis", *Med. & Biol. Eng. & Comput.*, Vol. 25, pp. 487-491, Sept. 1987.

[38] L-G Durand, Y. E. Langlois, T. Lanthier, R. Chiarella, P. Coppens, F. Lemire, M. Jarry, A. Solignac and Y. Latour, "Acoustic Transmission of the Aortic Component of the Second Heart Sound in Humans, Dogs and Pigs". *Innov. Tech. Biol. Med.*, Vol. 10, No. 4, pp. 383-393, April 1989.

[39] J. Rouanet, "Analyse des Bruits du Coeur", Paris thesis 1832, *cited in* [19].

[40] E. Craige, "On the Genesis of Heart Sounds", *Circulation*, Vol. 53, No. 1, pp. 207-209, Feb 1976.

[41] H. N. Sabbah and P. D. Stein, "Relation of the Second Sound to Diastolic Vibration of the Cosed Aortic Valve", *Am. J. Physiol.*, Vol. 3, pp. 696-700, 1978.

[42] P. D. Stein, H. N. Sabbah, J. B. Lakier, S. R. Kemp and D. J. Maglligan, "Frequency Spectra of the First Heart Sound and of the Aortic Component of the Second Heart Sound in Patients with Degenerated Porcine Bioprosthetic Valves", *The Am. J. Cardiol.* , Vol. 53, pp. 557-561, Feb. 1984.

[43] D. E. Harken, H. S. Soroff,W. J. Taylor, A. A. Lefemin, S. K. Gupta and S. Lunzer, "Partial and Complete Prostheses in Aortic Insufficiency". *J. Thorac. Cardiovas. Surg.*, Vol. 40, pp. 744-762, 1960.

[44] D. N. Ross, "Results After Biological Heart Valve Replacement", In "Quality of Life After Open Heart Surgery", P. J. Walter (Ed), *Kluwer Academic Publishers*, pp. 9-12, 1992.

[45] V. O. Bjork "The Bjork–Shiley Tilting Disc Valve: Past, Present and Future". In *Cardiac Surgery: State of the Art Reviews*, Vol 1. No. 2, pp. 183–211, Feb. 1987.

[46] A. Aris, C. Crexells, J. M. Auge. A. Oriol and J. M. Caralps, "Haemodynamic Evaluation of the Integral Monostrut Bjork–Shiley Prosthesis in the Aortic Position". *The Ann. of Thoracic Surgery*, Vol 40, No 2, pp. 234-240, 1985.

[47] T. H. Reif, T. J. Schulte and N. H. C. Hwang "Estimation of the Rational Undamped Natural Frequency of Bilaflet Cardiac Valve Prostheses",*J. of Biomechanical Eng.*, Vol. 112, pp. 327-332, Aug. 1990.

[48] J. C. Hylen, "Mechanical Malfunction and Thrombosis of Prosthetic Heart Valves". *The American Journal of Cardiology*, Vol. 30, pp. 396-404, Sept. 1972.

[49] E. Braunwald "Artificial Cardiac Valves", In "Heart Disease-A Textbook of Cardiovascular Medicine", Third Edition, *WB Saunders Company*, pp. 1078–1081, 1988.

[50] D. Horstkotte and R. Korfer, "The Influence of Prosthetic Valve Replacement on the Natural History of Severe Acquired Heart Valve Lesions". In "Advances in Cardiac Valves–Clinical Perspective" , DeBakey M.E.(Ed.), *Yorke–Medical Books*, pp. 47-87, 1982.

[51] L. I. Thulin, H. Reul, M. Giersiepen and C. L. Olin, "An *in Vitro* Study of Prosthetic Heart Valve Sounds", *Scand. J. Thor. Cardiovasc. Surg.*, No. 23, pp. 33-37, 1989.

[52] E. G. Butchart "Surgery for Heart Valve Disease", *Hospital Update*, Vol. 16, No. 12, pp. 963-973, Dec. 1990.

[53] N.E. R. Goodfield and P. Bloomfield, "Surgery for Valvular Heart Disease". *Hospital Update*, No. 1, pp. 1026-1034, 1992.

[54] D. P. Stein, N. H. Sabbah, E. A. Albert and J. E. Suyder "Spectral Signature of the Opening Sound of the Bjork–Shiley Convexo-Concave Valve as a Potential Indicator of Strut Fracture", *Am. Journal Noninvas. Cardiol.*, Vol. 1, pp. 369-372, 1987.

[55] A. Starr, "Ball Valve Prostheses: A Perspective After 22 Years". In "Advances in Cardiac Valves, Clinical Perspective", DeBakey (Ed.), *Yorke Medical Books*, pp. 1-14, 1982.

[56] B. Kingsley, "Acoustic Evaluation of Prosthetic Cardiac Valve in the Audio Spectrum", *Journal of the Audio Engineering Society*, Vol. 20, No 9, pp. 750-755, Nov. 1972.

[57] L-G. Durand, J. De Guise, G. Cloutier, R. Guardo and M. Brais, "Evaluation of FFT–Based and Modern Parametric Methods for the Spectral Analysis of Bioprosthetic Valve Sounds". *IEEE Trans. on BME*, Vol. 33, No 6, pp. 572-578, June 1986.

[58] R. Gordon, M. Najmi, B. Kingsley, B. L. Segal and J. W. Linhart, "Spectroanalytic Evaluation of Aortic Prosthetic Valves". *Chest*, Vol. 66, pp. 44-49, July 1974.

[59] J. C. Hylen, F. E. Kloster, R. H. Herr, A. Starr and H. Griswold, "Sound Spectrographic Diagnosis of Aortic Ball Variance", *Circulation*, Vol. 39, pp. 849-857, June 1969.

[60] Y. Kagawa, Sh. Nitta, N. Satoh, K. Saji, Y Shibota, T. Horiuchi and M. Tanaka, " Sound Spectroanalytic Diagnosis of Malfunctioning Prosthetic Heart Valve", *Tohoku J. Exp Medical*, Vol. 123, pp. 77-89, 1977.

[61] A. Iwata, N. Ishii, N. Suzumura and K. Ikegaya, "Automatic Classification of the Phonocardiogram: II. Discriminant Method", *Automedica*, Vol. 3, pp. 175-181, 1980.

[62] D. Nandagopal, J. Mazudar and R. E. Bogner, "Spectral Analysis of Second Heart Sounds in Normal Children by Selective Linear Prediction Coding" *Med. & Biol. Eng. & Comput,* Vol. 22, pp. 229-239, July 1984.

[63] A. Iwata, R. H. Boedeker, J. Dudeck, W. Pabst and N. Suzumura, "Computer Aided Analysis of Phonocardiogram", In *MEDINFO-83,* Bemmel Ball, Wiwertz, (Eds), *North-Holland,* pp. 569-572, 1983.

[64] D. Picard, J. Charara, R. Guidoin, Y. Haggag, D. Poussart, D. Walker and T. How, "Phonocardiogram Spectral Analysis Simulator of Mitral Valve Prostheses", *Journal of Medical Engineering & Technology,* Vol. 15, No 6, pp. 222-231, Nov. 1991.

[65] F. Schondube, H. Keusen and B. J. Messmer, "Physical Analysis of the Bjork-Shiley Prosthetic Valve Sounds", *J. Thorac Cardiovasc Surg.,* Vol. 86, pp. 136-141, July 1983.

[66] D. K. Walker and L. N. Scotten, "Discrimination *In Vitro* Between the Acoustic Emissions from Bjork–Shiley Convexo-Concave Valves with and Without a Broken Minor Strut". *Med & Bio. Eng. & Comput.,* Vol 29, pp. 457-464, Sept. 1991.

[67] Y. Kagawa, Sh. Nitta, M. Tanaka and T. Horiuchi, " Real-Time Sound Spectroanalysis for Diagnosis of Malfunctioning Prosthetic Valves", *J. Thorac Cardiovasc Surg.,* Vol. 79, pp. 671-679, May 1980.

[68] H. Koymen, B. K. Altay and Y. Z. Ider, "A Study of Prosthetic Heart Valve Sounds", *IEEE Trans. on BME,* Vol. 34, No. 11, pp. 853-863, Nov. 1987.

[69] H. Koymen, Y. Z. Ider and B. K. Altay, "A New Approach for the Analysis of Heart Valve Sounds", *IEEE Ann. Conference of the Eng. in Med. & Biol. Society.* pp. 136-139, 1986.

[70] H. Koymen, A. Baykal and Z. Ider, "Comparative Time Domain Modelling of Natural Heart Valve and Mechanical Heart Valve Sounds", *IEEE Ann. Conference of the Eng. in Med. & Biol. Society,* pp. 117-118, 1988.

[71] H. Koymen, A. Baykal, A. Z. Ider, Y. Zortuluna, O. Tasdemir, T. Tezcaner and K. Vural, "Study on the Generation of Closing Sounds From Metallic Prosthetic Heart Valve Implants", *IEEE Ann. Conference of the Eng. in Med. & Biol. Society,* pp. 55-56, 1989.

[72] A. Moritz, U. Steinseifer, G. Kobinia, K. Neuwirth–Riedl, H. Wolters, H. Reul and E. Wolner,"Closing Sounds and Related Complaints After Heart Valve Replacement with St. Jude Medical, Duromedics Edwards, Bjork–Shiley Monostrut, and Carbomedics Prostheses". *Br. Heart J.*, Vol. 67, pp. 460–465, 1992.

[73] M. Brais, L-G Durand, M. Blanchard, J. De Guise, R. Guardo and W. J. Keon, "Frequency Analysis of Ionesku-Shiley Prosthetic Closing Sounds in Patient with Normally Functioning Prostheses", *Med. & Biol. Eng. & Comput.*, Vol. 24, pp. 637-642, Nov. 1986.

[74] G. Cloutier, R. Guardo and L. G. Durand ," Spectral Analysis of Closing Sounds Produced by Ionescu-Shiley Bioprosthetic Aortic Heart Valves, Part 3: Performance of FFT-Based and Parametric Methods for Extracting Diagnostic Spectral Parameters", *Med. & Biol. Eng. & Comp.*, Vol. 25, pp. 497-503, Sept. 1987.

[75] G. Cloutier, L. G. Durand, R. Guardo, H. Sabbah and P. D. Stein," Bias and Variability of Diagnostic Spectral Parameters Extracted From Closing Sounds Produced by Bioprosthetic Valves Implanted in the Mitral Position", *IEEE Trans. on BME*, Vol. 26, No. 8, pp. 815-825, Nov. 1989.

[76] L-G. Durand, Z. Guo, H. N. Sabbah and P. D. Stein, " Comparison of Spectral Techniques for Computer-Assisted Classification of Spectra of Heart Sounds in Patients with Porcine Bioprosthetic Valve", *Med. & Biol. Eng. & Comput.*, Vol. 31, pp. 229-236, May 1993.

[77] R. A. Foale, T. H. Joo, J. H. McClellan, R. W. Metzinger, G. L. Grant and G. S. Myers, " Detection of Aortic Porcine Valve Dysfunction by Maximum Entropy Spectral Analysis", *Circulation*, Vol. 68, pp. 42-49, July 1983.

[78] L-G Durand, M. Blanchard, G. Cloutier, H. Sabbah and P. D. Stein, "Comparison of Pattern Recognition Methods for Computer-Assisted Classification of Spectra of Heart Sounds in Patients With a Porcine Bioprosthetic Valve Implanted in the Mitral Position", *IEEE Trans. on BME*, Vol. 37, No. 12, pp. 1121-1129, Dec. 1990.

[79] L-G. Durand, P. D. Stein, M. C. Grenier, J. W. Henry, R. Inderbitzen and D. W. Wieting, "*In Vitro* and *in Vivo* Low Frequency Acoustic Analysis of Bjork-Shiley Convexo-Concave Heart Valve Opening Sounds". *Proc. 1994 IEEE Seventh Symposium on Computer-Based Medical Sys.*, pp. 61-66, June 1994.

[80] G. A. Kein, B. Jeffries, H. V. Katz, B. A. Herman, R. F. Carey, D. J. Chwirut and H. F. Bushar, "Digital Acoustical Analysis of Normal and Bimodal Bjork-Shiley 60° Convexo-Concave Heart Valves", *The Am. Journal of Cardiology*, Vol. 66, pp. 849-854, Oct. 1990.

[81] R. Fischer, V. Padmanabhan, J. Semmlow, W. Welkowitz and J. Kostis, "Comparative Evaluation of Cardiac Microphones" , *Proc. of 10th IEEE Annual Conf. in EMBS*, pp. 167-169, 1988.

[82] R. Bedi "Signal Processing and Frequency Analysis of Carpentier-Edwards Biprosthetic Heart Valve Sounds", *PhD Thesis*, University of Edinburgh 1994.

[83] L-G. Durand and R. Guardo "Comparison of Air and Contact Microphones for Estimating the Acoustic Transmission of Heart Sounds in Dogs", *Innov. Tech. Biol. Med.*, Vol 7, No 4, pp. 458-473, July 1986.

[84] Knowles Electronics, Inc, *Data Acquisition Manual*, 1992.

[85] V. Padmanabham, J. L. Semmlow and W. Welkowitz, " Accelerometer Type Cardiac Transducer for Detection of Low–Level Heart Sounds", *IEEE Trans. on BME*, Vol. 40, No 1, pp. 21-28, Jan. 1993.

[86] E. Van Vollenhoven, "Calibration of Contact Microphones Applied to the Human Chest Wall", *Med. & Biol. Eng.*, Vol. 9, pp. 365-373, 1971.

[87] R. S. Schwartz, J. T. Reeves, I. E. Sodal and F. S. Barnes, " Improved Phonocardiogram System Based on Acoustic Impedance Matching", *Amer. J. Physiol*, Vol. 238, pp. 604-609, 1980.

[88] N. Suzumura and K. Ikegaya, "Characteristics of the Air Cavities of Phonocardiographic Microphones and the Effects of Vibration and Room Noise", *Med. & Bio. Eng. & Comput.*, Vol. 15, pp. 240-247, May 1977.

[89] H. Vermarien and E. Van Vollenhoven, "The Recording of Heart Vibrations: A Problem of Vibration Measurement on Soft Tissue". *Med & Biol. Eng. & Comput.*, Vol. 22, pp. 168–178, March 1984.

[90] R. L. Donnerstein, W.A. Scott, A. Vasu and J. G. Copeland, "Acoustic Analysis of the Closing Sounds of Bileaflet Prosthetic Valves in a Sheep Model". *J. Thorax Cardiovasc. Surg.*, Vol. 101, pp. 1060-1068, 1991.

[91] R. E. Challis and R. I. Kitney, " Biomedical Signal Processing (in four parts), "Part 1: Time-Domain Methods", *Med. & Biol. Eng. & Comput.*, Vol. 28, pp. 509-524, Nov. 1990.

[92] A. Baykal, Y. Z. Ider and H. Koymen, "Use of Signal Averaging in Analysis of the Digital Phonocardiograms" *IEEE Ann. Conference of the Eng. in Med. & Biol. Society*, Vol. 13 , No 5, pp. 2103–2104, 1991.

[93] G. M. Freisen, Th. C. Jannett, M. A. Jadallah, S. L. Yates, S.R. Quint and H.T. Nagle, "A Comparison of the Noise Sensitivity of Nine QRS Detection Algorithms", *IEEE Trans. on BME,* Vol. 37, No. 1, pp. 85-98, Jan. 1990.

[94] P. O. Borjesson, O. Pahlm, L. Sornmoand and M-E Nygards, "Adaptive QRS Detection Based on Maximum a Posteriori Estimation", *IEEE Trans. on BME*, Vol. 29, pp 341-351, May 1982.

[95] J. Fraden and M. R. Neuman, "QRS wave detection", *Med. & Biol. Eng. & Comput.*, Vol. 18, pp. 125-132, 1980.

[96] J. G. Proakis and D. G. Manolakis, "Digital Signal Processing-Principles, Algorithms and Application" *Maxwell Macmillan Inter. Editions*, 1992.

[97] R. E. Challis and R. I. Kitney, " Biomedical Signal Processing (in four parts), Part 2: The Frequency Transforms and Their Iter-Relationships" *Med. & Biol. Eng. & Comput.*, Vol. 29, pp. 1-17, Jan. 1991.

[98] D. A. Linkens, "Short-Time-Series Spectral Analysis of Biomedical Data", *IEE Proceedings*, Vol. 129, Pt A, No. 9, pp. 663-672, Dec. 1982.

[99] S. M. Kay and S. L. Marple, "Spectrum Analysis–A Modern Perspective", *Proceedings of the IEEE*, Vol. 69, No. 11, pp. 1380- 1419, Nov. 1981.

[100] S. Hykin, "Adaptive Filter Theory", *Prentice-Hall International*, 1991.

[101] J. W. Cooley and J.W. Tukey, "An Algorithm for Machine Calculation of Complex Fuorier Series", *Math. Comput.*, Vol. 19, pp. 297-301, Apr. 1965.

[102] P. M. Grant, C. F. N. Cowan, B. Mulgrew and J. H. Drips, "Analogue and Digital Signal Processing and Coding", *Chartwell-Bart (Publishing and Training) Ltd.*, 1989.

[103] B. I. Helme, Ch. L. Nikias, "Improves Spectrum Performance Via a Data-Adaptive Weighted Burgh Technique", *IEEE Trans. on ASSP*, ASSP-33, No. 4, pp. 903-910, August 1985.

[104] S.L. Marple, "Digital Spectral Analysis (with Application)", *Prentice-Hall*, 1987.

[105] L. Marple, "A New Autoregressive Spectrum Analysis Algorithm", *IEEE Trans. on ASSP*, Vol. ASSP-28, No. 4, pp. 441-454, Aug. 1980.

[106] S. M. Kay " The Effects of Noise on the Autoregressive Spectral Estimator", *IEEE on ASSP*, Vol. ASSP-27, No. 5, pp. 478-485, Oct. 1979.

[107] L. L. Scharf "The SVD and Reduced Rank Signal Processing", *Signal Processing*, Vol. 25, pp. 113-133, Oct. 1991.

[108] V. C. Klema and A. J. Lamb, "The Singular Value Decomposition: Its Computation and Applications", *IEEE Trans. on Automatic Control*, AC-25, No. 2, pp 164-176, April 1980.

[109] J. A. Cadzow, B Baseghi and T. Hsu, "Singular-Value Decomposition Approach to Time Series Modelling", *IEE Proceedings*, Vol. 130, Pt. F, No. 3, pp. 202-210, April 1983.

[110] D. W. Tufts and R Kumaresan, " Singular Value Decomposition and Improved Frequency Estimation Using Linear Prediction", *IEEE Trans. on ASSP*, ASSP-30, No. 4, pp. 671-675, Aug. 1982.

[111] J. A. Cadzow and D. Mitchell Wilkes, "Enhanced Rational Signal Modelling", *Signal Processing*, Vol. 25, pp. 171-188, Oct. 1991.

[112] J.A. Cadzow, " Spectral Estimation: An Overdetermined Rational Model Equation Approach", *Proceedings of the IEEE*, Vol. 70, No 9, pp. 907-939, Sept. 1982.

[113] B. Friedlander and B. Porat, "The Modified Yule–Walker Method of ARMA Spectral Estimation", *IEEE Trans. on ASE*, ASE-20, No. 2, pp. 158-172, March 1984.

[114] J. A. Cadzow, "ARMA Time Series Modelling: An Effective Method", *IEEE Trans. on Aerospace and Electronic Systems*, AES–19, No. 1, pp. 49-58, Jan. 1983.

[115] R. Kumaresan and D. W. Tufts, "Estimating the Parameters of Exponentially Damped Sinusoids and Pole–Zero Modelling in Noise", *IEEE Trans. on ASSP*, ASSP-30, No.6, pp. 833-840, Dec. 1982.

[116] K. Minami, N. Schlumberger and S. Kawata, " Prony's Method Based on Eigenanalysis and Overdetermined System Aproach", *IEEE Ann. Inter. Conf. on ASSP*(ICASSP), pp. 1393-1396, Tokyo 1986.

[117] M. Van-Blaricum and R. Mittra " Problems and Solutions Associated with Prony's Method for Processing Transient Data", *IEEE Trans. on Antennas and Propagation*, AP-26, No. 1, pp. 174-183, Jan. 1978.

[118] J. Laroche, "A New Analysis-Synthesis of Musical Signals Using Prony's Method: Application to Heavily Damped Percussive Sounds", *IEEE Ann. Conf. on ASSP*(ICASSP), Glasgow, pp. 2053-2056, May 1989.

[119] B. Porat and B. Friedlander, "On the Accuracy of the Kumaresan-Tufts Method for Estimating Complex Damped Exponentials", *IEEE Trans. on ASSP*, ASSP-35, No. 2, pp. 231-235, Feb. 1987.

[120] R. Kumaresan, D. W. Tufts and L. L. Scharf " A Prony Method for Noisy Data: Choosing the Signal Components and Selecting the Order in Exponential Signal Models", *Proc. of the IEEE*, Vol. 72, No. 2, pp. 230-233, Feb. 1984.

[121] D. V. B. Rao "An Explanation to the Limitation Observed in the Kumaresan-Prony Algorithm", *IEEE Trans. on ASSP*, ASSP-34, No. 5, pp. 1338-1340, Oct. 1986.

[122] E. F. Deprettere (Ed) "SVD and Signal Processing Algorithms, Applications and Architectures", *Elsevier Publ., North Holland*, 1988.

[123] T. Yu, "Improving the Accuracy of Parameter Estimation for Real Exponentially Damped Sinusoids in Noise", *IEE Proc.* Vol. 137, Pt. F, pp. 192-196, June 1990.

[124] W.H. Press, B. P. Flannery, S. A. Teukolsky and W. T. Vetterling "Numerical Recipies in C", *Cambridge Univ. Press*, 1988.

[125] B. C. Kuo, "Digital Control Systems", *Holt-Saunders International Editors*, Tokyo 1983.

[126] H. P. Sava and J.T.E. McDonnell, "Comparison of Spectral Analysis Algorithms for Use in Spectral PCG", In *Proceedings of EUSIPCO-94*, pp. 62-66, Sept. 1994.

[127] M. Wax and Th Kailath, "Detection of Signal by Information Theoretic Criteria", *IEEE Trans. on ASSP*, ASSP-33, No. 2, pp. 387-392, April 1985.

[128] K. Kostantinides and K. Yau, "Statistical Analysis of Effective Singular Values in Matrix Rank Determination", *IEEE Trans. on ASSP*, ASSP-36, No. 5, pp. 757-763, May 1988.

[129] M. Bouvet and H. Clergeot, "Eigen and Singular Value Decomposition Techniques for the Solution of Harmonic Retrieval Problems", In SVD and Signal Processing (Algorithms, Applications and Architectures), E. F. Deprettere (Ed), pp. 93-115, *Elsevier Publ., North Holland*, 1998.

[130] D. N. Swingler, "A Modified Burgh Algorithm for Maximum Entropy Spectral Analysis", *Proceedings of the IEEE*, Vol. 67, No. 9, pp. 1368-1369, Sept. 1979.

[131] T. J. Ulrych, Th. N. Bishop, "Maximum Entropy Spectral Analysis and Autoregressive Decomposition", *Rev. Geophysics and Space Physics*, Vol. 13, No. 1, pp. 183-200, Feb. 1975.

[132] R. Rangayyan and R. J. Lehner, "Phonocardiogram Signal Analysis: A Review", *Critical Reviews in Bio. Eng.*, Vol 15, Issue 3, pp. 211-236, 1988.

[133] W. Campbell and D. N. Swingler, "Frequency Estimation Performance of Several Weighted Burg Algorithms", *IEEE Trans. on Sig. Proc.* Vol. 41, No3, pp. 1237-1247, March 1993.

[134] R. Erickson, L. Thulin and G. Richard, "*In-Vitro* Study of Mechanical Heart Valve Sound Loudness as Measured by ISO-532/B" *Proc. of 1994 IEEE Seventh Symposium on Comp.-Based Medical Systems*, pp. 53-54, June 1994.

[135] H.P. Sava, E. McDonnell and P. Bentley, "Analysis of Phonocardiographic Signals Using Advanced Signal Processing Methods", *IPSM–Signal Proc. in Medicine Meeting*, London, pp. 17, Nov. 1994

[136] J-J Fuchs, "Estimating the Number of Sinusoids in Additive White Noise", *IEEE Trans. on ASSP*, Vol. 36, No 12, pp. 1846-1853, Dec. 1988.

[137] J. A. Cadzow, "Signal Processing Via Least Squares Error Modelling", *IEEE ASSP Magazine*, Vo. 7, No. 4, pp. 12-31, Oct. 1990.

[138] V. U. Reddy and L. S. Biradar, "SVD-Based Information Theoretic Criteria for Detection of the Number of Damped/Undamped Sinusoids and Their Performance Analysis", *IEEE Trans. on Sig. Proc.*, Vol. 41, No. 9, pp. 2872-2881, Sept. 1993.

[139] D. W. Tufts and R Kumaresan, " Estimation of Frequencies of Multiple Sinusoids: Making Linear Prediction Perform Like Maximum Likelihood", *Proceedings of the IEEE*, Vol. 70, No. 9, pp. 975-989, Sept. 1982.

[140] G. Liang, M. Wilkes and J. A. Cadzow, "ARMA Model Order Estimation Based on the Eigenvalues of the Covariance Matrix" *IEEE Trans. on Sig. Proc.* Vol. 41, No 10, pp. 3003-3009, Oct. 1993.

[141] W. Craelius, M. Restivo, M. A. Assadi and N. El-Sherif,"Criteria for Optimal Averaging of Cardiac Signals", *IEEE Trans. on BME*, Vol. 33, No. 10, pp. 957-966, Oct. 1986.

[142] L-G Durand, Y-E Langlois, T. Lanthier, R. Chiarella, P. Coppens, S. Carioto, S. Bertrand-Bradly. "Spectral Analysis and Acoustic transmission of Mitral and Aortic valve Closure Sounds in Dogs(Part 2)", *Med.& Biol. Eng. & Comput.*, Vol. 28, pp. 278-286, July 1990.

[143] L.E .Kinsler, A. R. Frey, A.B. Coppens and J. V. Sanders, "Fundamentals of Acoustics (Third Edition)", *John Wiley and Sons*, Inc, pp. 262, 1982.

[144] N. D. Smith, V. Raizada and J. Abrams, "Auscultation of the Normally Functioning Valve", *Ann. Intern. Med.*, Vol 95, pp. 595, 1981.

[145] Zh. Guo, L-G Durand, H. C. Lee, L. Allard, M-C. Grenier, and P. Stein, "Artificial Neural Networks in Computer Assisted Classification of Heart Sounds in Patients with Porcine Bioprosthetic Valves",*Med. & Biol. Eng. & Comput.*, Vol. 32, pp. 311-316, May 1994.

[146] S. Haykin, "Neural Networks; A Comprehensive Foundation", *Macmillan College Publishing Comp.*, 1994.

[147] R. P. Lippmann, "An Introduction to Computing with Neural Nets", *IEEE ASSP Magazine*, Vol. 4, No. 2, pp. 4-22, April 1987.

[148] R. Beale and T. Jackson, "Neural Computing: An Introduction", *IOP Publishing Ltd*, 1990.

[149] J. M. Mendel, "Tutorial on Higher–Order Statistics(Spectra) in Signal Processing and System Theory: Theoretical Results and Some Applications", *Proceedings of the IEEE*, Vol. 79, No. 3, pp. 277-305, March 1991.

[150] L. Cohen, "Time–Frequency Distributions-A Review", *Proceedings of the IEEE*, Vol. 77, No. 7, pp. 941-981, July 1989.

[151] J.C. Wood, A. J. Buda, D. T. Barry, "Time–Frequency Transforms: A new Approach to First Heart Sound Frequency Dynamics", *Trans. of IEEE on BME*, Vol 39, No. 7, pp. 730-740, July 1992.

[152] Ch. Nikias, "Higher-Order Spectral Analysis",*Proceedings of the 15th Annual International Conference IEEE in Engineering in Medicine and Biology Society*, Vol. 1, pp. 319, 1993.

[153] G-J. Cheon and K. B. Chandran, "Dynamic Behaviour Analysis of Mechanical Monoleaflet Heart Valve Prostheses in the Opening Phase". *J. of Biomech. Engineering*, Vol. 115, pp. 389-395, Nov. 1993.

[154] D. T. Barry and T. Cole, "Muscle Sounds are Emitted at the Resonant Frequencies of Skeletal Muscle" *IEEE Trans. on BME.*, Vol. 37, No. 5, pp. 525-531, 1990.

[155] P. Bently, J.T.E. McDonnell, "Time-Frequency Analysis and Diagnisis of Native Heart Valves", *IEE Colloquim in DSP methods in Cardiology*, London, Colloquim Digest, pp. 91-96, March 1995.

[156] D. Chen, L-G Durand, H. Lee, "Selection of a Time-Frequency representation for Analysis of the First Heart Sound Signal". *Proceedings 16th Annual International Conference IEEE Engineering in Medicine and Biology Society*, Baltimore (USA), pp. 1276-1278, 1994.

[157] J.G.J. Chin, H. Vermarien, E. Van Vollenhoven, J. Koops, P.J. Voogd, "Clinical Application of the Biaxial Esophagus Microphone, Especially in the Mitral regurgitation". *Acta Cardiologica*, Vol. 43, No. 3, pp. 297-300, 1988.

[158] H. Vermarien, J.G.J. Chin, E. Van Vollenhoven, J. Jacqueloot, D. Vandewoude, J. Koops, "Technical Improvements on Biaxial Esophageal Heart Vibration Recording". *Acta Cardiologica*, Vol. 43, No. 3, pp. 403-407, 1988.

Appendix A: Data Records

| Patient's | Patient Information | | | |
Code	Valve Type	Sex	Age	Diagnosis
P1BM	24M SE	F	65	AVD
P2BM	2M SE	F	56	SMVD
P3BM	31mm C	M	70	SMS
P4BM	4M SE	M	72	GMR+CAD
P5BM	19mm C	F	54	MS+MR
P6BM	27mm C	F	55	SMVD
P7BM	29mm AT	F	66	MR+CAD
P8BM	29mm SB	M	44	GMR
P9BM	27mm C	F	55	SMS
P10BM	27mm AT	F	69	SMS
P11BM	31mm C	M	62	AVD
P12BM	31mm C	F	62	MS+MR
P13BM	33mm C	M	77	SMS
P14BM	27mm SB	F	66	SMR
P15BM	29mm AT	F	51	AVD

Table 8.1:   Clinical data for normal patients who underwent mechanical heart valve implantation in the mitral position(S-E=Star-Edwards, C=Carbomedics, SB=Sorin-Bicarbon, AT=Aortech, AVD=Aortic Valve Disease, SMS=Severe Mitral reflux, MR=Mitral Regurgitation, SMVD=Severe Mitral Valve Disease, GMR=Gross Mitral Reflux, CAD=Coronary Artery Disease, MS=Mitral Stenosis).

Patient's Code	Patient Information			
	Valve Type	Sex	Age	Diagnosis
P1BA	19mm SB	F	72	SAS
P2BA	21mm SB	M	58	CAS
P3BA	25mm AT	M	51	CAS
P4BA	23mm AT	M	51	CAS
P5BA	27mm AT	M	65	SAS
P6BA	21mm C	M	58	SAS
P7BA	21mm C	M	62	SAS
P8BA	23mm C	M	74	SAS
P9BA	21mm C	F	74	SAS
P10BA	23mm C	M	6	ADV
P11BA	27mm C	M	52	SAS
P12BA	25mm SB	M	62	SAS
P13BA	19mm C	F	62	SAS
P14BA	27mm AT	F	54	AVD
P15BA	23mm C	F	67	AVD

Table 8.2:   Clinical data for normal patients who underwent mechanical heart valve implantation in the aortic position (SE=Star-Edwards, C=Carbomedics, SB=Sorin-Bicarbon, AT=Aortech, SAS=Severe Aortic Stenosis, CAS=Calcified Aortic Stenosis, AVD=Aortic Valve Disease).

Patient's	Patient Information		
Code	Valve Size	Sex	Age
P1BShA	25mm	M	63
P2BShA	23mm	F	54
P3BShA	23mm	F	67
P4BShA	21mm	F	51
P5BShA	19mm	F	65
P6BShA	23mm	M	53
P7BShA	17mm	F	56
P8BShA	25mm	M	49
P9BShA	25mm	M	46
P10BShA	31mm	F	56
P11BShA	23mm	M	29
P12BShA	25mm	F	36
P13BShA	25mm	M	56
P14BShA	23mm	M	66
P15BShA	21mm	M	51
P16BShA	25mm	M	65
P17BShA	23mm	M	53
P18BShA	21mm	F	48
P19BShA	19mm	F	60
P20BShA	19mm	F	56
P21BShA	21mm	F	35

Table 8.3:   Clinical data for normal patients with Bjork-Shiley valves in the aortic position who were investigated in this study.

Patient's	Patient Information		
Code	Valve Size	Sex	Age
P1CA	19mm	M	29
P2CA	21mm	M	45
P3CA	18mm	F	50
P4CA	21mm	M	54
P5CA	18mm	F	37
P6CA	21mm	M	56
P7CA	21mm	M	58
P8CA	23mm	M	62
P9CA	21mm	F	74
P10CA	23mm	M	66
P11CA	27mm	M	62
P12CA	19mm	F	62
P13CA	19mm	F	46

Table 8.4: Clinical data for normal patients with Carbomedics valves in the aortic position who were investigated in this study.

Patient's	Patient Information		
Code	Valve Size	Sex	Age
P1SEM	28mm	F	56
P2SEM	27mm	M	65
P3SEM	28mm	F	52
P4SEM	24mm	F	53
P5SEM	26mm	M	72
P6SEM	23mm	M	62
P7SEM	30mm	F	54
P8SEM	30mm	M	68
P9SEM	24mm	M	38
P10SEM	28mm	M	58
P11SEM	32mm	M	72

Table 8.5: Clinical data for normal patients with Starr-Edward valves in the mitral position who were investigated in this study.

Patient's	Patient Information		
Code	Valve Size	Sex	Age
P1BShM	27mm	F	60
P2BShM	25mm	F	42
P3BShM	21mm	F	57
P4BShM	29mm	F	50
P5BShM	31mm	F	57
P6BShM	21mm	F	66
P7BShM	27mm	M	54
P8BShM	31mm	M	51

Table 8.6:   Clinical data for normal patients with Bjork-Shiley valves in the mitral position who were investigated in this study.

Patient's	Patient Information		
Code	Valve Size	Sex	Age
P1CENA	21mm	M	76
P2CENA	19mm	M	79
P3CENA	19mm	F	82
P4CENA	21mm	F	77
P5CENA	25mm	M	78
P6CENA	21mm	M	78
P7CENA	21mm	F	80
P8CENA	23mm	M	63
P9CENA	19mm	F	83
P10CENA	21mm	F	84
P11CENA	25mm	M	73
P12CENA	21mm	F	76
P13CENA	25mm	M	69
P14CENA	21mm	M	71

Table 8.7:   Clinical data for patients with normal functioning Carpentier-Edwards bioprosthesis valves in the aortic position who were investigated in this study.

Patient's	Patient Information		
Code	Valve Size	Sex	Age
P1CEMA	21mm	F	55
P2CEMA	23mm	M	81
P3CEMA	19mm	M	80
P4CEMA	21mm	F	74
P5CEMA	23mm	M	67
P6CEMA	25mm	M	81
P7CEMA	19mm	F	76
P8CEMA	23mm	M	78
P9CEMA	23mm	M	66
P10CEMA	25mm	F	69
P11CEMA	21mm	M	42
P12CEMA	23mm	F	68

Table 8.8: Clinical data for patients with malfunctioning Carpentier-Edwards bioprosthesis valves in the aortic position who were investigated in this study.

Appendix B: Authors publications

The work described in this thesis has been reported in the following publications:

1. H. Sava and J.T.E. McDonnell "Comparison of Spectral Analysis Technique for Use in PCG", *Proceedings EUSIPCO 94 Conference*, Edinburgh 1994, pp 60-64 (see accompanying reprint).

2. H. Sava, J .T.E. McDonnell and K.A.A. Fox, "Spectral Analysis of First and Second Heart Sounds Before and After Mechanical Heart Valve Implantation", *Proceedings 16th Annual International Conference IEEE Engineering in Medicine and Biology Society* pp. 1274-1275, Baltimore (USA) 1994.

3. H.Sava, and J.T.E. McDonnell "New Analysis-Synthesis of First Heart Sounds Using Forward-Backward Overdetermined Prony's Method" *Proceedings 16th Annual International Conference IEEE Engineering in Medicine and Biology Society* pp. 1280-1281, Baltimore (USA) 1994.

4. H. Sava, J.T.E. McDonnell and P. Bentley "Analysis of PCG Signals Using Advanced Signal Processing Methods" *Digest of Abstracts Institute of Physical Sciences in Medicine and Biological Engineering Society Meeting on Signal Processing in Medicine*, IPSM/BES Colloquium, p 17, London 1994.

6. H. Sava and J.T.E. McDonnell " A Modified Forward-Backward Overdetermined Prony's Method and Its Application in Modelling Heart Sounds", *Proceedings of IEE Vision Image and Signal Processing*, submitted for review.

7. H. Sava and J.T.E McDonnell "Difference in Spectral Composition Between Monostrut Bjork-Shiley and Carbomedics Valves in Aortic Position" *Medical and Biol. Eng. and Computing*, 1994, accepted for publication.

8. H.Sava and J.T.E. McDonnell " Spectral Composition of Heart Sounds Before

and After Mechanical Heart Valve Implantation Using a Modified Forward-Backward Prony's Method" *IEEE Transactions on Biomedical Engineering*, 1994, submitted for review.

9. H. P. Sava, P. M. Grant and J. T. E. McDonnell, "Spectral Characteristics and Classification of Normally and malfunctioning Carpentier-Edwards Bioprosthetic Heart Valves Implanted in the Aortic Position", *IEEE Transactions on Biomedical Engineering*, 1995, submitted for publication.

10. H. P. Sava, J. T. E. McDonnell and K. A. Fox, "Frequency Characteristics Produced By Mechanical Prosthetic Heart Valves (Review)", *Innovation et Technologie en Biologie et Medicine*, submitted for publication.

11. H.P Sava, R. Bedi, J.T.E. McDonnell and P. M. Grant, "Classification of Carpentier-Edwards Bioprosthetic Heart Valves Using an Adaptive Single Layer Perceptron", *submitted for publication in* Proc. of the 17th Annual International Conf. of the IEEE Eng. in Medicine and Biology Society.

12. H.P Sava, J.T.E. McDonnell and P. M. Grant, "Spectral Composition of Closing Sounds Produced by Mechanical Prosthetic Heart Valves ", *submitted for publication in* Proc. of the 17th Annual International Conf. of the IEEE Eng. in Medicine and Biology Society.

13. H.Sava and J.T.E. McDonnell " Performance of Parametric Methods in Spectral PCG" *Medical and Biol. Eng. and Computing*, 1995 submitted for review.

Comparison of Spectral Analysis Algorithms for Use in Spectral Phonocardiography

Herkole P. SAVA and Edward McDONNELL

Dept. of Electrical Eng., The University of Edinburgh, Edinburgh EH9 3JL,

Scotland U. K., Tel/Fax +44 [31] 650 5655 / 650 6554. E-mail: hsava@ee.ed.ac.uk

Abstract. The use of spectral analysis of heart sounds has been found to be an effective method for detecting different valvular diseases, monitoring the condition of prosthetic heart valves and of studying the mechanism of heart action. In this context, the method used for this analysis is of crucial importance because diagnostic criteria depend on the accuracy of estimation of the spectrum. This paper compares the performance of the Fast Fourier Transform (FFT), Maximum Entropy or Burg algorithm, autoregressive moving-average (ARMA) and modified backward Prony's method (MBPM) when applied to analysis of the first (S1) and the second (S2) heart sounds. From the results achieved, it is concluded that MBPM based on principal eigenvalues achieves the best results for both simulated and real signals. In all cases parametric methods are more appropriate than the FFT provided the proper model order is selected.

1 Introduction

Spectral phonocardiography (SPCG) is an effective noinvasive method of diagnosing human heart diseases and of studying the mechanism of heart action [2, 8]. This is based on the premise that any significant alternation in the mechanical properties of the heart should cause changes in the sound spectrum emitted from the heart. However, the method used is very important for qualitative analysis of heart sounds due to the fact that S1 and S2 are short-time transient signals with frequency components close to each others.

The objective of this paper is to compare results achieved from the FFT and different parametric methods in the analysis of first (S1) and second (S2) heart sounds and their ability to detect different frequency components associated with S1 and S2.

Results are compared from the following algorithms: FFT, Maximum Entropy, ARMA, and MBPM when applied to simulated and actual heart sounds recorded from normal and abnormal subjects.

2 Spectral Estimation

In an attempt to alleviate the inherent limitations of the FFT approach, many alternative spectral estimation procedures have been proposed during the last two decades. These alternatives, called 'parametric' methods, assume a generating model for the signal process and the spectrum is calculated from this model. However, straightforward application of the standard parametric methods can lead to poor performance, especially for short and noisy data records [1, 3]. This case arises often in recorded heart sounds.

In this paper a singular value decomposition (SVD) technique is used in the ARMA and Prony's methods as a tool to enhance the signal components in data records. The linear equation for the extended order ARMA (p_e, q_e) model may be expressed in matrix form as follows

$$\mathbf{R_{XX}a} = -\mathbf{r_{XX}} \qquad (1)$$

where

$$R_{xx} = \begin{bmatrix} R_{xx}[q_e] & R_{xx}[q_e-1] & \cdots & R_{xx}[q_e-p_e+1] \\ R_{xx}[q_e+1] & R_{xx}[q_e] & \cdots & R_{xx}[q_e-p_e+2] \\ \vdots & \vdots & \cdots & \vdots \\ R_{xx}[q_e+m-1] & R_{xx}[q_e+m-2] & \cdots & R_{xx}[q_e-p_e+m] \end{bmatrix} \qquad (2)$$

is the extended order autocorrelation matrix, and

$$a = \begin{bmatrix} a[1] \\ a[2] \\ \vdots \\ a[p_e] \end{bmatrix}, \quad r_{xx} = \begin{bmatrix} R_{xx}[q_e+1] \\ R_{xx}[q_e+2] \\ \vdots \\ R_{xx}[q_e+m] \end{bmatrix} \qquad (3)$$

are respectively the model parameters and data vector, whereas p_e, and q_e are the extended order of the matrix. In the ARMA method SVD is applied in three different versions. In the first case the SVD technique is applied to the autocorrelation matrix, $\mathbf{R}_{xx}$. To eliminate the noise effects from the data vector, a simple variation of the above mentioned technique is used by working with the extended coefficient matrix $\mathbf{R}'$ [1, 5] where :

$$\mathbf{R'_{XX}} = [\mathbf{r_{XX}}, \mathbf{R_{XX}}] \qquad (4)$$

and then to compute the minimum norm solution

$$\hat{\mathbf{R}}_{\mathbf{XX}}^{(\mathbf{p})} \begin{bmatrix} 1 \\ a \end{bmatrix} = 0 \qquad (5)$$

In this case SVD was applied to the extended order matrix $\mathbf{R}'$ after which $\hat{R}_{xx}^{(p)}$ is decomposed into $(\mathbf{R}')^{(p)} =$

1

$[\mathbf{r}_1^p \mid \mathbf{R}_1^p]$. In both cases mentioned above the size of the $\mathbf{R}_{xx}^{(p)}$ matrix is $m \times p_e$, the third ARMA algorithm has been implemented by reducing the dimension of the left-hand matrix in eq. 1 to $p \times p$. This matrix is given by

$$R_{xx}^{(p)} = \sum_{k=1}^{p_e - p + 1} (\hat{R}_k^{(p)})^* \hat{R}_k^{(p)} \qquad (6)$$

where $\hat{R}_k^{(p)}$ are the submatrices of $\hat{R}xx^{(p)}$ composed of its columns: k to $p+k$. The SVD methods described above enhances the accuracy of the estimates from the Modified Yule-Walker equations. In order to complete the ARMA modelling, it is necessary to determine the associated moving average parameters of the model. MA-components are estimated by using the forward and backward residual time–series associated with an ARMA time series [1]. In the next section these three methods of computing the ARMA model are called respectively ARMA1, ARMA2 and ARMA3.

The SVD technique is also applied successfully to MBP-M. The main advantage of this method is that it gives full parametrisation of the spectrum of the signal: amplitude, frequency, phase and bandwidth information of its significant spectral components [6]. There are four basic steps in this method [3, 6]:

1. The linear prediction parameters are computed from the available data. The principal eigenvalues are used to find these parameters. In our algorithm, SVD is applied to the overdetermined backward noisy data matrix in order to replace it with the least squares approximation matrix of lower rank [5]. For the backward direction case, it has been shown [5] that the poles of the signal can easily be separated from those introduced by noise (i.e. the norm of the signal roots is $\lambda[i] \geq 1$).

2. The roots of a polynomial formed from the linear prediction coefficients will yield the estimates of damping and sinusoidal frequencies of each of the exponential terms. This polynomial has the form

$$B(z) = \sum_{m=0}^{p} a[m] z^{p-m} \qquad (7)$$

The roots of this polynomial are found from the eigenvalues of the matrix A:

$$A = \begin{bmatrix} 0 & 1 & 0 & \cdots & 0 \\ 0 & 0 & 1 & \cdots & 0 \\ \vdots & \vdots & \vdots & \cdots & \\ 0 & 0 & \cdots & 0 & 1 \\ -a[p] & a[p-1] & \cdots & -a[2] & -a[1] \end{bmatrix} \qquad (8)$$

which gives better results than other standard procedures. This procedure is based on (1) reduction of the A matrix to the Hessenberg form and (2) a balancing procedure is applied afterwards to reduce the sensitivity of the estimated eigenvalues to the rounding errors [7].

3. A set of linear equations is solved, which will yield the estimates of the amplitude exponential and initial phase of the sinusoid. With p roots computed from eq. 7 the Vandermonde matrix is created [3, 6]

4. Computation of the spectral estimator. To compute the spectrum from the exponential model we use the two–sided function since it is found more to give sharper spectral peaks [6].

The paper is also focused on the criteria used for order selection of parametric models. As it is very difficult to estimate the order of the model in the case of real data, several model order determining criteria are considered [6]. The four following criteria are used in the case of Maximum Entropy algorithm [3, 6]

- final prediction error (FPE),

$$FPE[p] = \hat{\sigma}_{wp} \left(\frac{N + p + 1}{N - p - 1} \right) \qquad (9)$$

where $\hat{\sigma}_{wp}$ is the estimated variance of the linear prediction error and N is the number of data samples.

- Akaike information criterion (AIC),

$$AIC[p] = N ln \hat{\sigma}_{wp} + 2p \qquad (10)$$

- Criterion autoregressive transfer (CAT)

$$CAT[p] = \left(\frac{1}{N} \sum_{j=1}^{p} \bar{\rho}_j^{-1} \right) - \bar{\rho}_j^{-1} \qquad (11)$$

- Minimum description length (MDL)

$$MDL[p] = N ln(\hat{\sigma_{wp}}) + p ln(N) \qquad (12)$$

where $\bar{\rho}_j = \left[\frac{N}{N-j} \right] \hat{\sigma}_{wj}$.

In the case of ARMA and Prony's method, the order is decided by the relative magnitude of the principal eigenvalues (RME) of the covariance matrix [1, 5].

3 Method

Twenty patients were tested. For each patient, the electrocardiogram (ECG) and phonocardiogram (PCG) were recorded. A Helwett-Packard (21050A) contact microphone was used to pick up the PCG. The microphone was placed on the second right interspace ('aortic' area) and the cardioapex or the 'mitral' area. In these locations the contribution of the heart valve movements is the 'primary source' of the acoustic energy for S2 and S1. The PCG was preprocessed by a third-order high-pass Butterworth filter with a cutoff frequency of 50 Hz and a sixth-order low-pass filter with cutoff frequency of 2kHz was used as an anti-aliasing filter. The ECG and PCG were then digitised to 12-bits at a sampling rate of 5kHz.

156

4 Results

4.1 Simulation Results

The performances of the algorithms are demonstrated by testing them on a synthetic signal, which has characteristics similar to those of heart sounds, namely:

$$x[n] = (0.98)^n sin(0.123n) + (0.98)^n sin(0.423n)$$
$$+w[n] \quad n = 1, 2, \cdots, 128 \quad (13)$$

where $w[n]$ is a Gaussian white noise. The criterion used for choosing the above time series was based on the fact that S1 and S2 are composed of transient sinusoidal signals of short duration and fast decaying amplitude, superimposed on a background of random noise [2, 4]. A percentage error for the estimated frequency is calculated for all methods with different levels of SNR as follows:

$$err(\%) = \frac{\left| \hat{f_i} - f_i \right|}{f_i} \times 100 \quad (14)$$

Table 1 summarises the results and figures 1-5 show the results achieved with the different methods.
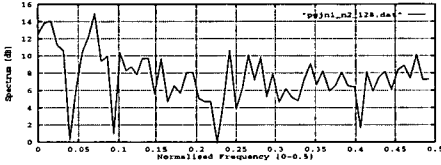
Figure 1: FFT Spectrum
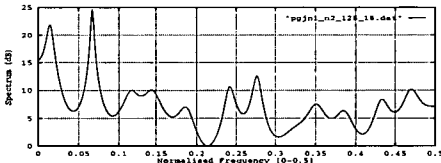
Figure 2: Burg Spectrum (order 30)
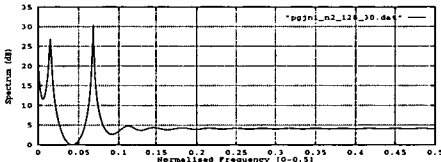
Figure 3: ARMA1 Spectrum (order 4)
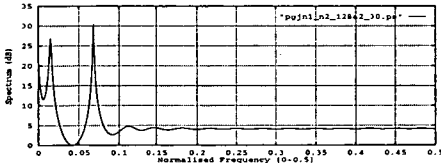
Figure 4: ARMA2 Spectrum (order 4)
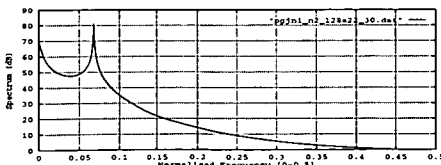
Figure 5: ARMA3 Spectrum (order 4)
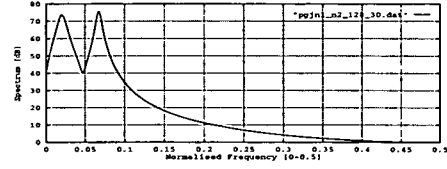
Figure 6: Prony's Method Spectrum (order 4)

Method	SNR(dB)	f_1	f_2	err f_1%	err f_2%
FFT	3	0.0155	0.0704	20.82	4.57
Max. E.	3	0.0147	0.0672	23.5	0.18
ARMA1	3	0.0159	0.0679	18.7	0.93
ARMA2	3	0.0158	0.0679	18.9	0.98
ARMA3	3	fail	0.0675	100	0.26
Prony	3	0.0199	0.0674	1.6	0.01

Table 1: Frequency error estimation

4.2 Real Data

By using the QRS part of the ECG signal as a time reference [2] S1 and S2 are extracted from the PCG signal. An ensemble average was taken of S1 and S2 respectively. This process was achieved automatically using cross-correlation with a known S1 and S2 template. Only sounds achieving a cross-correlation of 80% or more were admitted into the ensemble average. Figures 7-10 show the results of the different methods when applied to S1 of a normal subject.

5 Discussion and Conclusion

By comparing these results it is clear that in the most cases the FFT is not an appropriate method for studying the spectrum of heart sounds. Regarding the fact that S1 and S2 vary in duration from 10-60ms and the PCG spectral components of interest are, in most cases, spread in a narrow band(30-300Hz) [8] the FFT resolution (30-100Hz) is insufficient to detect all the significant components present in S1 and S2. From figure 7 it is very difficult to estimate accurately the different components of the spectrum, especially in the band 100-300Hz where is well known that S1 has many components [8].
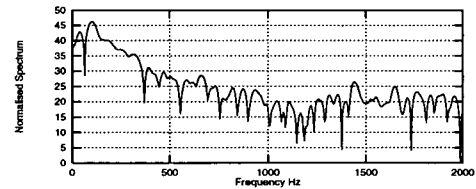

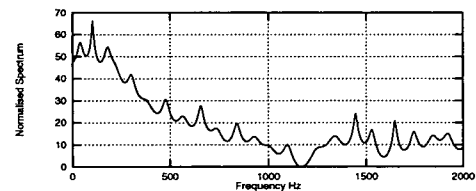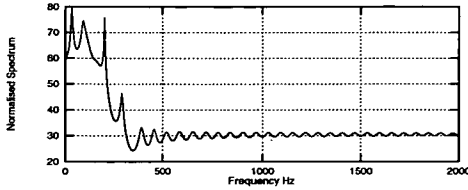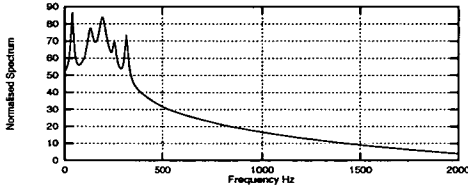Figure 7: FFT Spectrum of first heart sound

Figure 8: Burg Spectrum of first heart sound (p=50)

Figure 9: ARMA1 Spectrum of first heart sound (p=q=10)

Figure 10: Prony's Spectrum of first heart sound (p=10)

Amongst the parametric methods, MBPM is the best one to characterise the frequency components of a closing heart valve. It is also found that the maximum entropy method gives very smooth spectra especially when the order model is given by the minimum value of FPE, AIC, CAT or MDL. To combat this effect a higher model order is required which automatically will yield in extra components of the spectrum(fig. 2). This finding is in accordance with Cloutier's results [2] when analysing closing sounds produced by bioprostheses. The same conclusion can be drawn for the ARMA3 algorithm. However, ARMA1 and ARMA2 give better results compared with ARMA3 and the maximum entropy algorithms(see fig 9).

Regarding the order of the model we have found that FPE, AIC, CAT and MDL do not return a consistent value and their estimated model orders vary between 8-32 (fig 12). In the case of ARMA modelling and MPBM the relative magnitude of eigenvalues (K) was used for deciding the order of the model. It was found that the optimum model order p lies for RME in range between -32 to -40dB. In this context the SVD technique returns a model order which closely relates to what would be expected from the anatomical construction of the heart valves and is very consistent (fig. 11). Furthermore, the SVD technique applied here is in accordance with the theory of the 'primary sources' of the PCG signals because it extracts from the overall signal (i.e. the external recorded PCG) the p strongest components which are assumed to be related to heart-valve action. Therefore, these components can be used as a feature vector for parameterization of the valvular condition.
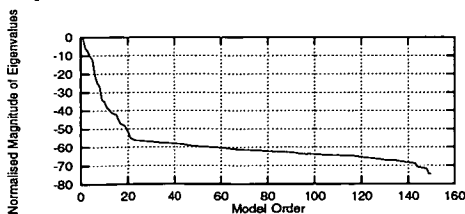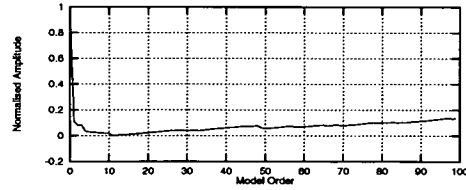

Figure 11: SVD Order Selection

Figure 12: AIC Order Selection

In addition, these methods not only give a good representation of the frequency components of S1 and S2 but also provide a method for the further investigation of the origin of S1 and S2 since they give good spectral resolution even for short data records.

Acknowledgments

References

[1] J.A. Cadzow, "Spectral Estimation: An Overdetermined Rational Model Equation Approach", *Proc. of the IEEE*, Vol. 70, No 9, 907–939, Sept. 1982.

[2] G. Cloutier, M. C. Grenier, R. Guardo, L. G. Durand, "Spectral Analysis of Closing Sounds Produced by Ionescu-Shiley Bioprosthetic Aortic Heart Valves", *Med. & Biol. Eng. & Comput.*, No. 25, 492–496, Sept. 1987.

[3] S. M. Kay, S. L. Marple, "Spectrum Analysis–A Modern Perspective", *Proceedings of the IEEE*, Vol. 69, No. 11, 1380–1419, Nov. 1981.

[4] H. Koymen, B. K. Altar, Y. Z. Ider, "A Study of Prosthetic Heart Valve Sounds", *IEEE Trans on BME*, Vol 34, No. 11, pp 853–863, 1987.

[5] R. Kumaresan, D. W. Tufts, "Estimating the Parameters of Exponentially Damped Sinusoids and Pole–Zero Modeling in Noise", *IEEE Trans on AS-SP*, Vol ASSP-30, No.6, pp 833–840, Dec. 1982.

[6] S. L. Marple, "Digital Spectral Analysis (with applications)",*PRENTICE-HALL*, INC, Englewood Cliffs, NewJersey 07632, 1987.

[7] W. H. Press *et al.*, "Numerical Recipies in C", *Cambridge Univ. Press*, 1988.

[8] R. Rangayyan, R. J. Lehner, "Phonocardiogram Signal Analysis: A Revieew",*CRC Critical Review in Boim. Eng.*, Vol. 15(3), 1988.